

Aus dem Institut für Biochemie
der Medizinischen Fakultät Charité – Universitätsmedizin Berlin

DISSERTATION

**Perturbations of proteostasis networks in Alzheimer´s disease:
Focus on the ubiquitin proteasome system.**

zur Erlangung des akademischen Grades
Doctor of Philosophy (PhD)

vorgelegt der Medizinischen Fakultät
Charité – Universitätsmedizin Berlin

von

Eileen Josephine Schormann
aus Hamburg

Datum der Promotion: 01.03.2019

Vorwort

Die Alzheimer-Krankheit stellt die häufigste Form der Demenz dar und ist bis heute unheilbar. Obwohl sich mittlerweile ein bemerkenswertes Wissen über die Erkrankung angesammelt hat, stellt ihre Komplexität die Forschung vor große Herausforderungen. Ich halte es für unabdingbar, dass aktuelle und zukünftige Wissenschaftler mit Neugier und Mut sowie einer Portion Flexibilität in ihren Denkstrukturen an die weitere Aufklärung neurodegenerativer Erkrankungen herangehen. Nur so lassen sich die immer noch bestehenden Lücken schließen und dadurch hoffentlich eine wirksame Therapie entwickeln.

Die von mir vorgelegte Dissertation wurde während meiner Tätigkeit als Wissenschaftliche Mitarbeiterin im Institut für Biochemie der Charité Universitätsmedizin Berlin erarbeitet. Während der gesamten Zeit wurde ich umfassend von meiner Doktormutter Frau Prof. Dr. rer. nat. Elke Krüger (heute Universitätsmedizin Greifswald, Institut für Medizinische Biochemie und Molekularbiologie) betreut. Im Rahmen meiner Teilnahme am internationalen Graduiertenprogramm Medical Neurosciences der Charité wurde meine Forschungsarbeit von Prof. Dr. med. Christoph Harms (Charité Universitätsmedizin, Centrum für Schlaganfallforschung) und Dr. Alessandro Prigione (Max Delbrück Centrum Berlin, Mitochondria and cell fate reprogramming) co-betreut.

Der überwiegende Anteil meiner Forschungsarbeit entstand im Rahmen des vom Berliner Institut für Gesundheitsforschung (BIH) geförderten Collaborative Research Grants (CRG) „Elucidating the proteostasis network to control Alzheimer’s disease“ unter der Koordination von Prof. Dr. Erich Wanker und Prof. Dr. Frank Heppner. Dazu gehören die Arbeiten an organotypischen Hirnschnitten und die Einbeziehung des Alzheimer Mausmodells 5xFAD. In einer weiteren Kooperation mit Prof. Dr. Frank Heppner sind die in Kapitel 3.1.10. (Figure 24) dargestellten Daten in die Veröffentlichung *Wagner et al. (2017)* eingeflossen (Figure 1c+d).

Die Basis meiner Arbeit, das synthetische A β Peptid, wurde in unserer Institutseigenen Peptid-Facility von Frau Petra Henklein hergestellt. Die Umsetzung der mikroskopischen Aufnahmen, mein persönliches Herzstück, wurde ermöglicht durch einen von COST Proteostasis geförderten Aufenthalt in der Forschungsgruppe von Prof. Huib Ovaas am Netherlands Cancer Institute in Amsterdam, der in diesem

Zusammenhang auch die pan-reaktive active site probe zur Verfügung gestellt hat. Viele Stunden habe ich dann in der Charité-eigenen Advanced Medical Bioimaging (AMBIO) Core Facility verbracht und bedanke mich für die Beratung und Unterstützung von Dr. Jan Schmoranzer und Robyn Brackin-Helmers.

Forschung lebt nicht nur von Zusammenarbeit sondern auch von Austausch. In diesem Sinne habe ich meine aktuellsten Erkenntnisse auf Symposien und Konferenzen, wie z.B. auf der ENCODS (2017) oder dem Proteasome & Autophagy Workshop (2016), präsentiert und mich mit anderen Wissenschaftlern darüber ausgetauscht. Sollte meine Arbeit auch darüber hinaus zu wissenschaftlichem Diskurs anregen, hat sich der Einsatz aller Beteiligten gelohnt.

*„Es wird ja fleißig gearbeitet und viel mikroskopiert,
aber es müsste mal wieder einer einen gescheiterten Gedanken haben.“*

Rudolf Virchow

Berlin, Juni 2018

Content

Vorwort.....	0
Abstract.....	3
Zusammenfassung.....	4
1. Introduction	5
1.1. Aspects of neuroinflammation in Alzheimer’s disease	5
1.1.1. Alzheimer’s disease (AD)	5
1.1.2. Amyloid- β oligomers as drivers of neuroinflammation	6
1.1.3. Microglia and astrocytes in Alzheimer’s disease.....	8
1.2. The ubiquitin proteasome system in the central nervous system	9
1.2.1. General aspects of the ubiquitin proteasome system.....	9
1.2.2. The role of the immunoproteasome in immune response.....	11
1.2.3. The mTOR pathway as the intersection between the IFN signaling and the UPS ...	12
1.2.4. The ubiquitin proteasome system in brain homeostasis.....	13
1.3. Alzheimer’s disease and dysregulations in the ubiquitin proteasome system	15
1.3.1 Altered proteasome networks in Alzheimer’s disease	15
1.3.2. Altered inflammatory pathways related to the UPS in AD.....	16
1.4. Scientific aims.....	17
1.4.1. Perturbations in proteasome networks in experimental models of AD.....	17
1.4.2. Interventions in proteasome-associated signaling in an AD mouse model.....	17
2. Material and methods.....	19
2.1. Mouse models of immunoproteasome-deficiency and Alzheimer’s disease	19
2.1.1. Genotyping	19
2.1.2. Brain tissue sampling.....	21
2.2. Organotypic brain slice culture (OBSC).....	21
2.2.1. Neural dissociation and microglia separation (MACS)	22
2.3. Preparation of amyloid- β oligomers (A β Os).....	23
2.3.1. Blue native PAGE	23
2.4. Assessment of proteasome activity	24
2.4.1. Fluorogenic substrate based assay	24
2.4.2. Active site probes	24
2.5. Analysis of protein expression and ubiquitination	25
2.5.1. Protein extraction.....	25
2.5.2. Analysis of protein expression by western blot.....	25
2.5.3. Analysis of ubiquitinated proteins by dot blot	26

2.5.4.	Immunodetection	26
2.6.	Immunofluorescent stainings and confocal microscopy	27
2.7.	Analysis of mRNA expression	28
2.7.1.	RNA extraction	28
2.7.2.	cDNA synthesis	29
2.7.3.	Pre-amplification	29
2.7.4.	Quantitative real-time PCR	30
2.8.	Statistics.....	31
3.	Results.....	32
3.1.	Perturbations of proteasome networks in Alzheimer`s disease	32
3.1.1.	Characterization of amyloid- β oligomer preparation	32
3.1.2.	A β O-induced decrease of active proteasome subunits is abolished by immunoproteasome deficiency	33
3.1.3.	Proteasome impairment results in the accumulation of Ub-conjugates, immunoproteasome formation and a Type-I IFN response	35
3.1.4.	A β oligomers activate mTOR signaling pathway	42
3.1.5.	A β O-induced autophagy in immunoproteasome deficiency.....	45
3.1.6.	A β O alter glial activities dependent on the immunoproteasome	46
3.1.7.	Cell type specific response upon A β O-treatment	51
3.1.8.	Increased proteasome activity and immunoproteasome expression in aged APP/PS1 mice	56
3.2.	Rapamycin decreases the amount of active proteasome subunits in 5xFAD mice	58
4.	Discussion.....	62
4.1.	Perturbations in proteasome networks in experimental models of AD	62
4.2.	Interventions in proteasome-associated signaling in an AD mouse model.....	67
	Abbreviations	70
	List of figures.....	75
	List of tables	76
	References.....	77
	Eidesstattliche Versicherung	86
	Lebenslauf.....	87
	Publikationen.....	89
	Anteilerklärung an etwaigen erfolgten Publikationen.....	90
	Danksagung	91

Abstract

Alzheimer's disease (AD), one of the most prevalent neurodegenerative disorders, is characterized by the accumulation of amyloid- β as extracellular plaques. Nonetheless, the soluble forms of A β are thought to play a major role in driving disease progression, for example by promoting inflammatory processes. Furthermore, evidence suggests defects of protein degradation systems, in particular dysregulations in the ubiquitin proteasome system, play a pathogenic role. Proteotoxic stress and inflammation are associated with the upregulation of the specialized isoform immunoproteasome. Using organotypic brain slice cultures (OBSCs), we aimed to elucidate A β oligomer (A β O)-induced changes in proteasome networks and the role of the immunoproteasome. We further planned to compare our results to AD mouse models with established plaque pathology and aimed to interfere with signaling pathways involved in proteasome regulation.

Importantly, in OBSCs we were able to demonstrate that exposure to A β O resulted in a significant decrease of active β -subunits of the proteasome, upregulation of soluble Ub-conjugates and moderate increase of immunoproteasome subunit LMP7. Proteasome impairment was accompanied by activation of mTOR signaling and an increase in activated microglia. Interestingly, in the absence of the immunoproteasome, A β O did not alter the amount of active β -subunits or the number of activated microglia but changed the characteristics of astrocytes and induced the autophagy-marker LC3b-II. In contrast, in aged APP/PS1 mice we detected a significant increase in proteasome activity as well as the upregulation of LMP7. Immunoproteasome deficient APP/PS1 mice, however, displayed significant lower proteasome activity levels compared to age matched WT and APP/PS1 mice. In 5xFAD mice we interfered with mTOR signaling with rapamycin that surprisingly resulted in a decrease of active proteasome β -subunits probably due to already established A β plaques.

Overall, we found that the immunoproteasome indeed plays a significant role in AD pathogenesis and might be a suitable target for therapy. Our results further indicate that A β O alter glial activities dependent on the presence of the immunoproteasome. Moreover, we demonstrated that the impact on proteasome activity is dependent on the time point and model used.

Zusammenfassung

Die Alzheimer-Krankheit, eine der häufigsten neurodegenerativen Erkrankungen, ist durch die Anhäufung von β -Amyloid in Form von extrazellulären Plaques charakterisiert. Dennoch nimmt man heute an, dass die lösliche Form von A β eine bedeutende Rolle beim Fortschreiten der Alzheimer Erkrankung spielt. Darüber hinaus stehen defekte Protein-Abbauege im Verdacht, insbesondere das Ubiquitin Proteasom System (UPS). Proteotoxischer Stress und Entzündungsprozesse werden mit der Bildung einer spezialisierten Isoform, dem Immunoproteasom (iP), in Verbindung gebracht. Mit organotypischen Hirnschnitten möchten wir die durch A β Oligomere (A β Os) induzierten Veränderungen im Proteasom System und die Rolle des iP untersuchen. Diese Ergebnisse sollen dann mit Erkenntnissen aus Alzheimer Mausmodellen verglichen werden, die bereits eine Plaque-Pathologie aufweisen und bei denen mit Inhibitoren in Proteasom-regulierenden Signalwegen eingegriffen wurde.

Unsere Daten haben bewiesen, dass A β Os eine signifikante Verringerung der aktiven β -Untereinheiten des Proteasoms, eine Anreicherung löslicher Ub-Konjugate und die moderate Hochregulierung der iP-Untereinheit LMP7 bewirken. Die Verminderung der Proteasom-Aktivität resultierte in einer Aktivierung des mTOR-Signalwegs und einer Erhöhung der Anzahl aktivierter Mikroglia. Interessanterweise hatten A β Os bei Abwesenheit vom iP keine Veränderung der aktiven β -Untereinheiten oder Mikroglia zur Folge. Stattdessen haben sich die Eigenschaften der Astrozyten verändert und Autophagy wurde aktiviert. Im Gegensatz zu den ex-vivo Daten wurden in APP/PS1 Mäusen im Vergleich zum Wildtyp eine Erhöhung der Proteasom-Aktivität sowie die signifikante Erhöhung der iP-Menge detektiert. Die Inhibierung des mTOR Signalwegs durch Rapamycin hatte in 5xFAD Mäusen überraschenderweise eine Verringerung der aktiven Proteasom-Untereinheiten zur Folge, möglicherweise durch die bereits bestehende Plaque-Pathologie.

Zusammenfassend haben wir nachgewiesen, dass das iP eine entscheidende Rolle bei der Alzheimer Pathologie spielt und ein mögliches Ziel für therapeutische Ansätze darstellt. Unsere Ergebnisse zeigen ferner, dass A β Os - abhängig vom Vorhandensein des iP - die Aktivität von Gliazellen beeinflussen. Außerdem wurde deutlich, dass die Effekte auf das UPS vom Fortschritt der Erkrankung und damit dem Aggregationszustand von A β abhängig sind.

1. Introduction

1.1. Aspects of neuroinflammation in Alzheimer's disease

1.1.1. Alzheimer's disease (AD)

More than 100 years ago, Alois Alzheimer first described the pathology of the nowadays most common neurodegenerative disorder based on a female patient, Auguste D., who showed novel behavioral and cognitive symptoms and suspicious deposits in post-mortem brain tissue [1]. While macroscopically the brain of Auguste D. clearly showed signs of atrophy, microscopically Alois Alzheimer found neuronal loss with fibrillary debris and extracellular plaques. Today it is known that these intracellular fibrillary structures, called neurofibrillary tangles (NFTs), contain hyperphosphorylated tau protein and the observed extracellular plaques consist of aggregated amyloid- β peptide. Although both tau and A β deposits still remain histological hallmarks of Alzheimer's disease (AD), the scientific view on their contribution to disease progression changes. Reasons for the major economic burden for the health care system by AD are in particular the lack of suitable biomarkers and therapeutic approaches, although major advances are expected in the near future. Nevertheless, today the highly complex AD remains incurable. In addition, the number of AD patients increases due to the ageing population [2].

The source of the small amyloid- β peptide is the stepwise cleavage of the amyloid precursor protein (APP), a type I transmembrane glycoprotein, by β - and γ -secretases (Figure 1A). In the course of the so-called amyloidogenic pathway, APP that is internalized into endosomes is cleaved by β -secretases 1 and 2 (BACE1 and 2) resulting in two fragments, the long soluble APP β (sAPP β) and the short C-terminal fragment (β -CTF or C99) that comprises the A β sequence and is bound to the membrane [3]. Finally, γ -secretase generates an APP intracellular domain (AICD) and two peptides A β_{48} and A β_{49} , depending on the cleavage site. The two peptides are subsequently cleaved to A β_{42} and A β_{40} , respectively, and a number of other A β variants [4], [5]. Although the majority of A β peptides produced is A β_{40} , the longer variant A β_{42} is more prone to aggregate due to its higher hydrophobicity (Figure 1B, [6]). A third enzyme – the α -secretase - initiates the non-amyloidogenic pathway which is therefore not producing any pathogenic A β fragments.

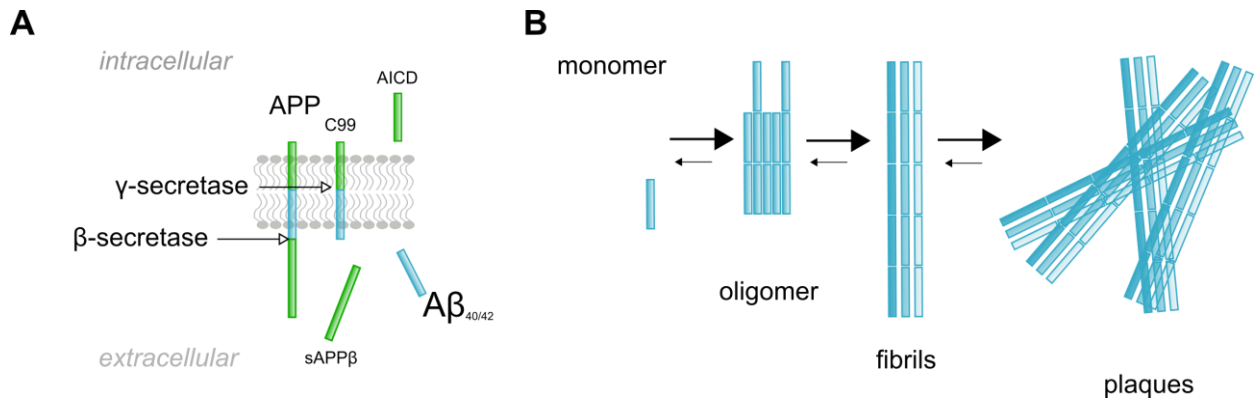


Figure 1: Cleavage of amyloid-β from APP.

A Membrane-bound APP is first cleaved by β-secretases resulting in the two fragments sAPPβ (soluble) and C99 (β-CTF, still membrane bound). C99 is then cleaved by γ-secretase into intracellular AICD and Aβ₄₈ and Aβ₄₉ that are further processed to Aβ₄₀ and Aβ₄₂. **B** Aβ₄₂ with its higher hydrophobicity tends to aggregate to oligomeric structures that can form fibrils and finally plaques.

APP as well as its cleavage products have been attributed to physiological roles in the brain with, for example, sAPPβ being involved in calcium-homeostasis or Aβ production being influenced by synaptic activity and plasticity [7]. Depending on the location of Aβ secretion, Aβ can impair neuronal functions by synaptic toxicity, mitochondrial dysregulation, microglial over-activation as well as by cross-talk with tau [7], [8]. The complexity of Alzheimer's disease is also reflected by the growing knowledge of the interaction of the various cell types, like neurons, microglia, astrocytes and the lesser studied oligodendrocytes, in response to Aβ stress [9]. In addition, the neuroinflammatory component, in particular the chronic activation of innate immunity, has gained attention in the research field of AD [10], [11]. Therefore, the cellular and inflammatory aspects of AD, with special regard to oligomeric species of Aβ, will be reviewed in more detail in the following chapters.

1.1.2. Amyloid-β oligomers as drivers of neuroinflammation

For a long time the involvement of neuroinflammation in Alzheimer's disease has been considered to be merely a concomitant feature rather than being relevant for disease progression or even initiation. In contrast to classical inflammatory diseases of the central nervous system (CNS) like multiple sclerosis (MS), AD is thought to involve cells and responses mainly of the innate immunity [10], [11]. Support for the neuroinflammatory hypothesis arises from epidemiological studies stating that long-term treatment with nonsteroidal anti-inflammatory drugs reduces the risk for AD development [12]–[14]. Although results about cytokine and chemokine levels in plasma or cerebrospinal fluid (CSF) of patients are conflicting, they indicate a quite early

involvement of inflammation at the stage of mild cognitive impairment (MCI) [15]. Importantly, the findings of genetic alterations in genes encoding for triggering receptor expressed on myeloid cells 2 (TREM2) and myeloid cell surface antigen CD33 [16]–[18] strongly supported the view of AD as a neuroinflammatory disorder. Interestingly, it has been demonstrated that prenatally infection with polyriboinosinic-polyribocytidilic acid (PolyI:C) of wild type (WT) mice is sufficient to induce an AD like phenotype with ageing that could be enhanced with a second infection in adulthood or infection of transgenic AD mice [19].

Amyloid- β coexists in a continuous equilibrium of monomers, oligomers and fibrils. The literature reports the existence of numerous oligomeric assembly states as a result of biological variety as well as different techniques for in vitro generation of A β oligomers (A β O_s) or their extraction from brain tissue (as critically reviewed in [20]). The potential toxic action of A β oligomers depends on the location of A β , intra- or extracellularly, and is very diverse. Besides the secretion of A β peptide to the extracellular space by cleavage of APP at the outer membrane, it has been proposed, that A β plaques might serve as a source for A β oligomers [20]. In either way, it is conceivable that A β oligomers interact with receptors at the surface of cells and induce, for example, inflammatory signaling cascades. Indeed, it has been shown that A β oligomers activate microglia in a similar manner as lipopolysaccharide (LPS) via scavenger receptor A (SRA) and calcium-activated potassium channel KCa3.1, already at nanomolar concentrations [21]. Moreover, IgG-binding Fc γ receptors have been shown to play a role in A β oligomer induced toxicity. Researchers found increased levels of Fc γ RIIb in neurons of AD patients in co-localization with oligomeric A β structures. Furthermore, in the same study it has been demonstrated that inhibition of Fc γ RIIb-A β interaction blocks A β oligomer-induced neurotoxicity [22]. Another A β sensor, receptor for advanced glycation end products (RAGE), became the focus of attention since it has not only been shown that RAGE provides binding sites for A β resulting in an inflammatory cascade leading to neuronal death but also its prevention by blockage of the V_d domain of RAGE [23]. Another receptor of the innate immunity, toll-like receptor 4 (TLR4), has been shown to be affected by A β oligomers. Thus, A β O_s lead to an increase in pro-inflammatory cytokines, enhanced expression of TLR4 and caused neuronal death. Both - anti-inflammatory drugs and TLR4 antagonists - have been shown to prevent A β O-induced cognitive impairment [24], [25]. Interestingly, in the hippocampus of a pre-

plaque AD mouse model, researchers found upregulation of major histocompatibility complex class II (MHCII), inducible nitric oxide synthase (i-NOS) and CD40 before plaque deposition but along with intraneuronal A β oligomers surrounded by microglia [26].

1.1.3. Microglia and astrocytes in Alzheimer's disease

The “biochemical phase” of AD, meaning the abnormal production of A β , the formation of A β assemblies and the resulting proteopathic stress, is per se not considered to be determining for the manifestation of AD [9]. It is rather assumed, that only if compensating mechanisms of protein homeostasis collapse, for example due to ageing, the “cellular phase” with alterations in glial functions and chronic inflammation finally results in cell death visible as “clinical phase” in AD [9].

The main cell types studied in terms of neuroinflammation is microglia. Although they are classified as brain resident macrophages and inspect the CNS for pathogens, recent advances highlight their heterogeneity and differences to other tissue resident macrophages. Thus, in addition to their role in innate immunity, microglia support CNS homeostasis and plasticity by, for example, synaptic remodeling [27]. Considering the broad spectrum of their actions, it is not surprising that impairment of microglia has various effects on cells of the CNS. Microglia are found in close association to amyloid plaques [28] and to express a variety of receptors that sense A β peptides [11] and induce the release of pro-inflammatory cytokines. Furthermore, although microglia have been shown to bind and internalize A β via receptors, recent evidence suggest that microglia-dependent A β clearance mechanisms are impaired in AD. In AD mouse models using in vivo two photon microscopy, it has been demonstrated that microglia dysfunction (impaired motility and phagocytosis) correlated with the accumulation of A β plaques [29]. This finding was supported by Orre et al. [30] showing a reduction in expression of phagocytosis genes in microglia isolated from AD mice. In addition, intracellular aspects of protein clearance, namely autophagy, have been linked to AD by showing reduced levels of Beclin-1 in microglia isolated from AD brains [31]. The idea of microglia featured with a disturbed A β clearance capacity in the course of AD has been promoted by a study that found no effect on A β plaque burden in microglia-depleted AD mice [32].

Although astrocytes exceed microglia in numbers in the CNS, their role in

neuroinflammation is still relatively poorly understood [33]. In healthy CNS tissue, astrocytes assure normal neuronal function by serving as a connection between neurons and the blood brain barrier (BBB). Functioning in a so-called “tripartite” synapse, astrocytes maintain transmitter homeostasis by either uptake or even release of transmitters like glutamate. Connected to blood vessels, astrocytes are able to influence, for example, the blood flow or transport energy metabolites to neurons [34]. Astrocytes can be challenged by injury or in disease and thereby - similar to microglia - change their phenotype into at least two reactive states A1 and A2 [33]. Interestingly, a recent study found that the neurotoxic state A1 is induced by the release of cytokines of activated microglia and these A1 astrocytes lose their beneficial characteristics which finally causes neuronal death [35]. Furthermore, transcriptional analysis of astrocytes isolated from AD mice revealed a pro-inflammatory phenotype and reduced levels in genes involved in neuronal support [30]. Astrocytes have been shown to surround A β plaques [36] and respond to A β oligomers by activation of cyclooxygenase 2 (COX-2) and the expression of cytokines interleukin 1 β (IL-1 β) and tumor necrosis factor α (TNF- α) mediated by nuclear factor κ -light chain enhancer of activated B-cells (NF κ B)-signaling [37]. In addition to their role in inflammatory signaling, astrocytes have been shown to degrade A β deposits [38], [39] and to influence microglial phagocytosis of A β via the release of apolipoprotein E (APOE), one of the proteins responsible for cholesterol export from the cell and considered as a genetic risk factor for AD [40]. By stimulation of astrocytes ex vivo with A β peptides it has been found that the secretion of proteolytic enzymes like neprilysin are involved in A β clearance [41]. Despite the demonstrated general ability of astrocytes to degrade A β , the morphological changes like atrophy - as observed in an AD mouse model - indicate an overload of their phagocytosis capacity [42].

1.2. The ubiquitin proteasome system in the central nervous system

1.2.1. General aspects of the ubiquitin proteasome system

Every protein has a definite lifespan that ends in its degradation to generate amino acids for the synthesis of new proteins. In addition, protein synthesis can fail and result in misfolded and therefore useless proteins. This constant need for a solid protein recycling machinery is covered mainly by the ubiquitin proteasome system (UPS) [43]. Besides the maintenance of protein homeostasis, the proteasome provides peptides for

antigen presentation via the major histocompatibility complex (MHC) class I [44].

The key player of the UPS, the proteasome, is a multimeric enzyme complex composed of over 60 subunits and complemented by many associated proteins. The proteasome structure is based on a barrel shaped 20S core consisting of two outer α -rings and two inner β -rings of 7 subunits each (Figure 2A). The inner β -rings harbor six catalytically active subunits - β 1, β 2 and β 5 – with caspase-like, tryptic-like, and chymotryptic-like activities, respectively. The 20S core alone is considered inactive until regulatory particles (19S, PA200 or 11S/PA28) are added to form the 26S proteasome. According to cellular requirements, the composition of the proteasome can be adjusted by differential gene expression resulting in the incorporation of alternative catalytic subunits or attachment of different combinations of regulators [45]. The immunoproteasome, for example, is formed de novo by the incorporation of three immuno-subunits β 1i/LMP2/PSMB9, β 2i/MECL-1/PSMB10, and β 5i/LMP7/PSMB8, and expressed constitutively in immune cells or induced in other cells in response to cytokines [46]. Due to its higher proteolytic capacity, the induction of the immunoproteasome enables cells to rapidly compensate the increased need for protein degradation upon proteotoxic stress or inflammation [47], [48].

Proteins determined for proteasomal destruction are marked with a poly-ubiquitin (poly-Ub) chain by ubiquitin ligases. Once the poly-Ub chain is reversibly bound to 19S subunits, de-ubiquitinylation of the protein substrate can either lead to the release of the

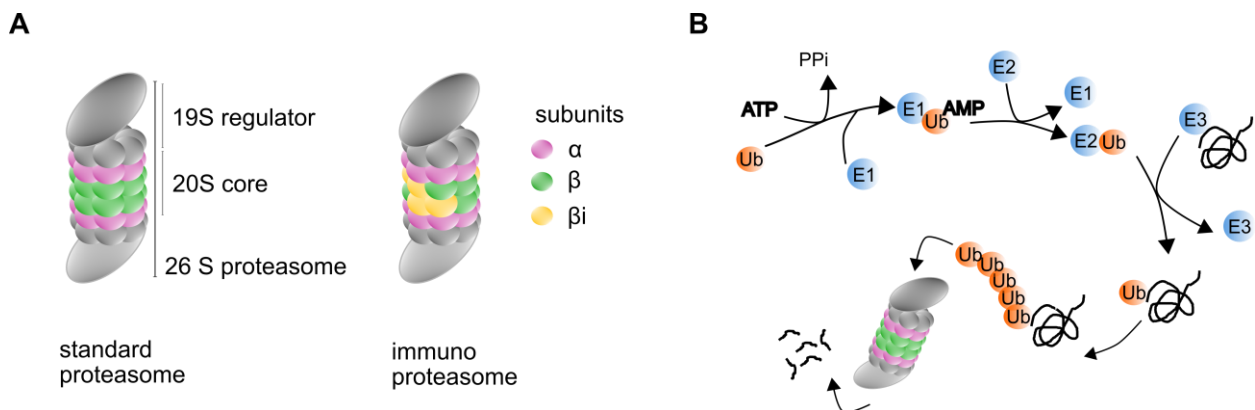


Figure 2: The structure of the proteasome and degradation of Ub-conjugated proteins.

A The proteasome consists of a barrel shaped 20S core build of two outer α -rings and two inner β -rings of 7 subunits each. The inner β -rings harbor six catalytically active subunits - β 1, β 2 and β 5. Alternatively within the immunoproteasome the catalytically β -subunits are substituted by respective β i subunits. In both – standard and immunoproteasome – the 20S core can be complemented by regulator particles, for example, 19S. **B** In an ATP-dependent enzymatic cascade (ubiquitin activation, E1; ubiquitin conjugation, E2; ubiquitin ligation, E3) proteins determined for degradation by the proteasome are poly-ubiquitinated. The poly-Ub-chain is recognized by regulatory particles, the protein translocated to the core, unfolded and de-ubiquitinated and finally degraded to short peptides.

protein or the interaction with ATPases promoted by a loosely folded region in the substrate and adenosintriphosphate (ATP) hydrolysis. When the competition results in tight binding to the proteasome complex and opening of the 20S gate, the protein substrate gets translocated, unfolded and finally de-ubiquitinated before peptide hydrolysis occurs [49]. This process is highly specific and tightly regulated, for example, via the ubiquitin-conjugation, the activity of de-ubiquitinating enzymes (DUBs) and the susceptibility of the substrate to the proteasome [49].

1.2.2. The role of the immunoproteasome in immune response

The ubiquitin proteasome system is capable to adjust its proteolytic capacity suitable to the changing cellular environment. Thus, for example, the pro-inflammatory cytokine interferon- γ (IFN γ) induces the expression of immuno-subunits to form the isoform immunoproteasome that possess higher chymotrypsin- and trypsin-like activity [50]. This way, the immunoproteasome has been proposed to serve as a more effective producer of antigens for MHC class I presentation as part of the adaptive immunity [51], [52]. However, the fact that the immunoproteasome can be cytokine-induced also in non-immune cells indicates an important role in innate immunity. Besides the formation of the immunoproteasome, cytokines induce the formation of reactive oxygen species (ROS) and reactive nitrogen species (RNS) [53]. In high amounts both forms of radicals cause oxidative stress by oxidant-damage of, for example, proteins. Evidence suggests the immunoproteasome to take care of the degradation of those oxidant-damaged and possibly toxic proteins to restore cell homeostasis and protect from cell death [48].

Evidence for the importance of the immunoproteasome emerged from studies using a mouse model of immunoproteasome deficiency (LMP7 KO). LMP7 KO mice lack exon 1 to 5 of the Psmb8 gene, encoding for the first 247 to 276 amino acids of the LMP7 protein, and thus lack one of the catalytic β -subunits of the immunoproteasome [54]. Thus, it has been found that lymphocytic choriomeningitis virus (LCMV)-induced meningitis is delayed and reduced in severity in mice deficient for the immunoproteasome [55], [56]. This study further showed a reduced LCMV-induced formation of the immunoproteasome in the WT brain compared to organs of the periphery. The immunoproteasome was located predominantly to microglia-like cells, suggesting that it is involved in microglia-driven aggravating harmful immune responses in the brain [55]. Furthermore, macrophages derived from different mouse strains

lacking the immunoproteasome displayed reduced nitric oxide (NO) production upon LPS indicating a role in the TLR4-IRF3 cascade [57]. This is in contrast, however, with the finding that LPS-challenged livers and experimental autoimmune encephalomyelitis (EAE)-diseased brains of LMP7 KO mice show significantly higher amounts of oxidant-damaged proteins [48]. Supporting this, coxsackie virus B3 (CVB3)-infection of mice lacking the immunoproteasome resulted in a severe enterovirus myocarditis [58]. This conflicting state of data regarding the particular role of the immunoproteasome underlines the need for elaborate research in the field, especially with regard to the central nervous system.

1.2.3. The mTOR pathway as the intersection between the IFN signaling and the UPS

Protein homeostasis is a delicate balance between protein synthesis and degradation. It is therefore not surprising that mammalian target of rapamycin (mTOR), one major control factor of protein synthesis, also determines the activity of protein degradation. Indeed, it has been demonstrated that the inhibition of mTOR by rapamycin increases the activity not only of autophagy but of the ubiquitin proteasome system as well [59]. It has been further shown that mTOR inhibition upregulates the expression of proteasome assembly chaperone Adc17 and the proteasome abundance in yeast [60]. Interestingly, rapamycin fed to aged mice extended their lifespan [61] and its immunomodulatory function is used as an immunosuppressant in transplantation [62]. mTOR signaling not only regulates overall protein synthesis but is involved in the development, survival and function of immune cells with a broad range of action in adaptive and innate immunity [62]. In this context, it has been reported that Toll-like-receptor-mediated type I IFN production in dendritic cells requires the activation of mTOR to establish the MyD88-TLR complex that further induces the nuclear translocation of IFN regulatory factors [63]. Co-treatment with rapamycin resulted in the significant reduction of IFN α and IFN β [63]. Type I IFNs in turn have been demonstrated to induce phosphorylation of p70 S6 kinase, a downstream target of mTOR, which further leads to the translation of IFN stimulated genes encoding for ISG15 and CXCL-10 [64], [65]. Therefore, it has been suggested that IFN induced mTOR signaling complements IFN mediated signal transducer and activators of transcription (STAT) signaling to promote immune responses [66].

The contribution of mTOR signaling to the regulation of both proteasome activity and IFN signaling as well as the intersection between IFN signaling and the modulation of proteasome networks via the induction of the immunoproteasome allows the assumption of an IFN-mTOR-immunoproteasome axis.

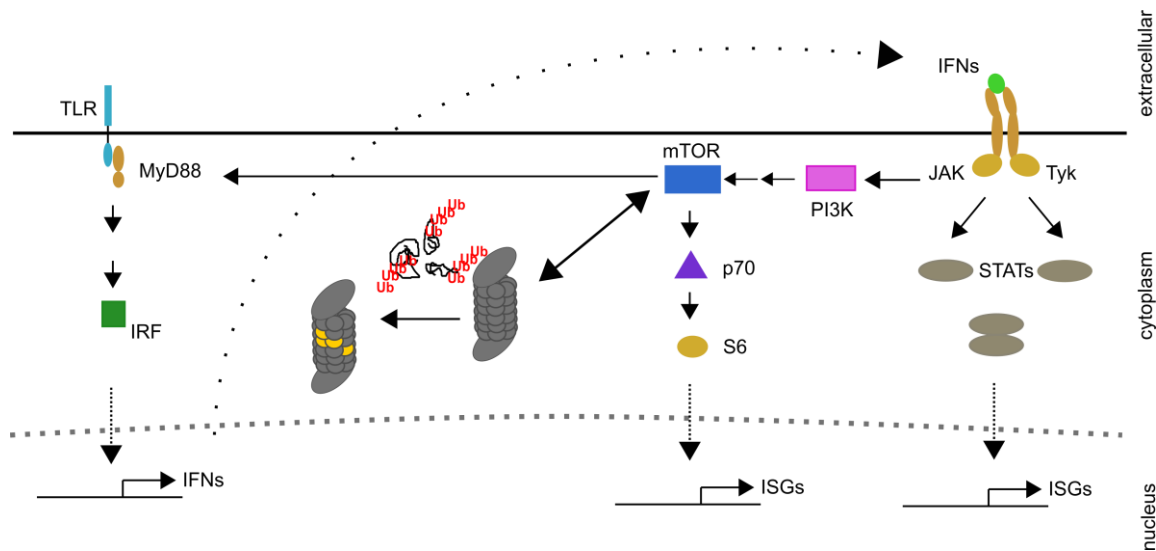


Figure 3: Intersections between IFN signaling and the UPS.

IFN signaling offers several points of interaction with mTOR promoting TLR-mediated production of IFNs that in turn activate STAT- and mTOR-mediated signaling that results in the production of ISGs. The proteasome system, in addition, has been shown to be influenced by mTOR activity and its impairment has been associated with IFN-induced upregulation of the immunoproteasome.

1.2.4. The ubiquitin proteasome system in brain homeostasis

A precisely regulated balance between protein synthesis and degradation is important for cellular functions in almost any cell type. Nonetheless, the appearance of protein aggregates in several neurodegenerative diseases suggests a particular susceptibility of neuronal cells to imbalances in degradative pathways as, for example, the UPS. In contrast to many other cell types, neurons are considered to be post-mitotic. Therefore, neurons are dependent on accurate protein recycling for their period of (human) life. In addition, neurons are characterized by a very unique morphology with long axons and highly branched dendritic trees. The axons and dendrites again are compartmentalized in axonal boutons and dendritic spines. These morphological features together with the constant need for changes in the synaptic proteome to maintain synaptic plasticity challenges the cellular regulation of protein synthesis and degradation. Although most of the knowledge about the UPS has been made by studying other than CNS cells, the understanding of CNS specific regulation of the UPS has gained in interest, especially regarding potential therapeutic interventions [67], [68].

The role of the UPS as a negative-feedback regulator in synaptic transmission has been shown simply by blocking the proteasome with lactacystin in cultured hippocampal neurons. Proteasome inhibition resulted in 76% increase in the recycling pool of synaptic vesicles, independent of protein synthesis but dependent on neuronal activity [69]. In particular, another study demonstrated the importance of E3 ubiquitin ligase SCRAPPER to control synaptic transmission by the specific degradation of its substrate RIM1, a modulator of synaptic activity that is upregulated upon proteasome inhibition [70]. The influence of the proteasome on the composition of the postsynaptic density (PSD) has been shown in cultured hippocampal neurons. Bicucullin-induced increase in synaptic activity did not result in changes in the PSD protein intensity profile if the neurons were treated with proteasome inhibitors MG132, lactacystin or epoxomicin [71]. Furthermore, evidence suggests that proteasome-mediated degradation is essential for the establishment of late-long term potentiation (LTP), indicating an indispensable role for memory formation [72], [73]. More specifically, researchers linked the loss of function of E3 ubiquitin ligase E6-AP, encoded by a gene mutated in the neurodevelopmental disorder Angelman syndrome, with the failure to induce LTP. Interestingly, E6-AP was found to be localized in dendrites and spines and E6-AP-deficiency changed spine number and morphology [74], [75].

The compartmentalization of neurons raises the question if protein turnover that is necessary for synaptic functions is regulated remotely in the soma or by proteasomes localized in defined spaces as the synapses themselves. Indeed, by microscopic studies in hippocampal neurons using green fluorescent protein (GFP)-labeled Rpt1 (a 19S subunit), it has been demonstrated that proteasomes are recruited to synapses from dendritic shafts along actin-filaments upon KCl-induced synaptic activity [76]. It has been further found that autophosphorylated protein kinase CaMKII α is required for the activity dependent recruitment of proteasomes to dendritic spines [77].

1.3. Alzheimer's disease and dysregulations in the ubiquitin proteasome system

1.3.1 Altered proteasome networks in Alzheimer's disease

The defective ubiquitin proteasome system as a driver in Alzheimer's disease was suggested about 30 years ago when NTFs and amyloid plaques in brain tissue of AD patients have been associated with ubiquitin by immunohistochemistry [78], [79]. Interestingly, van Leeuwen et al. [80] found a mutated variant of ubiquitin (Ub⁺¹) being selectively expressed in brains of AD patients and it has been further demonstrated in vitro that the proteasome fails to degrade poly-Ub⁺¹ chains [81]. Moreover, analysis of post-mortem brain tissue revealed a reduced proteolytic activity of the proteasome in AD patients compared to healthy age matched controls. The significant reduction was detected in hippocampus but not in AD-unaffected cerebellum and was not related to overall reduction in the amount of α - and β -subunits of the proteasome [82]. This finding has been supported by early in-vitro studies that reported inhibition of proteasome activity by direct binding of A β ₄₀ peptides to purified 20S [83], [84]. Proteasome inhibition by A β ₄₀- and A β ₄₂-oligomers and -fibrils has been confirmed in lysates of human neuroblastoma cell line SH-SY5Y in addition to accumulation of Ub-conjugates and enhanced protein oxidation [85]. In APP mutant neurons it has been shown that intraneuronal A β ₄₂ impairs multivesicular body (MVB) sorting via inhibiting the UPS, a mechanism that could explain synaptic dysfunction by the failure of endocytic trafficking of neuronal receptors [86]. In contradiction to these reports, Gillardon et al. [87] found the proteasome activity being unchanged in purified 20S proteasomes isolated from AD brains but identified altered post-translational modifications as acetylation and dephosphorylation of proteasome subunits. Furthermore, a more recent study reported increased proteasome activity in glial and neuronal cultures treated with A β as well as increased expression and activity of the immunoproteasome not only in microglia derived from AD mouse brains but also in post-mortem AD brain tissue [88]. These findings not only demonstrate the existing ambiguity regarding proteasome impairment in AD but highlight the role of the immunoproteasome and glial cells in AD pathogenesis. Evidence for the immunoproteasome in AD has been provided before by a study of Mishto et al. [89] that demonstrated elevated immunoproteasome (LMP2 subunit) expression in hippocampus tissue of AD patients compared to non-demented elderly with negligible or absent expression in young individuals. Surprisingly, LMP2

expression was localized predominantly to astrocytes and neurons [89]. Nonetheless, this study detected a decrease in proteasome (tryptic-like) activity in affected regions in AD brains. Alterations in proteasome composition have been further investigated in APP/PS1 transgenic AD mouse model. While the protein expression of standard subunit $\beta 5$ was downregulated in aged AD mice, immune-subunits LMP2 ($\beta 1i$) and MECL1 ($\beta 2i$) were significantly higher expressed compared to WT [90]. They further analyzed changes in proteasome activity and found an initial decrease in chymotryptic-like activity that despite of an increase at 12 months remained lower compared to age matches WT controls. In contrast, AD mice showed an initial increase in tryptic- and caspase-like activity that dropped after 12 months to WT levels [90].

1.3.2. Altered inflammatory pathways related to the UPS in AD

The ubiquitin proteasome system is especially challenged in innate immune response by for example the accumulation of oxidant-damaged proteins. When proteasome impairment is added, cells might be confronted with a vicious cycle of inflammatory response and perturbed proteostasis networks. In diseases such as the proteasome-associated autoinflammatory syndrome (PRAAS) it has been demonstrated that mutations in proteasome subunits, leading to reduced proteolytic activity of the proteasome, result in a prominent type I IFN response [91]. Dysregulations in cytokine signaling, so called "interferonopathies", have been observed in several CNS diseases as well [92]. Recent studies by Crack and colleagues highlight the involvement of IFNs in Alzheimer's disease. Thus, elevated IFN α and IFN β mRNA levels were detected in brain tissue of AD patients and AD mice and could be induced by A β peptides in neuronal cultures [93]. This study further demonstrated that the lack of type I IFN α receptor 1 (IFNAR1) reduced A β -induced pro-inflammatory cytokines and protected the neurons from cell death [93]. In addition, it has been shown in vitro that soluble A β -induced type I IFN response is mediated by TLRs and is dependent on MyD88 and IRF7 signaling [94]. Interestingly, analysis of aged AD mice lacking IFNAR1 displayed a reduced type I IFN response, reduced levels of A β monomers with unchanged plaque load and increased astrocyte activity with reduced microgliosis. These observations were complemented by improvement of cognitive behavior in IFNAR1 deficient AD mice [95].

Moreover, as described in *chapter 1.2.3* the mTOR pathway has been shown to interact

with IFN signaling and evidence point out the involvement in neuroinflammation in Alzheimer's disease. In particular, in mutant APP cell lines and in brains of transgenic AD mice, mTOR activity and signaling has been found increased [96]. Furthermore, the reduction of p70 S6 kinase expression has been shown to improve learning in an AD mouse model [97]. Interestingly, in a very recent study of synaptosomes in presymptomatic AD mice, researchers found ROS-induced modification of Akt1 to impair Akt1-mTOR signaling and consequently result in a deficiency of protein translation [98]. Thus, alterations in mTOR signaling might be the link to cognitive impairment in AD.

1.4. Scientific aims

1.4.1. Perturbations in proteasome networks in experimental models of AD

Alzheimer's disease is characterized by neuroinflammatory events that involve the production of proinflammatory cytokines, micro- and astrogliosis as well as ROS production. Moreover, evidence suggests several alterations in the ubiquitin proteasome system including proteasome impairment, accumulation of ubiquitin and perturbations in UPS regulating signaling pathways. In this context, the immunoproteasome could play a special role in the progression of AD. Nonetheless, the literature is full of conflicting studies supporting a persistent ambiguity about perturbations in proteasome networks in AD.

We therefore aim to elucidate the contribution of soluble A β oligomers to proteasome impairment including changes in proteolytic activity, ubiquitin-conjugated proteins and the expression of immunoproteasome subunits. In addition, we aim to analyze signaling pathways involved in the UPS as IFN and mTOR signaling as well as the cross-talk with autophagy. Since we are interested in particular in the immunoproteasome in the course of AD, we aim to perform these experiments in a model for immunoproteasome deficiency (LMP7 KO) as well. Our study will focus on an ex-vivo model (organotypic brain slice culture, OBSC, treated with oligomeric A β) and include in-vivo AD mouse models (APP/PS1, in collaboration with AG Heppner).

1.4.2. Interventions in proteasome-associated signaling in an AD mouse model

Evidence in the literature suggests the contribution of immunomodulatory pathways in both the impairment of the proteasome networks and Alzheimer's disease. This offers

manifold opportunities for therapeutic interventions. Inhibition of mTOR, for example, has been shown to extend life span in several organisms and to provide anti-inflammatory effects. Rapamycin, for example, is already used as an immunosuppressant in transplantation medicine.

We thus aim to intervene with mTOR signaling using rapamycin to treat mice that exhibit AD pathology (5xFAD). We subsequently aim to analyze the effects of rapamycin on proteasome activity and plan to refer our results to changes in microglia characteristics and cognitive behavior (in collaboration with AG Priller).

2. Material and methods

2.1. Mouse models of immunoproteasome-deficiency and Alzheimer's disease

Immunoproteasome deficient mice (LMP7 KO) and APP/PS1 mice were kept under the supervision of the lab of Prof. Heppner, Neuropathology (Charité), whereas 5xFAD mice were kept under the supervision of the lab of Prof. Priller, Molecular Neuropsychiatry (Charité). Mice or dissected tissue were provided in research collaboration of mutual projects within the CRG "Elucidating the proteostasis network to control Alzheimer's disease" of the Berlin Institute of Health (BIH).

LMP7 knock out (KO) mice lack exon 1 to 5 of the Psmb8 gene, encoding for the first 247 to 276 amino acids of the LMP7 protein, and thus lack one of the catalytic β subunits of the immunoproteasome [54]. To generate effectively littermate pups for organotypic brain slice culture, homozygous wild type and LMP7 KO mice from heterozygous breeding were mated. Pups thrown from these breeding were used at postnatal day 3 – 6 (P3-6).

APP/PS1 mice harbor the Swedish APP mutation KM670/671NL in conjunction with the presenilin 1 mutation L166P [99]. APP/PS1 mice were crossed to LMP7 KO mice, to generate immunoproteasome deficient APP/PS1 mice.

C57BL/6N mice (wildtype control for 5xFAD mice) were purchased from Janvier Labs and 5xFAD transgenic mice from The Jackson Laboratory. The 5xFAD mouse model [100] harbors the human APP and PSEN1 genes co-expressing five familial Alzheimer's diseases (FAD) mutations [APP K670N/M671L (Swedish) + I716V (Florida) + V717I (London) and PS1 M146LL286V].

Mice were group housed under pathogen-free conditions on a 12 h light/dark cycle and food and water were provided to the mice *ad libidum*. All animal experiments were performed in accordance with the national animal protection guidelines approved by the regional offices for health and social services in Berlin (LaGeSo).

2.1.1. Genotyping

Ear biopsies from LMP7 KO mouse line were incubated in lysis buffer (100 mM Tris pH 7.5, 200 mM NaCl, 5 mM EDTA pH 8, 0.2 % SDS and 100 μ g/mL Proteinase K [Sigma Aldrich]) at 55°C overnight. The next day, the samples were centrifuged at 13 000 rpm at 4°C for 15 min and the supernatant collected in a fresh tube. Equal amounts of

Isopropanol was added and the tube inverted several times. Next, the samples were centrifuged at 13 000 rpm at 4°C for 20 min and the supernatant carefully removed. The remaining pellet was washed by adding 75% ethanol and centrifugation at 13 000 rpm at 4°C for 10 min. The ethanol was removed and the pellet dried under a hood. The pellet was resuspended in DNase free H₂O and DNA concentration measured using the NanoDrop. For amplification 0.5 – 2 µl DNA (~300 ng) was added to 24 µl PCR reaction mixture containing 0.2 µl AmpliTaq DNA Polymerase (250 Units, ABI), 2.5 µl GeneAmp® 10X PCR Buffer I (ABI), 1 µl of each primer (Table 1), 0.5 µl dNTP's 10 mM and DNase free H₂O water. Polymerase chain reaction (PCR) was performed in a Thermocycler using the conditions depicted in Table 2. Sample buffer (50% glycerol, 50 mM EDTA pH 8, 0.25 % Xylencyanol) was added to the PCR products that were then separated in agarose gel electrophoresis using 1% agarose gel in TAE-buffer (Tris, acetic acid, EDTA pH 8) and Gel Red at 120 V. DNA bands were visualized using ultraviolet (UV) light.

The genotyping of APP/PS1 and 5xFAD mice was performed in the lab of Prof. Heppner and Prof. Priller, respectively.

Table 1: Primer sequences for LMP7 genotyping.

Primer	Sequence	PCR products	
LMP7 wt forward	GGA CCA GGA CTT TAC TAC GTA GAT G	wildtype	600 bp
LMP7 wt reverse	CTT GTA CAG CAG GTC ACT GAC ATC G		
LMP7 neo	CCG ACG GCG AGG ATC TCG TCG TGA	KO	700 bp

Table 2: PCR conditions for LMP7 genotyping.

PCR protocol		
Temperature	Time	
94°C	7 min	
94°C	45 s	cycle 35x
63°C	45 s	
72°C	1 min 10 s	
72°C	7 min	
8°C	hold/store	

2.1.2. Brain tissue sampling

Brain samples from APP/PS1 and APP/PS1xLMP7 KO mice were prepared in and provided by Neuropathology lab (Prof. Frank Heppner). Brain samples from 5xFAD mice were prepared in and provided by Molecular Neuropsychiatry lab (Prof. Josef Priller). Therefore, animals were euthanized and transcardially perfused with 1x phosphate buffered saline (PBS). Brains were carefully removed and snap-frozen in liquid nitrogen for brain homogenization and subsequent proteasome activity analysis.

2.2. Organotypic brain slice culture (OBSC)

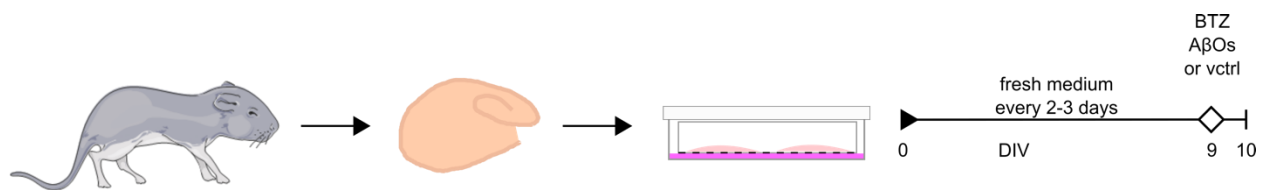


Figure 4: Experimental setup for organotypic brain slice culture.

The pup was anesthetized, decapitated and the brain quickly dissected. The brain was further separated in hemispheres that were cut into sagittal slices using a vibratome. Slices were placed in a membrane insert on culture medium and cultured for up to 10 days. Medium was replaced every 2-3 days and vitality of slices were checked macroscopically or by light microscopy.

OBSC was prepared from postnatal 3–6-day-old mice pups according to the regulations of animal care and protection. Pups were anesthetized by isoflurane and sacrificed by decapitation. Brains were then rapidly dissected and separated in hemispheres. The cut side was glued to the metal block of the vibratome (Leica VT1200S), which was then placed in cold Hank's balanced salt solution (HBSS, Gibco) supplemented with 1% penicillin/streptomycin (P/S, Pan Biotech), 0.6% glucose (Fluka), and 20 mM HEPES (Sigma-Aldrich), purged with Carbogen for dissection in sagittal slices of 300 μm . The cerebellum was removed using a razor blade. Slices were collected and placed onto membrane inserts (Millicell, 0.45 μm ; Merck Millipore) in six-well plates containing 1 ml of minimum essential medium Eagle (Gibco) supplemented with 25% horse serum (Gibco), 20.7% HBSS, 1% P/S, 0.6% glucose, and 2% B27 (Gibco). Two slices per insert were cultivated at 35°C and 5% CO₂ for minimum 8 days before starting the treatments. Medium was replaced every other day, and slice cultures were observed regularly using light microscopy. OBSCs were treated with either 0.5 – 5 μM A β Os (see chapter 1.3.) or 250 nM Bortezomib (BTZ) for 1 - 24 hrs. BTZ (Velcade) in 0.9% NaCl

solution was provided by Charité Apotheke, aliquoted and stored at -20°C until usage.

2.2.1. Neural dissociation and microglia separation (MACS)

Microglia were isolated from OBSCs using the Neural Dissociation Kit (P), gentleMACS Dissociator and CD11b (Microglia) microbeads from Milteny Biotec according to manufacturer's protocol. At least 20 slices per treatment were scratched from the membrane inserts to 1 mL HBSS (without Ca²⁺ and Mg²⁺, Sigma). For every sample 50 µl enzyme P and 1900 µL buffer X were pre-warmed at 37°C in a gentleMACS C tube for 15 min. Slices in HBSS were added to the enzyme mix in C tube and attached upside down onto the sleeve of the gentleMACS dissociator to run program m_brain_01. Subsequently, the sample was incubated rotating at 37°C for 15 min followed by running program m_brain_02 on the gentleMACS. For every sample 10 µL enzyme A and 20 µL buffer Y was added and the tube gently mixed by inverting. In the following the sample was incubated rotating at 37°C for 10 min, processed on gentleMACS running program m_brain_03 and again incubated rotating at 37°C for 10 min. Then the sample was collected on the bottom of the tube by brief centrifugation and transferred on moistened cell strainer (70µm) placed on a fresh 50 mL tube. The strainer was rinsed with 10 mL HBSS (with Ca²⁺ and Mg²⁺, Sigma) and the cell suspension centrifuged at 300xg for 10 min at room temperature (RT). The supernatant was removed completely and the cell pellet collected in 1 mL 1x PBS (pH 7.5) with 0.5% bovine serum albumin (BSA).

To isolate microglia from OBSC cell suspension, the suspension was centrifuged 300xg for 10 min at RT and the pellet collected in 90 µL 1xPBS/0.5%BSA (buffer). 10 µL of CD11b microbeads were added to the cell suspension mixed well by flicking the tube and incubated in the fridge for 15 min. Afterwards, 1 mL buffer was added and the cell suspension centrifuged at 300xg for 10 min at RT. The supernatant was removed and the cell pellet resuspended in 500 µl buffer. LS columns were placed in a magnetic separator and prepared with 3 mL buffer before applying the cell suspension. The flow through was collected and the column washed 3x with 3 mL buffer. The flow through was collected and combined with the flow through from step 1. The column was removed from the magnetic separator and placed on a collection tube. Finally, the CD11b-labeled cells were washed from the column by adding buffer and immediately pushing the plunger into the column. The cells from the flow through and the isolated

microglia were pelleted by centrifugation at 300xg for 10 min at RT and snap frozen in liquid nitrogen (N_{2(l)}) and stored at -80°C until analysis.

2.3. Preparation of amyloid- β oligomers (A β O_s)

Oligomeric amyloid- β was prepared according to Klein et al. ([101], see also [102] and <http://www.kleinlab.org/brochure.pdf>). In-house generated amyloid- β peptide 1-42 (A β ₄₂, Petra Henklein; Head of peptide synthesis facility, Inst. of Biochemistry, Charité) was dissolved in ice-cold 1,1,1,3,3,3-Hexafluoro-2-propanol (HFIP, Fluka Analytical) to a ratio of 2.5 mg peptide/1 mL HFIP. The peptide/HFIP mix was then incubated for 1 hour (h) at room temperature (RT) followed by 1 hour incubation on ice for monomerization. The monomerized A β ₄₂ was further aliquoted in low-bind Eppendorf tubes á 125 μ g and HFIP was evaporated overnight. Residual HFIP was eliminated using a Speedvac for 10 min. The resulting peptide film was then stored at -80°C. To generate oligomeric A β , the peptide film was solved in 5.5 μ L dimethyl sulfoxid (DMSO, Applichem) thoroughly and further diluted in phenol-red free Dulbecco's Modified Eagle Medium Nutrient Mixture F-12 (DMEM/F12, (+) L Glutamin, Gibco) to reach an A β concentration of approximately 100 μ M. For the analysis in confocal microscopy, 6 μ g tetramethylrhodamine (TAMRA)-labeled A β 42 (AnaSpec) dissolved in DMSO was added to the DMSO-solved A β prior to the dilution in DMEM/F12 to reach a fraction of 5% TAMRA-A β . After 16 h of oligomer formation in the cold room at 4 °C the peptide solution was centrifuged at 14 000 g for 15 min at 4 °C to remove fibrillary A β . The effective peptide concentration in the supernatant was determined using the bicinchoninic acid (BCA) protein assay Kit (Thermo Fisher) and 0.5, 2 and 5 μ M A β O_s were used for treatments.

2.3.1. Blue native PAGE

A β O preparation of different A β 42 peptide batches was validated using blue native polyacrylamide gelelectrophoresis (BN PAGE) and western blot with A β specific antibody 6E10. BN PAGE was performed using the NativePAGE Novex® Bis-Tris gel system (Invitrogen) according to the manufacturer's protocol. NativePAGE™ Sample Buffer (4X) was added to 25 μ l of the A β O preparation and loaded to a 4-16% Bis Tris gel. BN PAGE was performed at 150 V for 1 h and 250 V for several hours in the cold room until the blue front ran out. Afterwards, the gel was blotted on polyvinylidene difluoride (PVDF) membrane (Immobilon-P 0.45 μ m, Millipore) for 1.5 h in the cold room

using the wet tank system (Bio-Rad). The membrane was then blocked in 1x Roti-Block (Roth) for at least 1 h and incubated in 6E10 antibody (BioLegend, 1:3000) shaking over night at 4°C. The next day, after washing 3x for 10 min in 1x Tris-buffered saline/0.02%Tween20 (TBST) the membrane was incubated shaking in anti-mouse peroxidase labeled secondary antibody for 45 min at RT. The membrane was then washed 3x for 10 min in TBST before performing the detection using Clarity enhanced chemiluminescence (ECL) western blotting substrate (BioRad) according to manufacturer's protocol.

2.4. Assessment of proteasome activity

To measure the proteasome activity, lysates of the OBSC or adult mouse brain samples were prepared under native conditions on ice. Therefore, two slices of tissue samples were homogenized in native lysis buffer (10 mM Tris pH 7.5 at 4°C, 10 mM NaCl, 25 mM KCl, 1.1 mM MgCl, 0.1 mM EDTA pH 8, 2 mM Adenosintriphosphat [ATP], 1 mM Dithiothreitol [DTT], 10% glycerin) followed by 6 freeze-thaw cycles in N₂(l). Then, the lysates were centrifuged at 13 000 rpm at 4°C for 60 min and the supernatant collected in a fresh tube. The protein concentration was determined using the BCA protein assay Kit (Thermo Fisher).

2.4.1. Fluorogenic substrate based assay

Prior to assessment of chymotrypsin-like activity, 10 µg of the native lysate was incubated with 1 µM epoxomicin or DMSO, respectively, in assay buffer (50 mM Tris pH 7.5 at 37°C, 5 mM MgCl, 1 mM ATP, 1 mM DTT) for 10 min at 37°C and then transferred to a black 96 well plate (in triplicate). Subsequently, 100 µl of 50 µM fluorogenic substrate (Suc-Leu-Leu-Val-Tyr(LLVY)-7-amino-4-methycoumarin(AMC), Bachem) in assay buffer was added per well and the plate incubated with a lid at 37°C. Cleaved fluorescent AMC was measured using a plate reader (extinction 380 nm and emission at 440 nm). Remaining activity in lysates incubated with epoxomicin were considered to be of other proteases and was subtracted from DMSO incubated lysates.

2.4.2. Active site probes

To assess the availability of active sites within the proteasome, 25 µg of the native lysate was incubated with 2 µM of pan reactive active site probe (pan-ASP) Me4-BodipyFLAhx3Leu3VS (provided by Huib Ovaa, University Leiden) or ASP mix (β1c-

and β 1i-reactive Cy5-NC-001, β 2c- and β 2i-reactive BODIPY(FL)-LU-112 and β 5c and β 5i-reactive BODIPY(TMR)-NC-005-VS, provided by Herman Overkleeft, University Leiden) in assay buffer for 1 hour at 37°C. Afterwards, 3x Lämmli sample buffer (0.35 M Tris pH 6.8, 10% sodium dodecyl sulfate (SDS) (w/v), 9.3 % DTT (w/v), 30% glycerol (v/v), Bromphenol blue) was added to the lysate-probe-mix and heated at 95°C for 5 min. The samples were then loaded completely to a 18% SDS polyacrylamide gel and the electrophoresis was run in electrophoresis buffer (25 mM Tris, 0.2 M glycine, 0.1% SDS) for 20 min at 80V and then for several hours at 120-150V. The labeled proteasome subunits were detected in-gel in Fusion FX Spectra (Vilber) using the settings GFP for Bodipy-FL, Cy3 for Bodipy-TMR and Cy5. For normalization, the gel was then stained overnight shaking in a sensitive coomassie solution (150 mM $\text{Al}_2(\text{SO}_4)_3 \cdot \text{H}_2\text{O}$, 10% ethanol, 0.02% Coomassie Brilliant Blue, 2% ortho H_3PO_4) and scanned.

2.5. Analysis of protein expression and ubiquitination

2.5.1. Protein extraction

Two slices from OBSC or the cell pellets after subsequent magnetic activated cell sorting (MACS) were homogenized in lysis buffer (50 mM Tris pH 7.5, 150 mM NaCl, 1% NP40, 0.1% SDS, 1x cOmplete [ULTRA, Mini, EDTA-free, EASYpack, Roche], 1x phosStop [EASYpack Roche], 20 mM N-ethylmaleimide, 10 μ M MG132 and 0.5 % sodium deoxycholate) and incubated on ice for 1 hour. The lysates were then centrifuged at 13000 rpm at 4°C for 1 hour and the supernatant was transferred to a fresh tube. The protein concentration in the supernatant was determined using the BCA protein assay Kit (Thermo Fisher).

2.5.2. Analysis of protein expression by western blot

For immunodetection of proteins, 20 μ g of protein was heated 1x Lämmli SDS sample buffer for 5 min at 95°C and loaded to SDS polyacrylamide gels that were run in electrophoresis buffer at 80 V for 20 min and 120-150 V until the blue front ran out of the gel. Each gel was run with PageRuler Prestained Protein Ladder (Thermo Scientific) as a reference. The gel was then blotted semi-dry in 1x semi-dry blot buffer (electrophoresis buffer supplemented with 10% methanol) on PVDF membrane. After blotting, the membranes were stained for total protein using an amidoblack staining solution (0.1% amidoblack, 10% acetic acid, 45% methanol) and photographed for

normalization calculations.

2.5.3. Analysis of ubiquitinated proteins by dot blot

For immunodetection of poly-ubiquitinated proteins in particular, 10 µg of protein from the lysis supernatant was heated in 1x Lämmli sample buffer for 5 min at 95°C. The remaining pellet after lysis was resuspended in equal amounts (to homogenization volume) of 1x Lämmli sample buffer and heated for 5 min at 95°C as well. Supernatant and pellet was loaded in duplicates using a BioDot Microfiltration apparatus (BioRad) onto 1x TBS equilibrated 0.2 µm nitrocellulose membrane (Amersham Protran, GE Healthcare). The membrane was washed once with 1xTBS and stained for total protein using an amidoblack staining solution and photographed for normalization calculations.

2.5.4. Immunodetection

The membranes were blocked in 5 % non-fat dry milk in TBST or 1x RotiBlock at least for 1 hour at RT prior to incubation with the primary antibody (Table 3). The membrane was washed in TBST 3x for 10 min before and after incubation with the respective horse radish peroxidase (HRP)-conjugated secondary antibody (Table 3). Protein detection was performed using Clarity ECL western blotting substrate (BioRad) according to manufacturer's protocol and the Fusion-FX7 Spectra (Vilber) gel documentation system.

Table 3: Antibodies used for immunodetection in western or dot blot.

Antibody	Provider	Host	Dilution
anti-rabbit IgG peroxidase conjugated	Calbiochem Cat#401393	goat	1: 10000
anti-mouse IgG peroxidase conjugated	Calbiochem Cat#402335	goat	1: 10000
anti-poly-Ubiquitin	Dako Z0458	rabbit	1:5000- 1:10000
Anti-LMP7 K63	In-house	rabbit	1:10000
anti-p70 S6 kinase (49D7)	Cell Signaling L708P	rabbit	1:1000

anti-phospho-p70 S6 kinase (Thr389)	Cell Signaling 9234P	rabbit	1:1000
anti-S6 ribosomal protein (5G10)	Cell Signaling 2217S	rabbit	1:4000
anti-phospho-S6 ribosomal protein (Ser235/236)	Cell Signaling 2211S	rabbit	1:3000
anti-STAT1	Cell Signaling 9172S	rabbit	1:2000
Anti-phospho-STAT1 (Y701) 58D6	Cell Signaling 9167S	rabbit	1:1000
LC3b	Cell Signaling 27755	rabbit	1:1000

2.6. Immunofluorescent stainings and confocal microscopy

After treatment with either A β O_s or vehicle controls, organotypic brain slices were incubated with 500 nM pan reactive proteasome probe in the cell culture incubator at 35°C for 1 hour. In a 24 well plate, slices were subsequently fixed in cold 4% paraformaldehyde shaking for 20 min at RT, washed in 1x PBS/1% Triton-X for 20 min and incubated in blocking solution (10% normal goat serum (NGS), 0.3% Triton-X in 1x PBS [PBT]) shaking for 2 hrs at RT. Slices were then incubated in primary antibody diluted 1:500 in PBT/5% NGS for 48 hrs shaking in the cold room. Further, slices were washed twice for 30 min at RT and followed by overnight shaking in the cold room in PBT. The next day, slices were washed again twice for 30 min at RT in PBT followed by incubation in secondary antibody diluted 1:500 in PBT/5% NGS for 24 hrs shaking in the cold room. The following day, slices were washed 6x for 30 min in PBT at RT. PBT was replaced by MilliQ H₂O and immediately replaced by autofluorescence reduction solution (100 mM CuSO₄/50mM CH₃COONH₄). After 1 hour of incubation the solution was replaced by MilliQ H₂O and then by 1x PBS. Finally, slices were mounted in Fluoromount (aqueous, Sigma Aldrich) using the bridging technique. Thereby, two cover slips were glued onto the microscope slide, the slice in mounting medium placed between and covered by the final cover slip (#1.5). After resting for an hour, the edges were sealed using transparent gel nail polish.

Table 4: Antibodies for immunofluorescence stainings in organotypic brain slices.

Antibody	Provider	Host
Anti-MAP2	SynSys Cat no. 188004	guniea pig
Anti-Iba1	Wako Cat no. 019-19741	rabbit
Anti-GFAP	Dako Z0334	rabbit
Anti-guinea-pig-Alexa Fluor 405	Abcam, Ab175678	goat
Anti-rabbit-Alexa Fluor 633	Invitrogen, A21071	goat

Immunostained slices were further imaged using the Nikon A1r+ confocal microscope setup (AMBIO facility, Charité). First the hippocampal region of interest was examined using a 20x objective before magnification was increased by using a 60x water immersion (WI) objective. Z-stacks were obtained with 0.1 μm step size. Images were further processed in Image J. For quantification of pan proteasome probe signals the total intensity (applied on SUM stacks) was measured in defined areas (identical for every image analyzed) within the stratum pyramidale and stratum radiatum. Iba1+ microglia and GFAP+ astrocytes were counted using the “analyze particle” function (applied on SUM stacks). Thresholds were set equally for every image analyzed.

2.7. Analysis of mRNA expression

2.7.1. RNA extraction

Two organotypic brain slices were homogenized in 1 mL of TRIzol Reagent (Thermo Fisher) and incubated for 5 min at RT. Then 200 μl chloroform was added, the TRIzol-chloroform mix was vortexed for 10 sec and incubated for further 3 min at RT. Afterwards, the mix was centrifuged for 30 min at 13000 rpm at 4°C. The upper aqueous phase containing the RNA was removed carefully and transferred to a fresh tube without touching the interphase or the lower phenol-chloroform phase. The RNA was precipitated by adding 500 μl 2-propanol and incubating overnight at -20°C. The next day, the RNA was pelleted by centrifugation at 13000 rpm and 4°C for 30 min. The 2-propanol was removed completely and the pellet washed in 75% ethanol by centrifugation at 13000 rpm and 4°C for 20 min. The RNA pellet was dried under the lab hood, resuspended in Rnase-free H₂O and stored at -80°C.

2.7.2. cDNA synthesis

Prior to performing complementary DNA (cDNA) synthesis the RNA was incubated with TURBO DNase for 20 min at 37°C, followed by incubation with DNase inactivation reagent for 5 min at RT (TURBO DNA-free Kit, Thermo Fisher) to remove any genomic DNA. The remaining mRNA was transcribed using the PrimeScript First Strand cDNA Synthesis Kit (Takara) according to manufacturer's protocol. To reach a final cDNA concentration of 50 ng/μl, 1000 ng RNA was diluted in RNase-free H₂O up to a volume of 10 μl and added by 10 μl of cDNA synthesis mastermix (Table 5). The cDNA synthesis was performed at 37°C for 15 min followed by 85°C for 5 min in a Thermocycler. For every sample a no reverse-transcriptase (RT) control was performed (RNA plus master mix but excluding RT).

Table 5: cDNA synthesis master mix.

1x Mastermix	μl
5x prime script Buffer	4
Prime script RT Enzyme Mix I	1
oligo dT Primer (50 μM)	1
Random 6mers (100 μM)	4
total	10

2.7.3. Pre-amplification

To amplify the low amount transcripts *Ifna1* and *Ifnb1*, a fraction of the cDNA was pre-amplified using the TaqMan™ PreAmp Master Mix (Applied Biosystems) according to manufacturer's protocol. Therefore, *Ifna1*, *Ifb1* and *Hprt* were diluted 1:100 in 1x Tris-EDTA (TE) buffer (RNase-free, Thermo Fisher) to generate a 0.2x PreAmp pool. 250 ng cDNA in RNase-free H₂O was added to 1x PreAmp Master Mix and 0.05x PreAmp pool. Pre-amplification was performed in a Thermocycler according to the program depicted in Table 6. For qRT-PCR 1 μl of pre-amplified cDNA applied.

Table 6: Pre-amplification protocol.

temperature	time	
95°C	10 min	
95°C	15sec	cycle
60°C	4 min	
4°C	infinite	

2.7.4. Quantitative real-time PCR

Quantitative real-time PCR was performed based on Taqman PCR reagents and Taqman primer assays (Applied Biosystems). For each target gene the master mix was prepared (Table 8). Hprt served as housekeeping gene. For each sample 1 µl of cDNA or pre-amplified cDNA was added to 9 µl of respective master mix. PCR reaction was performed in technical duplicates according to the program depicted in

Table 9 using the Rotor Gene RG-3000 Real-Time machine (Corbett). In every run a H₂O negative control, non-template control and a RT control sample was included. Threshold was set equally for every sample.

The relative gene expression of a specific target gene was calculated as follows:

$$\Delta C_t (\text{cycle threshold}) = C_{t,\text{gene target}} - C_{t,\text{housekeeping gene}}$$

$$\text{Relative gene expression (RE)} = 2^{(-\Delta C_t)}$$

Table 7: Taqman primer assays.

Gene target	Assay number
Hprt (housekeeping gene)	Mm01545399_m1
Ifna2	Mm00833961_s1
Ifnb1	Mm00439546_s1
Isg15	Mm01705338_s1
Mx1	Mm01218004_m1
Cxcl-10	Mm00445235_m1

Psmb8	Mm00440207_m1
Psmb9	Mm00479004_m1
Psmb10	Mm00479052_g1
Cd11b	Mm00434455_m1
NeuN	Mm01248771_m1
Gfap	Mm01253033_m1

Table 8: Quantitative real-time PCR master mix.

1x master mix	μl
PCR H2O	3.5
TaqMan Universal PCR MasterMix 2x	5
Taqman assay	0,5
total	9

Table 9: Quantitative real-time PCR program.

temperature	time	
95°C	10 min	
95°C	15 sec	45 x
60°C	1min	

2.8. Statistics

Statistical analyses were performed using the GraphPad Prism 6 Software. Differences between two groups were evaluated by student's t-test. Data are represented as means \pm SEM. Statistical significance is indicated as follows: * $p < 0.05$, ** $p < 0.01$ and *** $p < 0.001$.

3. Results

3.1. Perturbations of proteasome networks in Alzheimer`s disease

The knowledge about the effects of A β on the ubiquitin proteasome system is limited and ambiguous. Whereas initial studies have shown an inhibitory effect of A β on the UPS [82]–[84], [86], recent findings suggest an activation of the proteasome in models of Alzheimer`s disease [87], [88]. In both studies, the involvement of the immunoproteasome gains in importance. In addition, in earlier studies we found that the immunoproteasome with its higher proteolytic capacity compensates increased proteotoxic stress under inflammatory conditions [47], [48]. For that reason, we aim to elucidate the impact of A β oligomers (A β O) in organotypic brain slice cultures (OBSCs) derived from wild type (WT) pups as well as those deficient for the immunoproteasome (LMP7 KO). Furthermore, we aim to analyze APP/PS1 (Alzheimer) mice with respect to the immunoproteasome.

3.1.1. Characterization of amyloid- β oligomer preparation

According to several studies in the past demonstrating that oligomeric amyloid- β plays a major role in the development of Alzheimer`s disease [8], [20], [103], we decided to use an A β O preparation to study the effects on proteasome networks in OBSCs. In the course of the study different batches of A β ₁₋₄₂ were monomerized in HFIP and regularly characterized by BN PAGE and western blot. The analysis of A β O preparations from four distinct A β ₁₋₄₂ batches that were used in a time period of 2.5 years showed the major proportion of protein smear above a protein size of 242 kDa. This pattern could be reproduced in all of the A β ₁₋₄₂ batches used for the following treatments of OBSCs (Figure 5A). From this analysis we describe the A β O preparations used in the following experiments as a heterogeneous mixture of high molecular weight oligomeric A β . In addition, to visualize the uptake of A β O applied to the medium, TMR-labeled A β O was generated and used to treat OBSCs. These TMR-A β O treated slices were further processed for immunofluorescence confocal microscopy. Imaging clearly showed assemblies of TMR-labeled A β (magenta) in the hippocampus of treated OBSCs (Figure 5B). Presumably, these A β assemblies were located extracellularly. However, conclusions about even smaller A β assemblies located intracellularly cannot be drawn by this data.

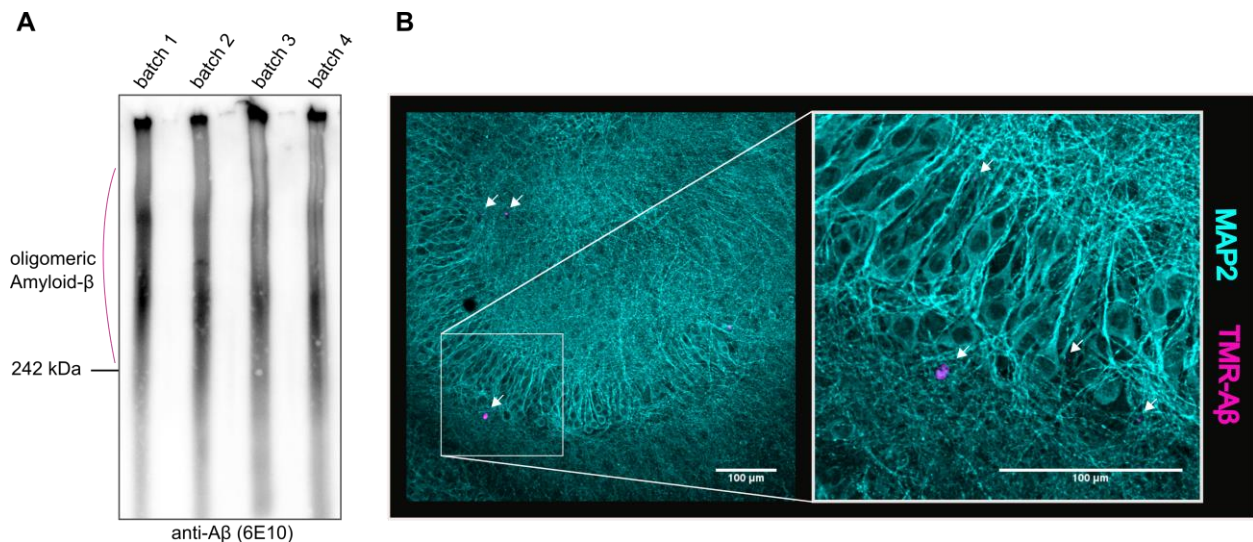


Figure 5: Characterization of A β O preparation.

A 25 μ l of each A β O preparation derived from 4 distinct A β_{1-42} batches were separated in a 4-16% Bis Tris gel followed by wet transfer on PVDF membrane. A β species were detected on the membrane using anti-A β antibody 6E10. A characteristic smear of A β protein aggregates of different sizes could be detected. **B** OBSCs treated with TMR A β O were subsequently stained with anti-MAP2 antibody and 405-secondary antibody to visualize neurons. Hippocampal regions of the slices were imaged with Nikon A1r+ confocal microscope setup and 20x (left) and 60x water immersion (WI, right) objectives. White arrows mark visible TMR A β O within the hippocampus.

3.1.2. A β O-induced decrease of active proteasome subunits is abolished by immunoproteasome deficiency

To analyze the effect of A β O on proteasome activity we decided to visualize the active sites β 1, β 2 and β 5 as well as the corresponding immunoproteasome subunits β 1i, β 2i and β 5i using a fluorescently labeled pan reactive proteasome inhibitor. Thereby, in WT OBSCs we could show that treatment with A β O decreases the amount of active β subunits already after 4 hrs of treatment and resulted in a significant decrease of 48 % after 24 hrs. In contrast, in OBSCs deficient for the immunoproteasome the treatment with A β O either resulted in an increase or no change of active β subunits (Figure 6AB). Whether this difference is due to a lower initial activity of the proteasome in LMP7 KO slices was analyzed by comparing the amount of active β subunits in vehicle controls of WT and LMP7 KO samples. Indeed, the basal level of active β subunits is significantly lower in immunoproteasome deficient OBSCs compared to wild type (Figure 6C), which is in agreement with our recent findings in adult LMP7 KO mouse brains [104].

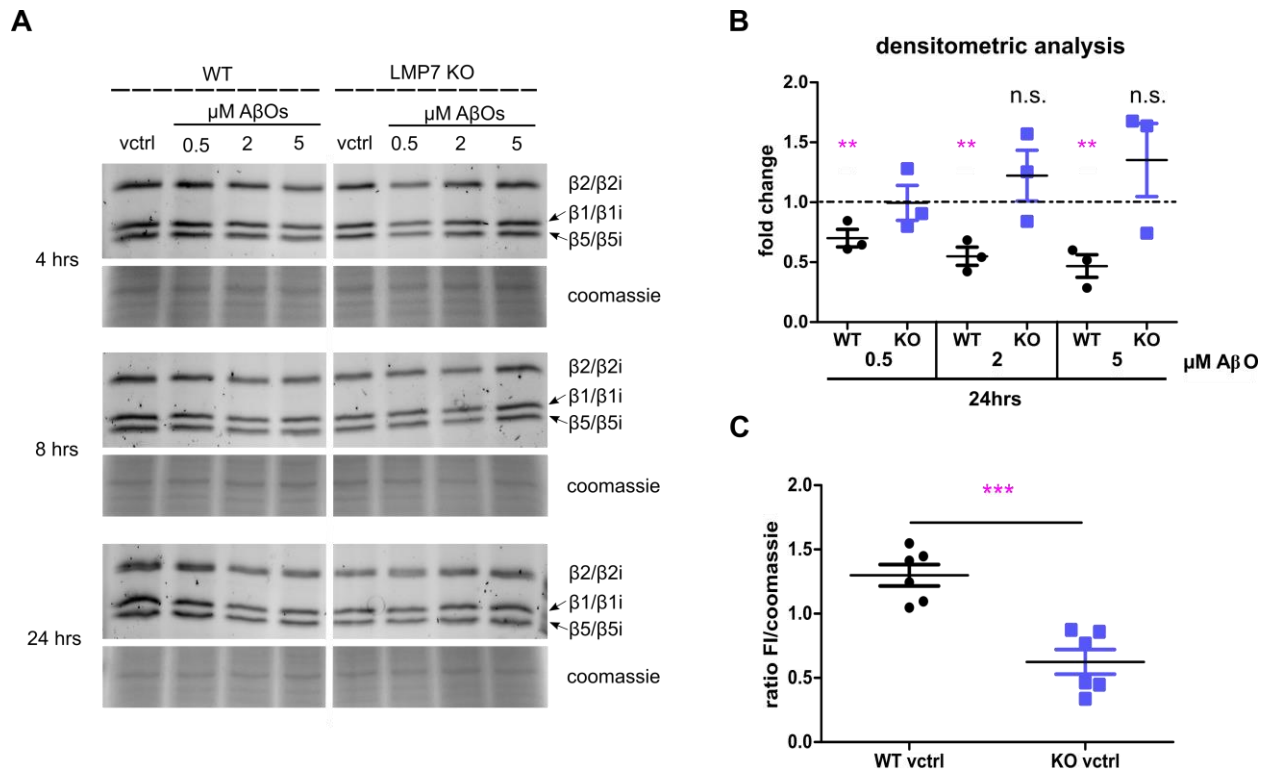


Figure 6: Concentration depended decrease of active subunits upon AβO treatment.

A Representative image of proteasome subunit activity using pan-reactive proteasome probe in native lysates of WT and LMP7 KO OBSCs treated with 0.5 – 5 μM AβOs or vehicle control. Coomassie staining served as protein loading control. **B** Corresponding densitometric analysis of 24 hrs time point (normalized to coomassie staining). Fold change was calculated to WT or LMP7 KO vctrl. **C** The fluorescence intensity (FI) of pan reactive proteasome probe normalized to coomassie of WT compared to LMP7 KO vehicle controls. Values represent mean with SEM (** p < 0.005, ***p<0.001, student-t test).

In order to differentially analyze the effect of AβOs on specific proteasome β subunits, we used a fluorescently labeled proteasome inhibitor mix with inhibitors specifically binding to β1/β1i and β5/β5i. The results showed that the decrease in active β subunits in WT OBSCs induced by AβO treatment is restricted to β1 subunits. Here, in WT we detected a decrease of 48% (2 μM AβO) up to 55% (5 μM AβO) of active β1 subunits after 24 hrs of treatment. In LMP7 KO, however, no changes in β1 or β5 could be detected, confirming the results above obtained with the pan reactive proteasome probe (Figure 7).

In summary, this data showed inhibitory effects of AβOs on proteasome activity in wild type OBSCs but no effects in those deficient for the immunoproteasome. Furthermore, we were able to show a specific effect on β1 subunits in the case of WT OBSCs. Nonetheless, using the fluorescent probes labeling active proteasome subunits we were not able to differentiate between standard and immuno subunits. This is possibly due to the very similar protein size of the β subunits and limits in resolution using SDS-PAGE.

Finally, we decided to focus on the A β O concentration of 5 μ M for further experiments since it lead to the highest inhibitory effect on β subunits.

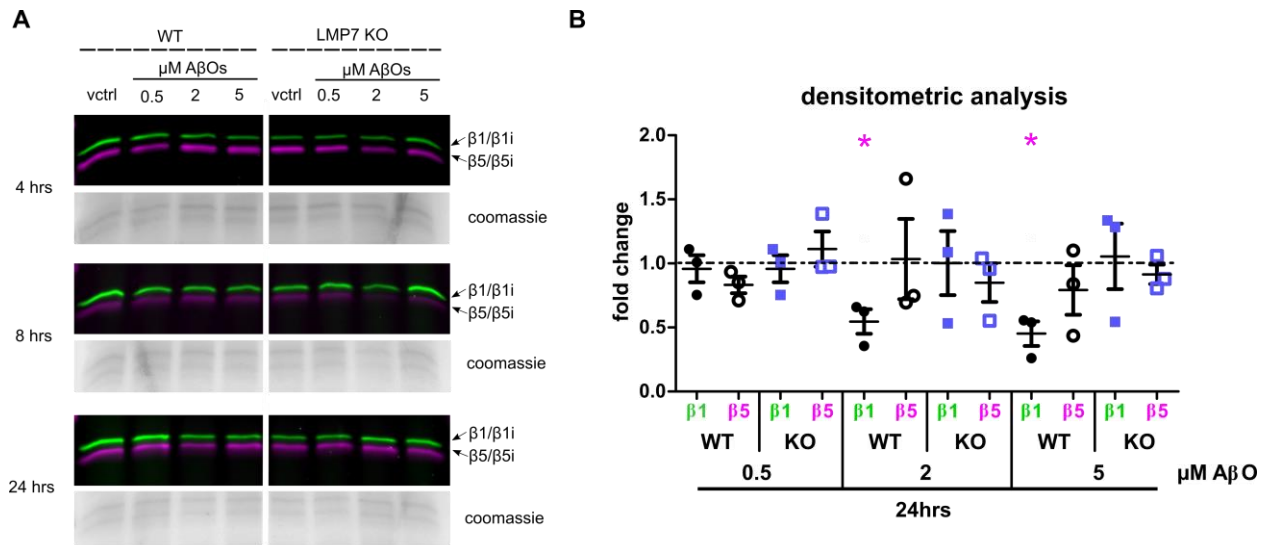


Figure 7: A β O-induced decrease of active β 1 subunits in WT OBSCs.

A Representative image of specific β 1/ β 1i (green) and β 5/ β 5i (magenta) subunit activity using a proteasome probe mix in native lysates of WT and LMP7 KO OBSCs treated with 0.5 – 5 μ M A β O or vehicle control. Coomassie staining served as protein loading control. **B** Corresponding densitometric analysis of 24 hrs time point (normalized to coomassie staining). Fold change was calculated to WT or LMP7 KO vctrl, respectively. Values represent mean with SEM (* $p < 0.05$, student-t test).

3.1.3. Proteasome impairment results in the accumulation of Ub-conjugates, immunoproteasome formation and a Type-I IFN response

Previous studies have shown that conditions that challenge the ubiquitin proteasome system (e.g. exposure to interferons) lead to the formation of the specialized isoform immunoproteasome and a transient accumulation of poly-ubiquitinated proteins [47], [48], [105]. Since we demonstrated an inhibitory effect of A β O on WT organotypic brain slices, we hypothesize that in response to A β O ubiquitinated proteins will accumulate, which in turn induce the formation of the immunoproteasome, accompanied by a Type-I IFN response. To verify the accumulation of ubiquitin-conjugated proteins (Ub-conjugates) by chemical inhibition of the proteasome, protein lysates and insoluble pellets of Bortezomib (BTZ)-treated OBSCs were analyzed in dot blot. Whereas Ub-conjugates of the soluble fraction (supernatant) started to accumulate at 4 hrs of BTZ treatment, those in the insoluble fraction (pellet) first accumulated at 24 hrs with significant amounts (3 fold increase, Figure 8A). Following this, we analyzed Ub-conjugate levels in OBSCs treated with A β O. Whereas in both, WT and LMP7 KO, the soluble Ub-protein levels in the supernatant were slightly decreased initially only in WT

the levels rose again after 24 hrs (42% towards vehicle control). After 24 hrs of A β O exposure, when proteasome inhibition was highest in WT, the levels of insoluble Ub-conjugates were increased by 30%. In contrast, in immunoproteasome deficient OBSCs

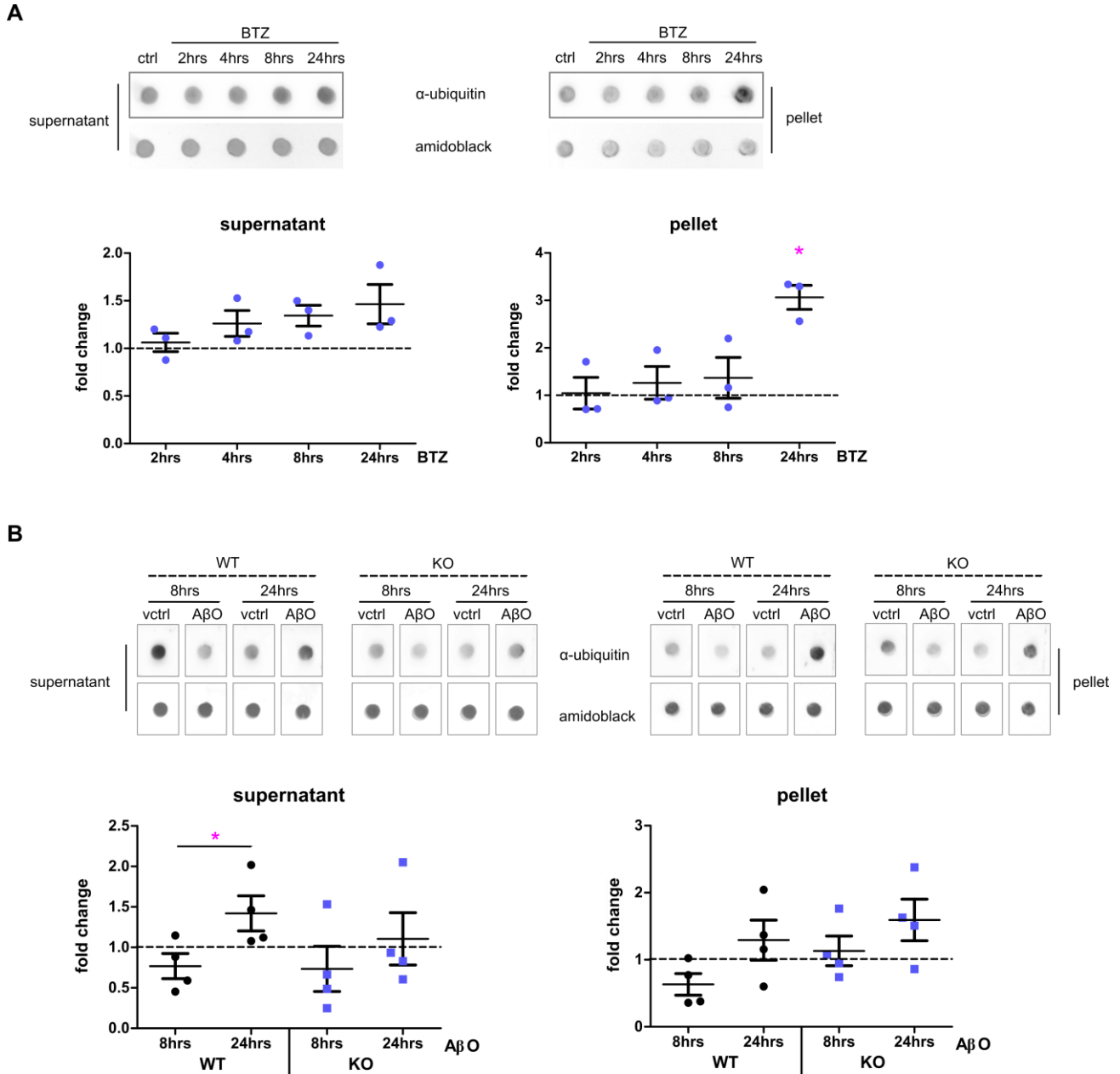


Figure 8: Proteasome inhibition by Bortezomib results in higher insoluble Ubiquitin positive fraction.

A Upper panel: Dot blot analysis of ubiquitinated proteins in RIPA protein lysates and pellets after fractionation of WT OBSCs treated with 250 nM BTZ using anti-poly-ubiquitin antibody (Dako). Amidoblack staining serves as protein loading control. **Lower panel:** Corresponding densitometric analysis of protein levels of n=3 normalized to amidoblack staining. Dot blot was performed in duplicates and fold changes calculated towards control. Values represent mean and SEM (significance refers to difference between ctrl and treatment, *p<0.05, student-t test).

B Upper panel: Dot blot analysis of ubiquitinated proteins in RIPA protein lysates and pellets after fractionation of WT and LMP7 KO OBSCs treated with 5 μ M A β O using anti-poly-ubiquitin antibody (Dako). Amidoblack staining serves as protein loading control. **Lower panel:** Corresponding densitometric analysis of protein levels normalized to amidoblack staining. Dot blot was performed in duplicates and fold changes calculated towards control. Values represent mean and SEM (significance refers to difference between 8 and 24 hrs time points, *p<0.05, student-t test).

the insoluble Ub-conjugate levels were raised by 60% after 24 hrs in response to A β O_s, although no proteasome inhibition was detected (Figure 8B).

Next we verified if chemical proteasome inhibition in general induces the upregulation of immunoproteasome subunit LMP7 in our OBSC model. Therefore, we treated WT OBSCs with proteasome inhibitor BTZ and analyzed LMP7 protein expression levels at different time points in western blot. In fact, we clearly demonstrated that BTZ induces an upregulation of LMP7 subunit on protein expression level (Figure 9A). In the following, we reviewed the protein expression of LMP7 in OBSCs treated with A β O_s. While LMP7 protein expression initially appeared decreased, 24 hrs of treatment resulted in a 30% increase versus vehicle control (Figure 9B).

The formation of the immunoproteasome is mediated by interferons that are generally known to activate JAK-STAT signaling resulting, for example, in the production of IFN stimulated genes (ISGs) (Figure 10A). We verified the activation of this pathway in our OBSC model using murine IFN β (mIFN β) and detected the transient phosphorylation of

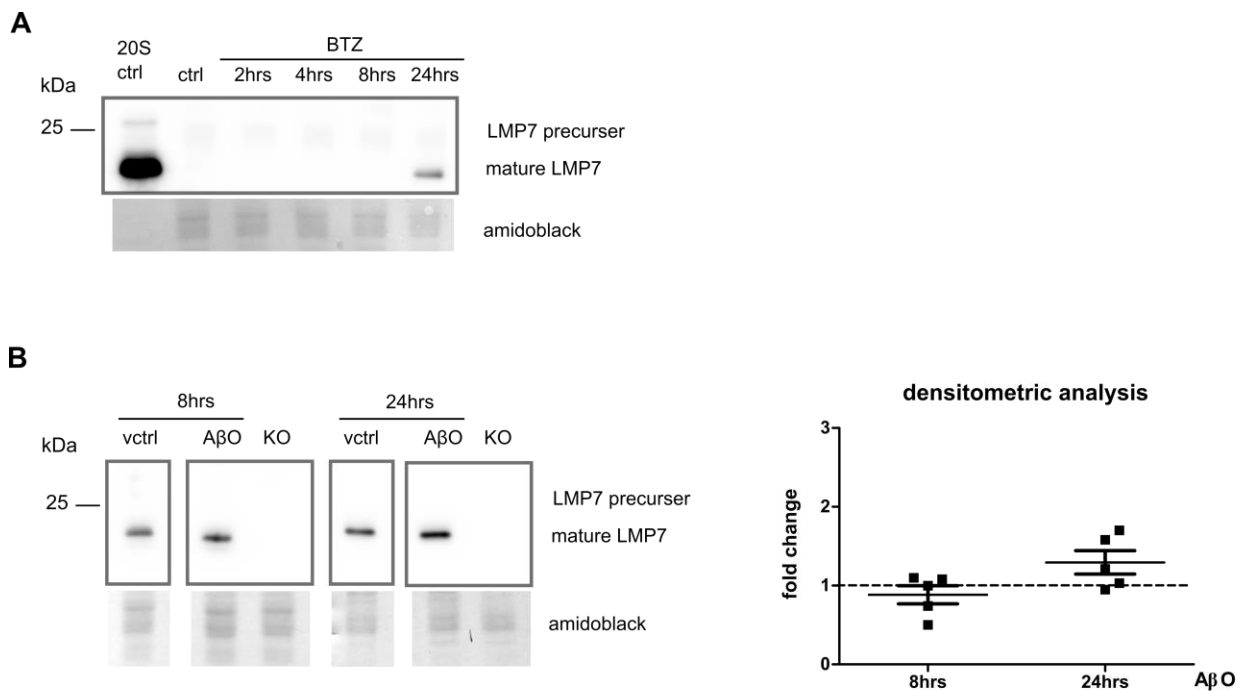


Figure 9: Chemical proteasome inhibition by Bortezomib upregulates LMP7 protein expression.

A Western blot analysis of LMP7 protein expression in OBSCs treated with 250 nM BTZ using in-house anti-LMP7 antibody. Purified 20S proteasome from mouse spleen serves as positive control and the amidoblack staining served as protein loading control. **B Left:** Representative western blot of LMP7 protein expression in OBSCs treated with 5 μ M A β O_s using in-house anti-LMP7 antibody. OBSCs from LMP7 KO pups serve as negative control and the amidoblack staining served as protein loading control. **Right:** Corresponding densitometric analysis of LMP7 protein levels normalized to amidoblack staining. Fold changes were calculated towards vehicle controls. Values represent mean and SEM (no significant changes were detected, student-t test).

STAT1 in western blots (Figure 10B). Moreover, we detected definitely elevated mRNA levels of a selection of ISGs – Cxcl10, Mx1 and Isg15 - by quantitative RT-PCR (Figure 10C).

Next, we examined if chemical proteasome inhibition or A β O exposure results in the production of Type I IFNs IFN α and IFN β with subsequent STAT activation and the transcription of ISGs. The results of gene expression analysis of OBSCs treated with proteasome inhibitor BTZ revealed elevated mRNA levels for *Ifna1* after 4 hrs by 2.7-fold and significantly elevated mRNA levels for *Ifnb1* already after 2 hrs by 1.8-fold, remaining stable until 8 hrs (Figure 11). Nevertheless, the results of OBSCs treated with A β O were less conclusive. Although occasionally elevated mRNA levels of *Ifna1* and

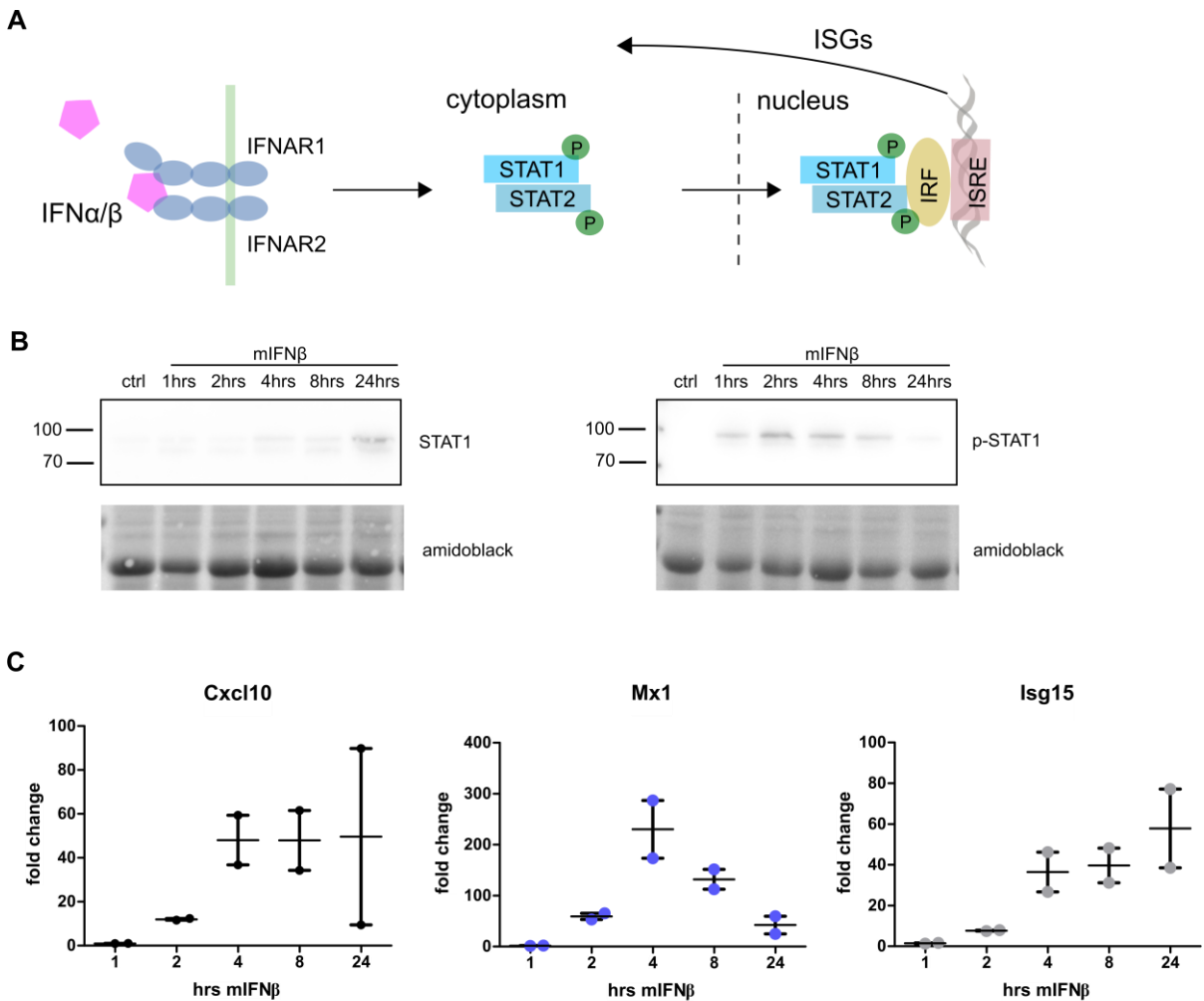


Figure 10: Type I IFN induced JAK-STAT signaling.

A Binding of Type I IFNs IFN α or IFN β to IFN receptors initiate a phosphorylation cascade resulting in the dimerization of STAT1 and STAT2 that finally translocate to the nucleus. Binding to IFN stimulated response elements (ISRE) IFN via IFN regulating factors (IRF) initiates the transcription of IFN stimulated genes (ISGs). **B** Western blot of STAT1 and phosphorylated STAT1 in OBSCs treated with murine IFN β . **C** Gene expression analysis of *Cxcl*-10, *Mx1* and *Isg15* mRNA levels in OBSCs treated with mIFN β . Fold changes were calculated towards control. Values represent mean with SEM.

Ifnb1 appeared in both WT and immunoproteasome deficient OBSCs, no significant pattern for upregulation could be observed (Figure 11).

Next, we analyzed the protein levels of STAT1 and its phosphorylation-status in OBSCs treated with BTZ in western blot. We were able to detect increased levels of STAT1 at 8 hrs of BTZ treatment compared to untreated control. Simultaneously, only at this time point STAT1 appears phosphorylated (Figure 12A). Corresponding, we detected significantly elevated mRNA levels of Cxcl-10 and Mx1. Interestingly, although the results suggest an upregulation of total STAT1 protein expression upon A β O-treatment (enhanced in WT compared with LMP7 KO), statements to phosphorylated STAT1 were more challenging since we were not able to detect a signal using the antibody directed against STAT1 phosphorylation sites (Figure 12A). However, assuming the upper protein band being the phosphorylated STAT1, we observe an activation of STAT1 in both WT and LMP7 KO. Corresponding, we found elevated ISG levels only for Mx1 in A β O-treated WT OBSCs (Figure 12B). Probably, the expected Type I IFN response only appears after much longer periods of proteasome inhibition.

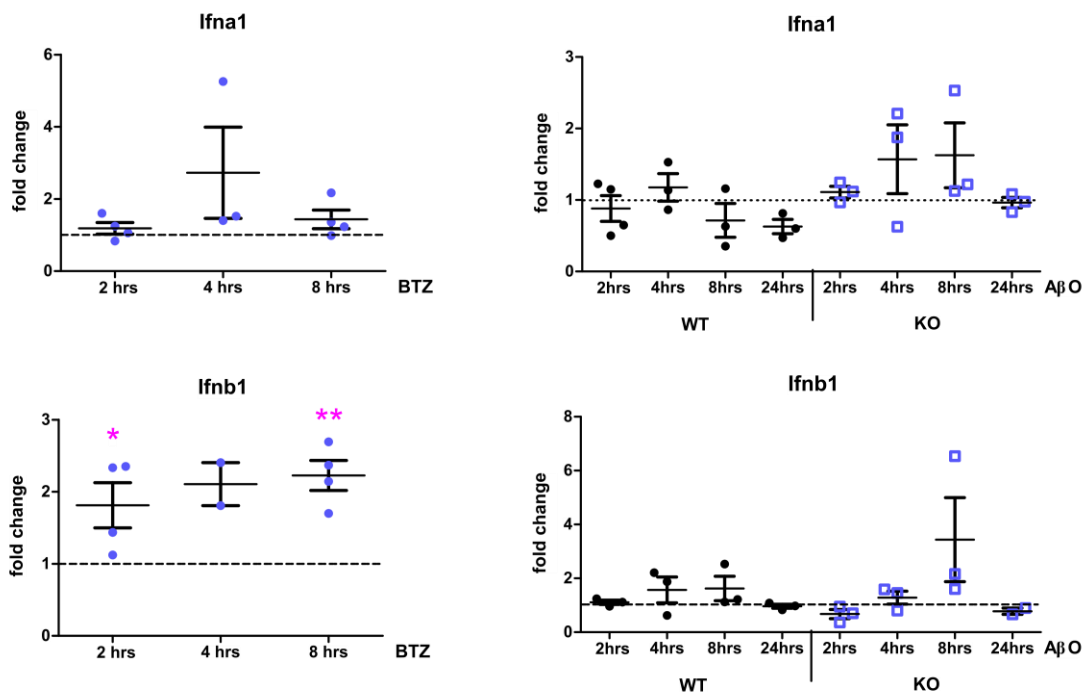


Figure 11: Bortezomib induces a Type I IFN response.

Gene expression analysis of Ifna1 and Ifnb1 mRNA levels in OBSCs treated with 250 nM BTZ or 5 μ M A β O. Fold changes were calculated towards control. Values represent mean with SEM (* p <0.05 ** p <0.005, student-t test).

To sum up, while proteasome inhibition by Bortezomib results in a significant accumulation of insoluble Ub-proteins in organotypic brain slices (3-fold), in WT OBSCs treated with A β O only a slight increase in insoluble Ub-protein levels could be detected (1.3-fold). Surprisingly, in A β O-treated OBSCs from LMP7 KO pups, that could not be associated with proteasome inhibition, we found a 1.6-fold increase in the insoluble Ub-protein fraction. Furthermore, chemical proteasome inhibition resulted in a clear upregulation of immunoproteasome subunit LMP7, whereas we could demonstrate that A β O-induced proteasome inhibition leads to a slight increase in LMP7 protein expression level. Finally, a Type-I IFN response with elevated levels of Ifnb1 mRNA, STAT1 phosphorylation and subsequent upregulation of IFN-stimulated genes could be shown for OBSCs treated with Bortezomib but not for those treated with A β O.

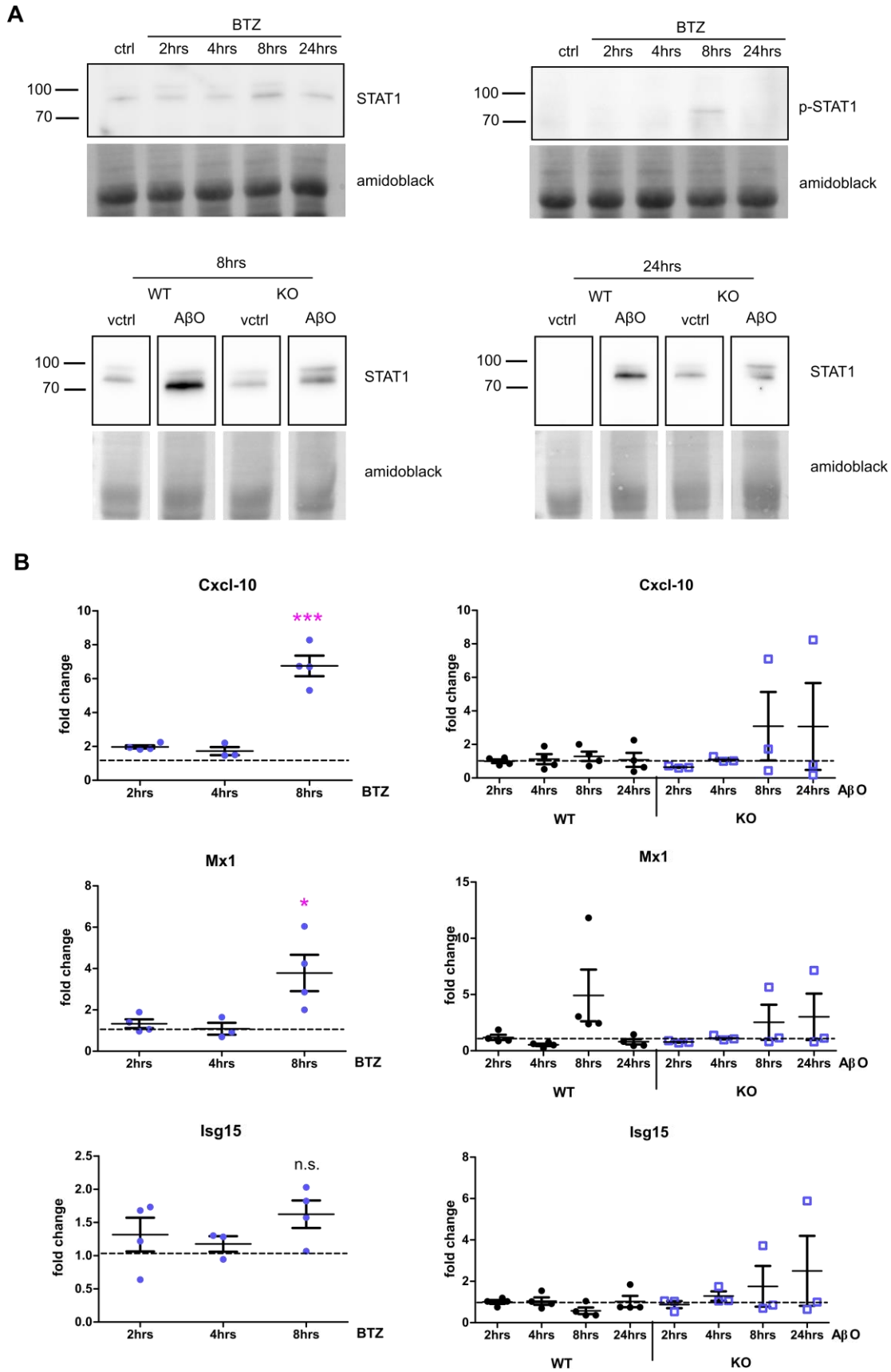


Figure 12: Bortezomib but not A β O_s activate STAT1 and ISG transcription.

A Western blot analysis of STAT1 and phospho-STAT1 in OBSCs treated with 250 nM BTZ or 5 μ M A β O_s. Amidoblack staining serves as protein loading control. **B** Gene expression analysis of Cxcl10, Mx1 and Isg15 mRNA levels in OBSCs treated with 250 nM BTZ or 5 μ M A β O. Fold changes were calculated towards corresponding vehicle control. Values represent mean with SEM. (* p <0.05 *** p <0.001, student-t test).

3.1.4. A β oligomers activate mTOR signaling pathway

Another sensor of immune signals – the mTOR pathway – has been shown to cooperate with JAK/STAT signaling [66] and act independently of STAT phosphorylation to induce IFN-stimulated genes [64]. In addition, the mTOR pathway plays a role in the regulation of the ubiquitin proteasome system and autophagy [60], [106]. For this reason, we aimed to include the analysis of mTOR signaling in the context with impairment of the UPS in our Alzheimer's disease model. Since it has been demonstrated that Type I IFNs activate mTOR signaling via phosphorylation of p70 S6 kinase and S6 ribosomal protein [65], we decided to study their protein expression and phosphorylation status in western blot.

First, in line with previous experiments, we treated OBSCs with proteasome inhibitor BTZ and analyzed p70 kinase and S6 ribosomal protein expression. While the protein expression levels of p70 and S6 remained nearly unchanged, we detected up to 2-fold increase in p70 phosphorylation and up to 13-fold increase in S6 phosphorylation (Figure 13).

In a similar manner, OBSCs from WT and LMP7 KO pups treated with A β O_s were examined regarding p70 and S6 protein expression and phosphorylation. Both, in WT and LMP7 KO, the protein expression and phosphorylation levels of p70 kinase appeared unchanged. Although in both genotypes the applied A β O_s increased the S6 protein levels, the results further showed significantly increased phosphorylation of S6 protein only in WT OBSCs - already after 8 hrs of A β O_s-treatment. In contrast, S6 phosphorylation levels prevailed unchanged in LMP7 KO at the tested time points (Figure 14).

Taken together, we found that chemical proteasome inhibition by Bortezomib lead to an activation of mTOR signaling resulting in phosphorylation of downstream target S6 ribosomal protein. In accordance with this notion, we were able to demonstrate that proteasome inhibition by A β O_s activated mTOR signaling as well. This is consistent with our finding in LMP7 KO OBSCs, which did not display further impaired proteasome activity, no increase in S6 phosphorylation was observed. The question remains though, how immunoproteasome deficient OBSCs compensate the A β O_s-induced proteotoxic stress.

Perturbations of proteasome networks in Alzheimer's disease

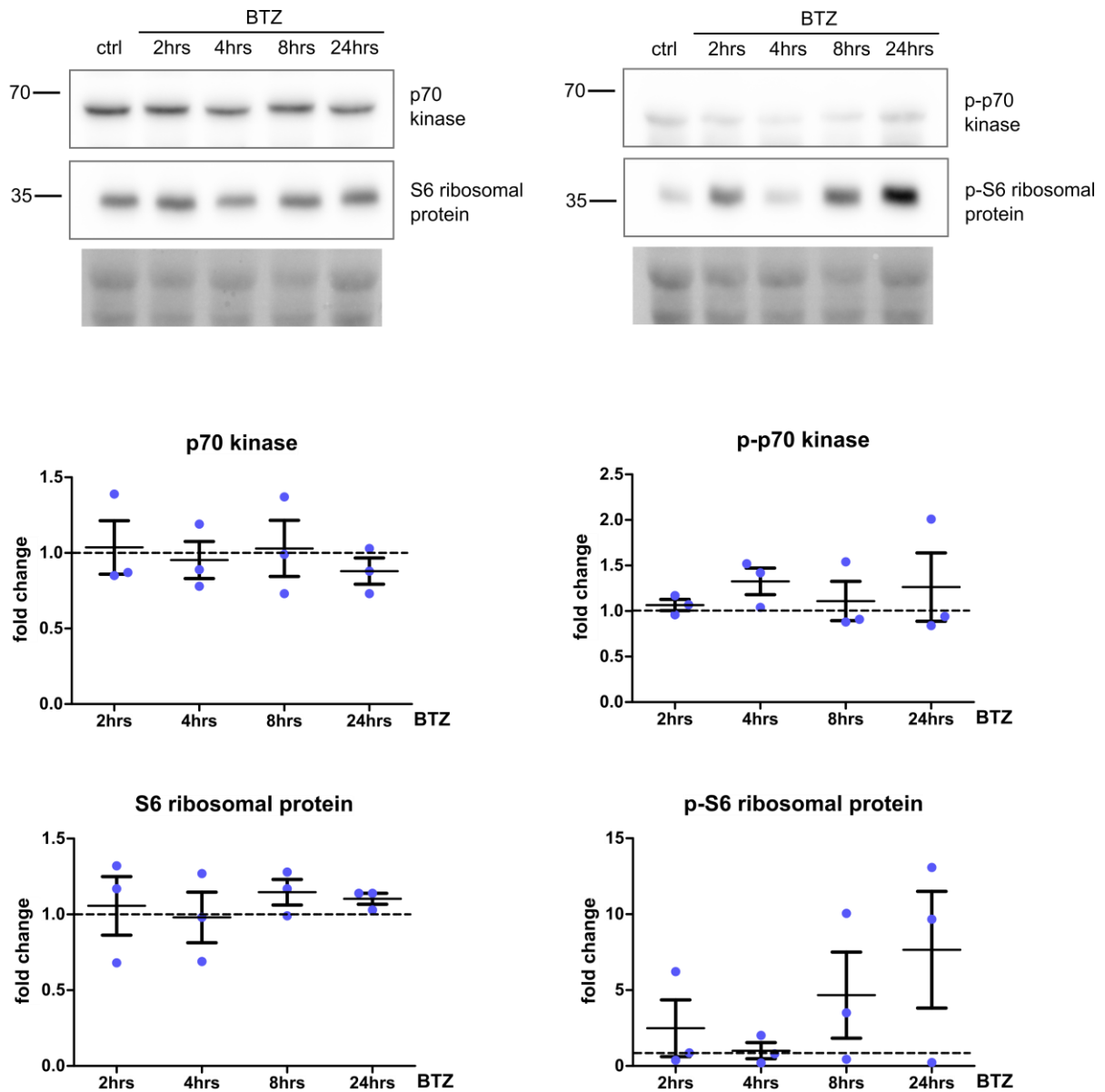


Figure 13: Proteasome inhibition by Bortezomib results in p70/S6 activation.

A Western blot analysis of p70 S6 kinase, S6 ribosomal protein and their phosphorylation in OBSCs treated with 250 nM BTZ. Amidoblack staining served as protein loading control. **B** Corresponding densitometric analysis of protein levels normalized to amidoblack staining. Fold changes were calculated towards control. Values represent mean with SEM.

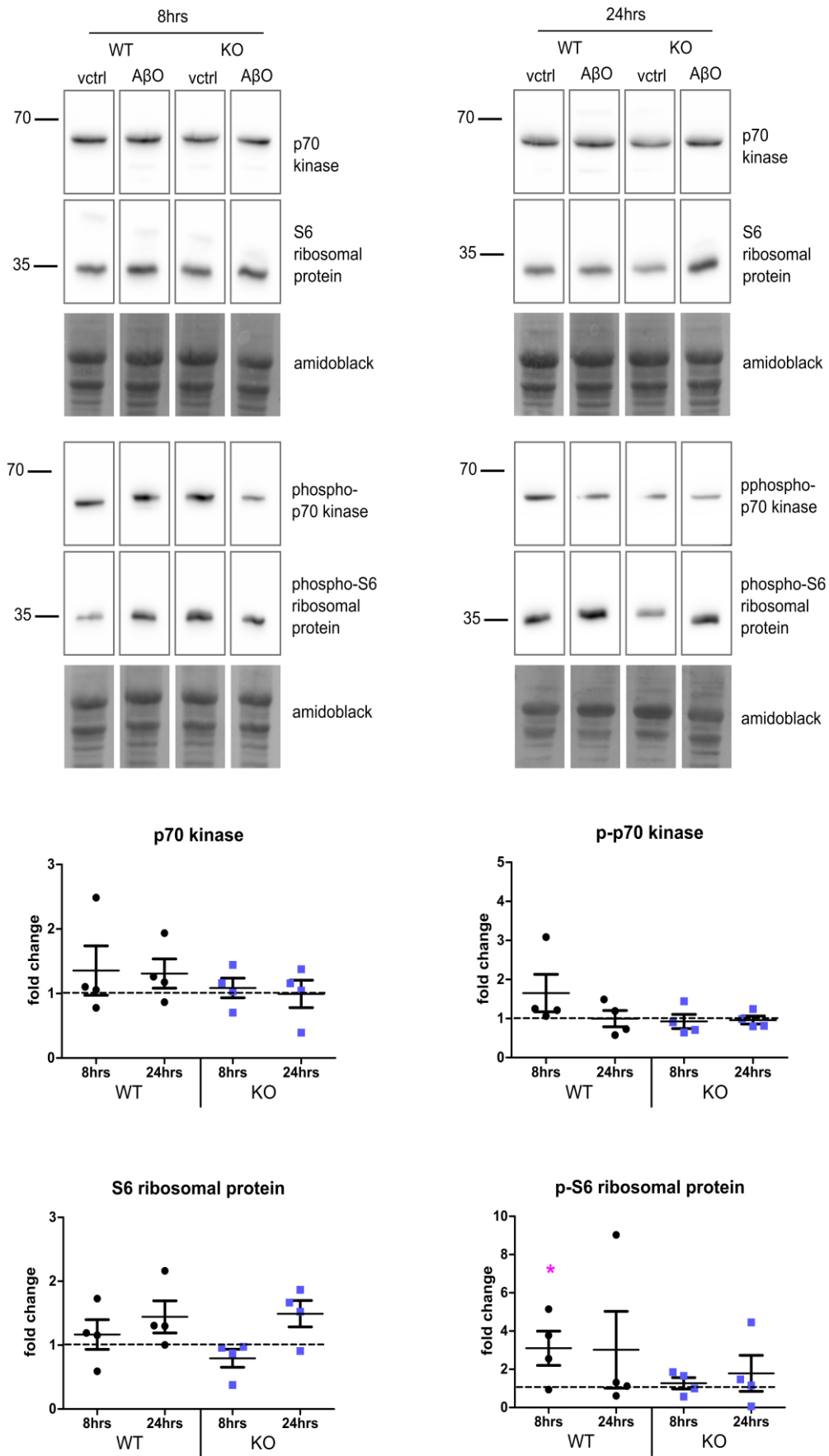


Figure 14: AβO-induced p70/S6 (mTOR) pathway in WT OBSCs.

Upper panel: Western blot analysis of p70 S6 kinase and S6 ribosomal protein and their phosphorylation in OBSCs treated with 5 μM AβOs. Amidoblack staining served as protein loading control. *Lower panel:* Corresponding densitometric analysis of protein levels normalized to amidoblack staining. Fold changes were calculated towards control. Values represent mean with SEM (*p<0.05, student-t test).

3.1.5. A β O-induced autophagy in immunoproteasome deficiency

It is a rather new way of thinking that the two major degradation pathways - the ubiquitin proteasome system and macroautophagy - are linked to each other. In fact, experimental data suggests a direct cross-talk between these pathways [107]. Since we observed no further proteasome inhibition and no mTOR activation in immunoproteasome deficient OBSCs treated with A β O, we suspected involvement of autophagy. Therefore, we analyzed the protein expression of the established autophagy marker microtubule-associated protein 1 light chain (LC3), in particular the conjugated variant LC3-II. In order to verify the interplay between the proteasome and autophagy, we performed western blot analysis of LC3-I and LC3-II in OBSCs treated with proteasome inhibitor BTZ. Surprisingly, we detected no changes in expression of the autophagy marker LC3-II and even significantly downregulated expression of LC3-I in the initial phase of proteasome inhibition (Figure 15A).

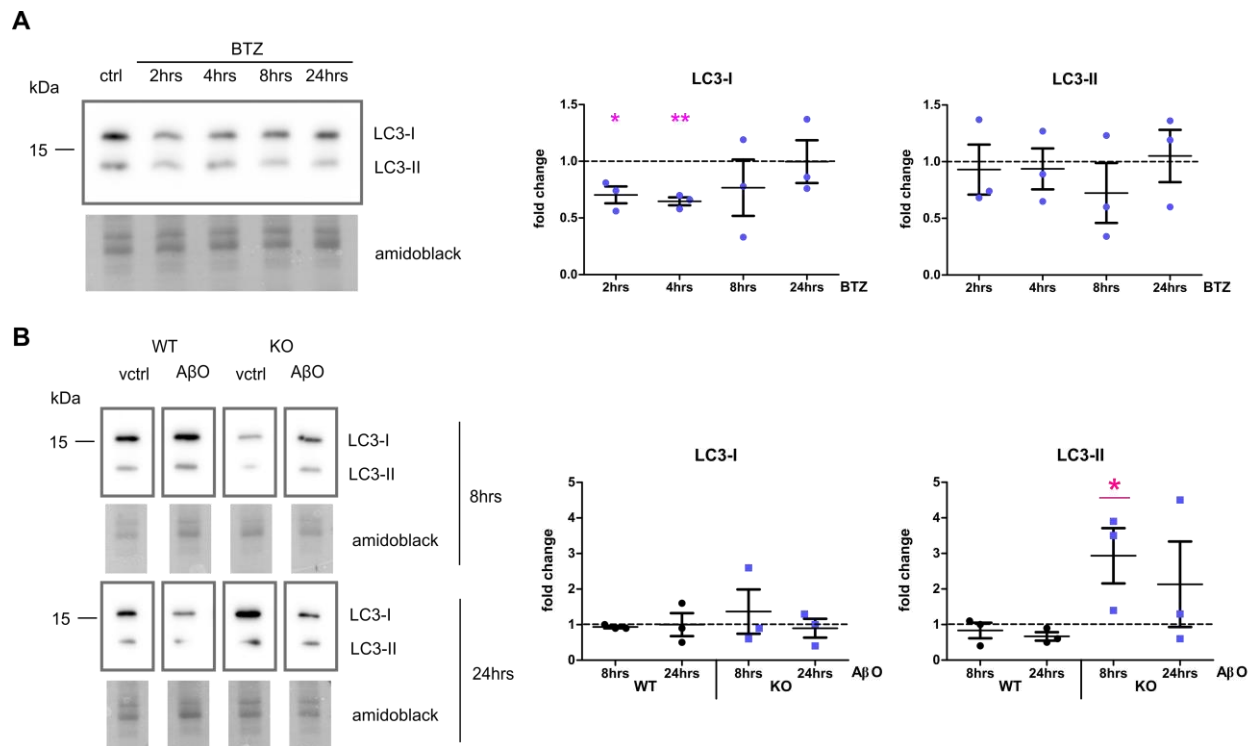


Figure 15: Suppression of autophagy upon Bortezomib and A β O-induced autophagy in LMP7 KO OBSCs.

A *Left panel:* Western blot analysis of LC3-I and LC3-II in OBSCs treated with 250 nM BTZ. Amidoblack staining serves as protein loading control. *Right panel:* Corresponding densitometric analysis of protein levels normalized to amidoblack staining. Fold changes were calculated towards control. Values represent mean with SEM (* $p < 0.05$, ** $p < 0.005$, student-t test).

B *Left panel:* Western blot analysis of LC3-I and LC3-II in OBSCs treated with 5 μ M A β O. Amidoblack staining serves as protein loading control. *Right panel:* Corresponding densitometric analysis of protein levels normalized to amidoblack staining. Fold changes were calculated towards control. Values represent mean with SEM (* $p < 0.05$, student-t test).

In agreement with this finding, proteasome inhibition by A β O in WT-derived OBSCs does not result in activation of autophagy at the tested time points as protein expression levels of both, LC3-I and LC3-II remain unchanged. Interestingly, when the immunoproteasome is absent, we observed significantly upregulated LC3-II protein levels indicating activation of autophagy (Figure 15B).

Collectively, our data show no activation or even downregulation of autophagy in WT-derived OBSCs treated with Bortezomib or A β O which differs from our expectations and the literature. In contrast, in OBSCs lacking for the immunoproteasome elevated levels of autophagy marker LC3-II were detected, possibly reflecting the compensation mechanism upon A β O-induced proteotoxic stress.

3.1.6. A β O alter glial activities dependent on the immunoproteasome

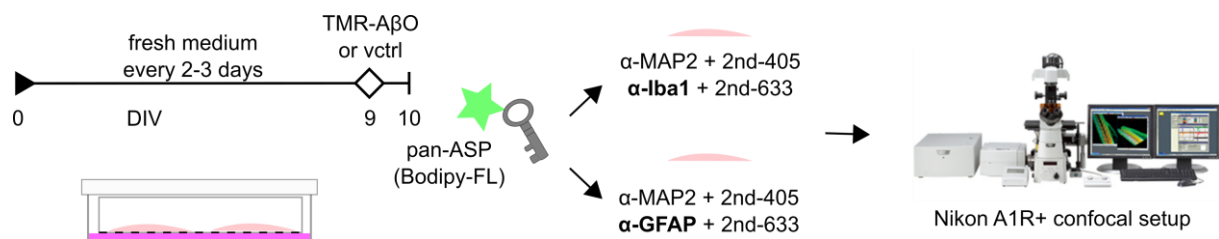


Figure 16: Experimental setup for confocal imaging.

Organotypic brain slices were cultured for 9 days in vitro (DIV) before treatment with either 5 μ M TMR-labeled A β O or vehicle control (vctrl) for 24 hrs followed. At day 10 the OBSCs were incubated with pan-reactive Bodipy-FL-labeled active site probe (ASP) for 1 hour in the incubator. Slices were subsequently fixed in 4% PFA and one slice further immunostained free floating for MAP2 and Iba1 or MAP2 and GFAP as described in material & methods section. Finally, the slices were mounted in aqueous Fluoromount using the bridge-technique and imaged with the Nikon A1R+ confocal setup using 20x objective and 63x water immersion (WI) objective.

The use of organotypic brain slices enables to investigate how amyloid- β oligomers impacts on proteasome networks in a tissue-like context. Thereby we aimed to include effects of A β O on all cell types and the interaction between them. In order to visualize the reaction of the different cell types, we performed confocal imaging using TMR-labeled A β O for treatments followed by incubation with the pan-reactive active site probe (proteasome, pan-ASP) and immunostaining for neuronal (MAP2), microglial (Iba1) and astrocyte (GFAP) markers (Figure 16).

As expected according to earlier findings (see Figure 6C), the quantitative analysis of pan-ASP fluorescence intensity in confocal images of OBSCs revealed significantly reduced proteasome activity signals in slices lacking the immunoproteasome (Figure 17). The reduction was observed under untreated and treated conditions and was

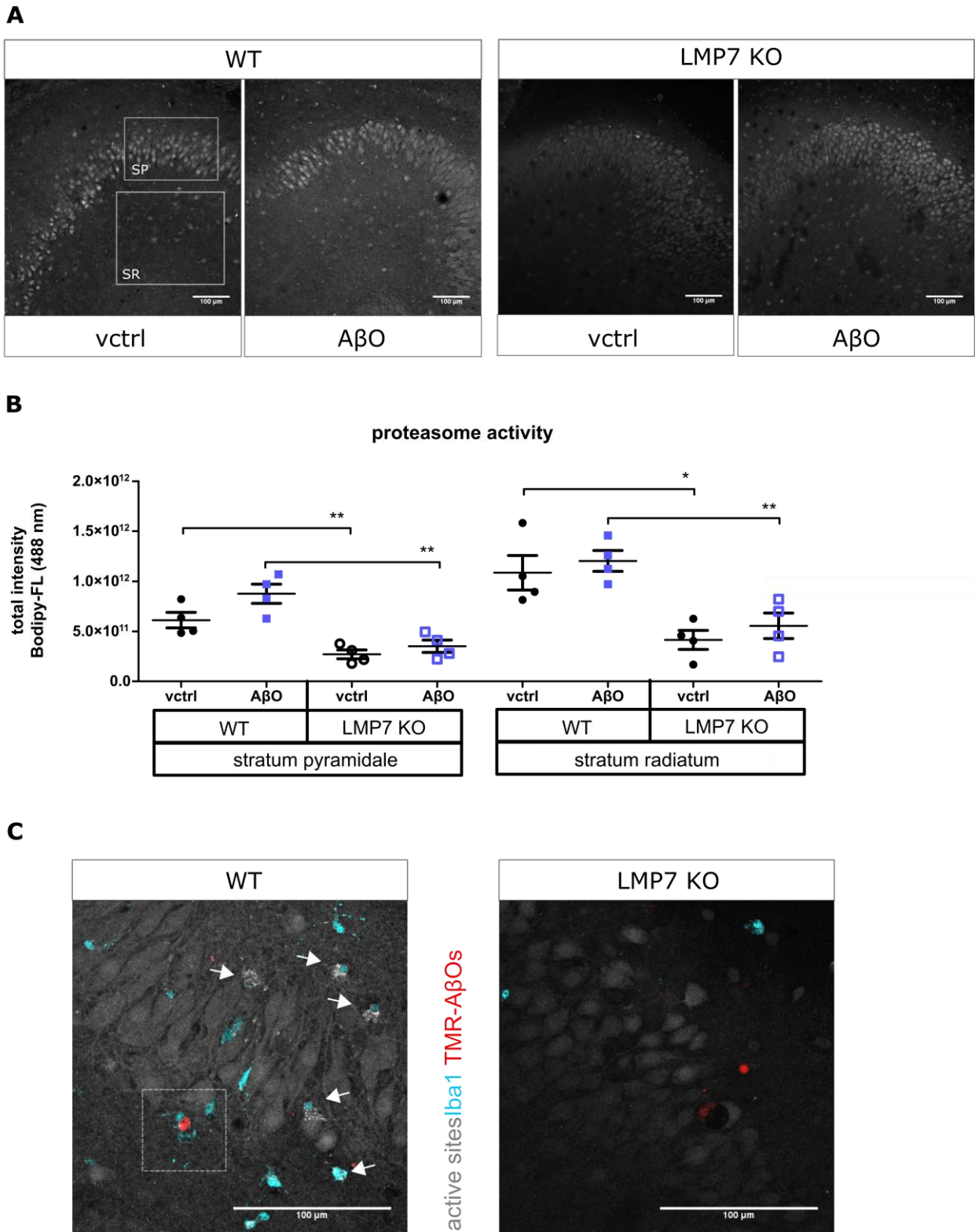


Figure 17: Reduced proteasome activity in immunoproteasome deficient OBSCs.

A Confocal images of WT and LMP7 KO OBSCs treated with vehicle control or A β O for 24 hrs and subsequently labeled with pan-ASP. Images were obtained with 20x objective using equal laser excitation (488 nm) for every slice. **B** Corresponding quantitative analysis of total fluorescence intensity in two different areas: stratum pyramidale (SP) and stratum radiatum (SR). Values represent mean with SEM (* $p < 0.05$, ** $p < 0.005$, student-t test). **C** Confocal images of WT and LMP7 KO OBSCs treated with A β O for 24 hrs and subsequently labeled with pan-ASP and α -Iba1 antibody. Images were obtained with 63x WI objective. White arrows indicate spotty ASP signals associated with Iba1+ microglia. White box highlights Iba1+ positive microglia engulfing TMR-A β O accumulations.

independent of the area analyzed. Nonetheless, the proteasome activity signal was not changed upon A β O-treatment (in contrast to the observed reduction in proteasome activity analyzed in SDS-PAGE, see Figure 6 and Figure 7). Using higher magnification (63x) we observed suspicious spotty ASP signals in close proximity to Iba1 positive microglia in WT OBSCs treated with A β O as well as microglia obviously embracing TMR-labeled A β O accumulations (Figure 17C). In contrast, in A β O-treated LMP7 KO slices fewer Iba1 positive microglia were detected that at the same time did not feature additional ASP signals. We therefore intended to quantify the Iba1 positive signals in confocal images to verify the difference in microglia activation between WT and

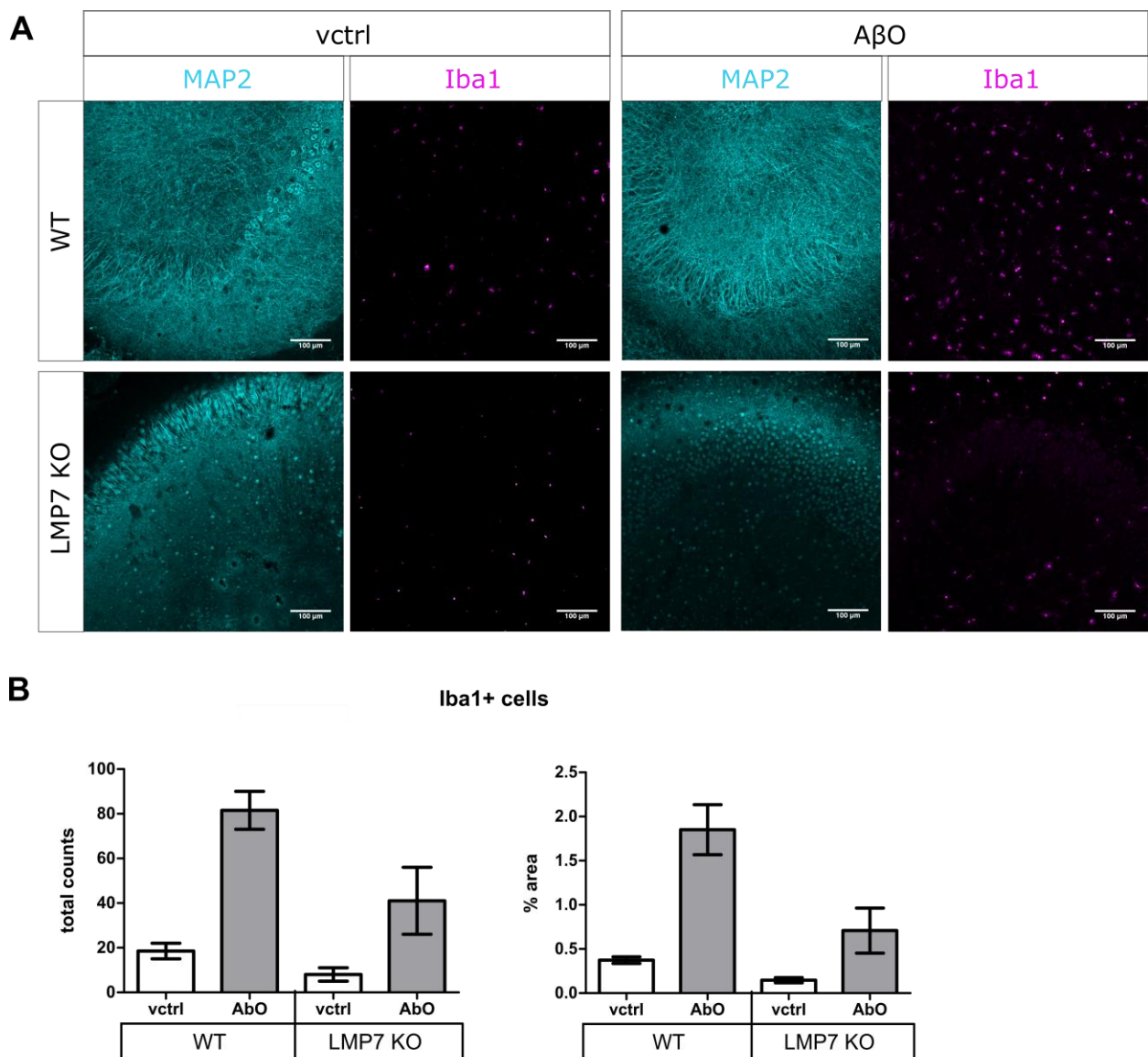


Figure 18: A β O-induced microgliosis.

A Confocal images of WT and LMP7 KO OBSCs treated with vehicle control or A β O for 24 hrs and immunostained for neurons (MAP2) and microglia (Iba1). Images were obtained with 20x objective. **B** Total counts and area covered by Iba1 positive microglia in image stacks obtained with 20x objective. n = 2 slices per group were analyzed.

LMP7 KO OBSCs upon A β O treatment. Indeed, the number of activated microglia was 4-fold higher in response to A β O in both WT and LMP7 KO although the total counts were 50 % lower in immunoproteasome deficient OBSCs (Figure 18C). This finding is in line with our earlier observations that demonstrated significantly lower numbers of Iba1 positive microglia in brain slices of aged APPPS1xLMP7 KO mice [104].

The second slice of each well treated with either vehicle control or TMR-A β O was immunostained for GFAP (astrocytes) in addition of MAP2 (neurons). The quantitative analysis of the respective images (Figure 19) revealed an interesting observation: Upon A β O-treatment, astrocytes appear more numerous in slices deficient for the

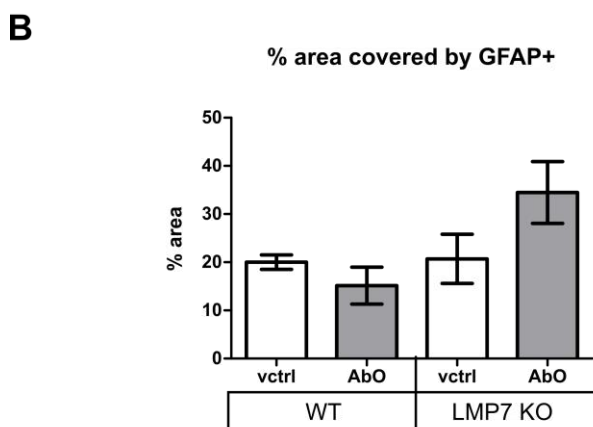
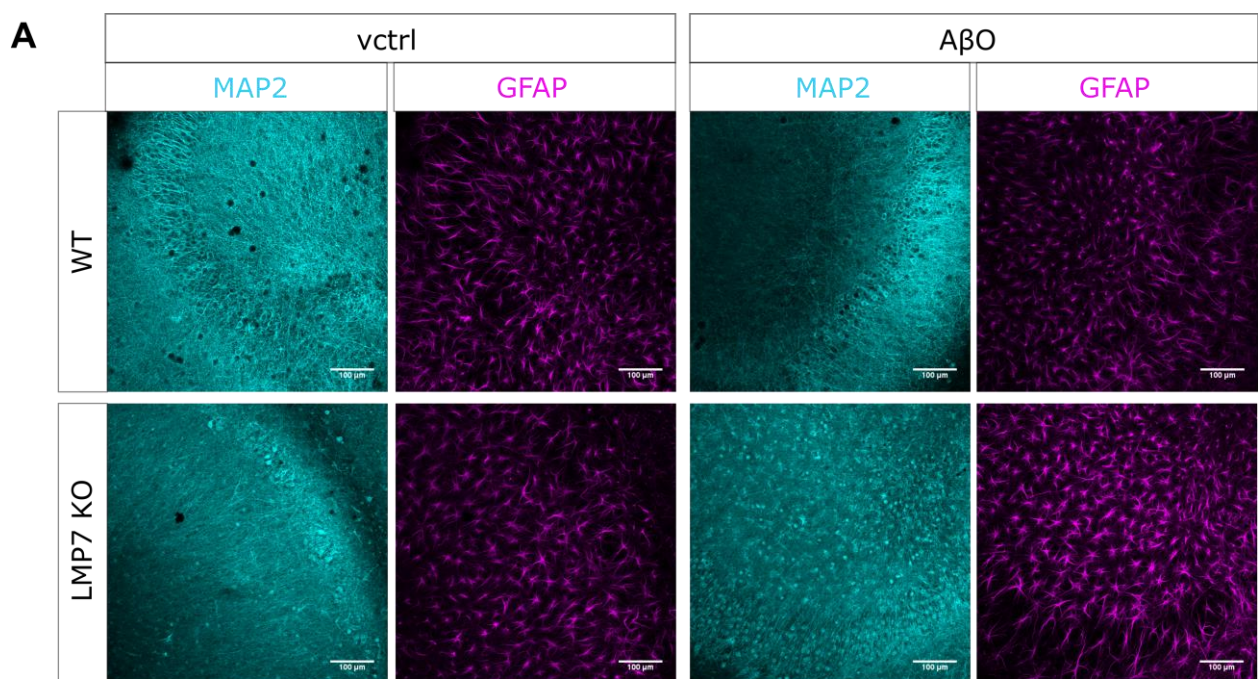


Figure 19: A β O-induced astrogliosis in immunoproteasome deficient OBSCs.

A Confocal images of WT and LMP7 KO OBSCs treated with vehicle control or A β O for 24 hrs and immunostained for neurons (MAP2) and astrocytes (GFAP). Images were obtained with 20x **B** Quantified area covered by GFAP positive astrocytes in image stacks obtained with 20x objective. n = 2 slices per group were analyzed.

immunoproteasome (LMP7 KO) compared to WT, reflected by an increase in area covered by GFAP positive cells (Figure 19B). Interestingly, recently we observed an enhanced astrogliosis in brain sections of AD mice deficient for the immunoproteasome as well [104].

Taken together, our data from confocal microscopy highlights the importance of glial cells and the immunoproteasome in our OBSC model of Alzheimer's disease. A β O_s increased the Iba1 (microglia) immunoreactivity in WT with associated increased signals for proteasome active sites. Although A β O-induced microgliosis appeared less pronounced in immunoproteasome deficient OBSCs, astrogliosis was enhanced.

3.1.7. Cell type specific response upon A β O-treatment

Following the observations of differential activation of microglia and astrocytes compared with neurons in response to A β oligomers in WT and LMP7 KO slices in confocal microscopy, we decided to analyze MACS-separated microglia from A β O-treated OBSCs on mRNA and protein level and compare the results with the flow through fraction. Therefore, at least 20 slices from each condition were collected, the tissue dissociated and microglia separated using CD11b magnetic beads (Figure 20A). We subsequently extracted either RNA for qRT-PCR or protein for western blot.

To validate the successful microglia separation, we measured the expression of marker genes for microglia (Cd11b), neurons (NeuN) and astrocytes (Gfap) in CD11b-positive cells and those cells from the respective flow through. The results clearly show high levels of Cd11b gene expression and negligible NeuN and Gfap gene expression levels

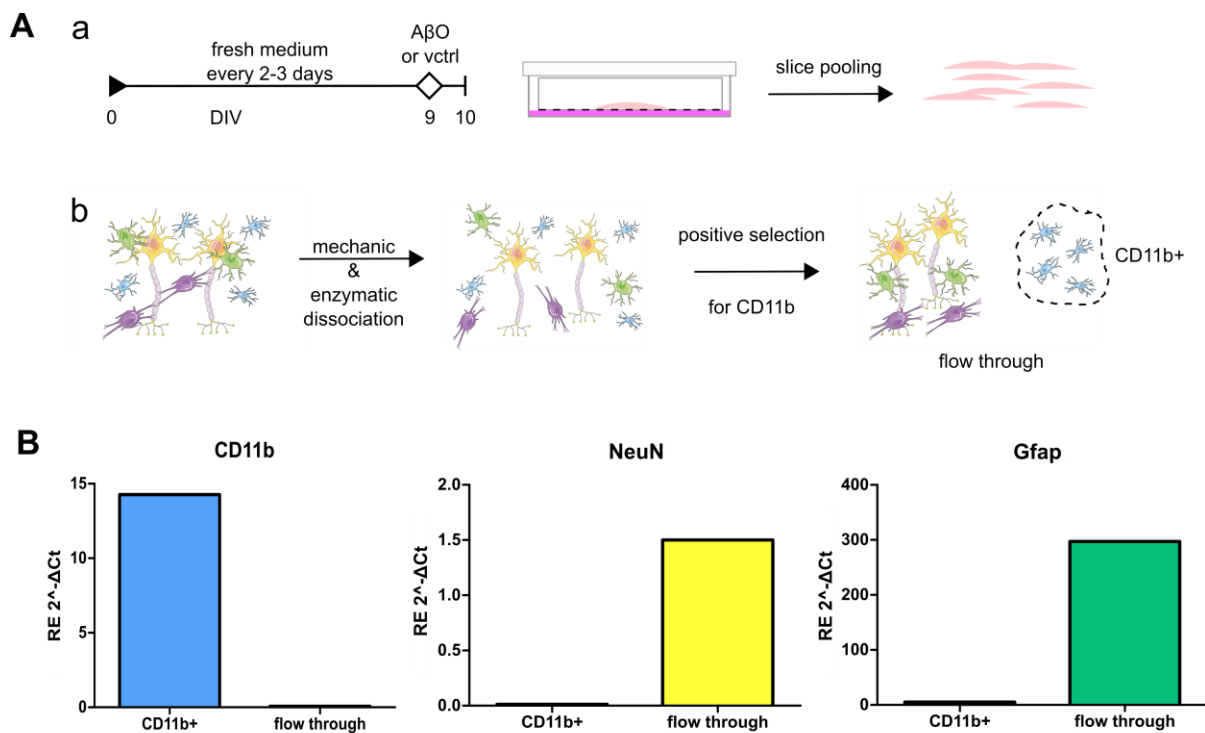


Figure 20: MACS-separating of Cd11b-positive microglia from OBSCs.

A Neural dissociation and MACS-separating of CD11b-positive microglia. OBSCs were cultured and treated as described in the methods section. Slices of at least 10 wells treated equally were pooled (a). Slices were subsequently dissociated mechanically using gentleMACS dissociator and enzymatically using papain. Cell suspension was incubated with CD11b-conjugated magnetic-beads and CD11b-positive cells were separated from flow through using by magnetic force. **B** CD11b-positive and flow through fractions were characterized by qRT-PCR using markers specific for microglia (CD11b), neurons (NeuN) and astrocytes (GFAP). Bars represent one single measurement (performed in technical duplicates) but includes a sample pool of at least 10 individually treated wells corresponding to 2-3 pups.

in the CD11b-positive fraction, whereas we detected only negligible levels of Cd11b gene expression but high expression levels of NeuN and Gfap gene expression in the flow through, respectively (Figure 20B).

We were first interested in the expression of immunoproteasome β subunits PSMB9 (encoding for LMP2, β 1i), PSMB8 (encoding for LMP7, β 1i) and PSMB10 (encoding for MECL1, β 2i) on the mRNA level and further analyzed the protein expression of LMP7 in microglia derived from OBSCs treated with A β O. As expected, the results of gene expression analysis in isolated microglia in WT OBSCs revealed that gene expression of PSMB9 and PSMB8 was increased 1.2 and 1.5 fold upon 24 hrs A β O-treatment (Figure 21A). The respective protein expression of LMP7 was slightly increased by 1.3-fold in western blot as well (Figure 21B). In contrast, regarding the flow through fraction, the gene expression of both PSMB9 and PSMB8 was reduced by 0.9- and 0.7-fold

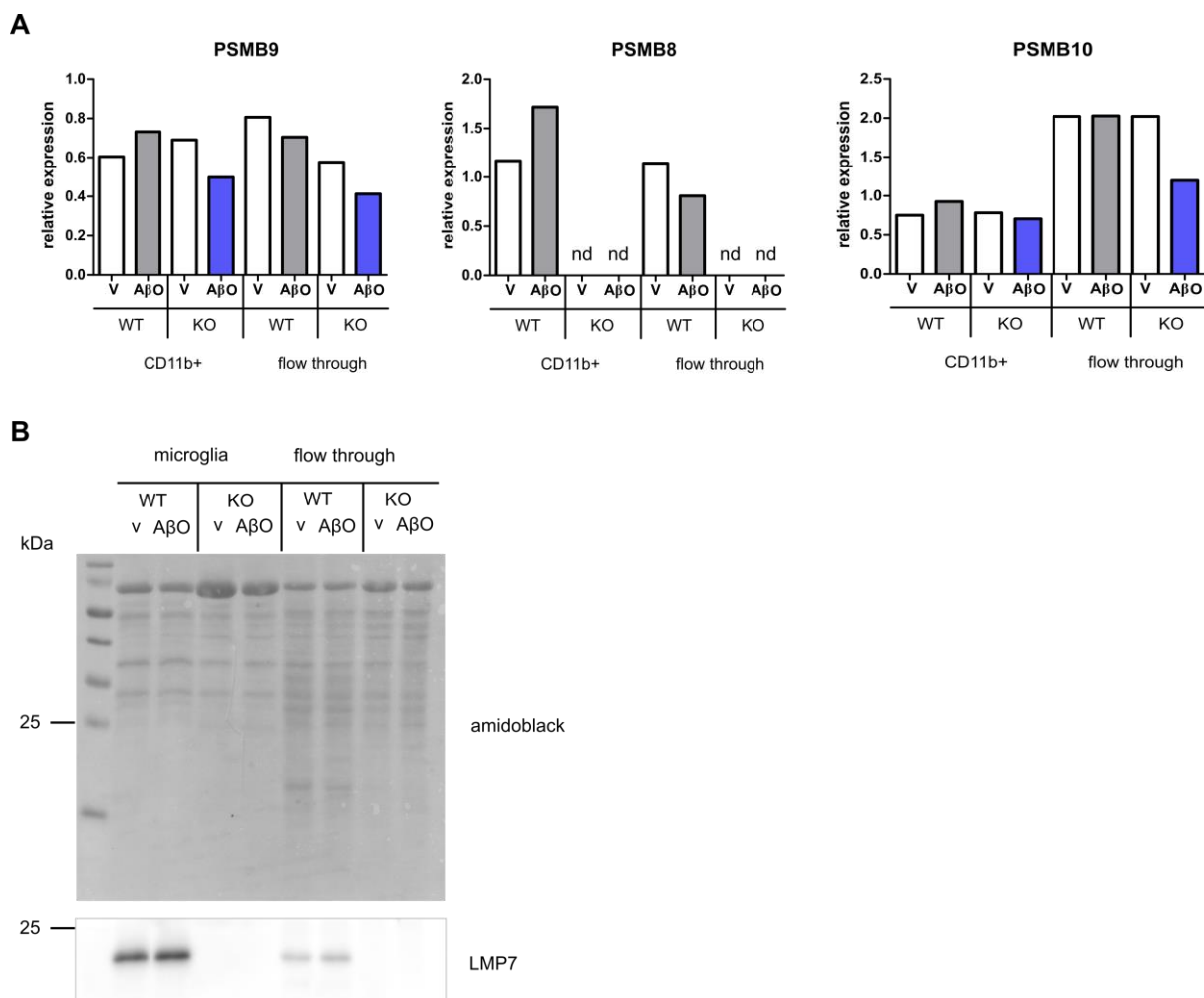


Figure 21: Differential expression of iP subunits in MACS-separated microglia versus flow through.

A Gene expression of immunoproteasome subunit genes PSMB9, PSMB8 and PSMB10 relative to housekeeping gene Hprt. **B** Western blot analysis of immunoproteasome subunit LMP7. Bars (qRT-PCR) and lanes (western blot) represent one single measurement (performed in technical duplicates) but includes a sample pool of at least 10 individually treated wells corresponding to 2-3 pups.

(Figure 21A). Protein expression of LMP7 was clearly lower compared with CD11b-positive fraction but contrary to gene expression results, A β O-treatment resulted in a slight increase in LMP7 signal in western blot (Figure 21B). Results of PSMB10 gene expression revealed an increase by 1.2 fold in the microglia fraction but no change in the flow through. Interestingly, in both the CD11-positive and flow through fraction we detected lowered gene expression of PSMB9 by 0.7- (both fractions) and PSMB10 by 0.9- (CD11+) and even 0.5-fold (flow through, Figure 21A).

Next, we were interested in the gene expression profile of Type-I IFN genes *Ifna1*, *Ifnb1* and a selection of IFN stimulated genes (*Cxcl10*, *Mx1* and *Isg15*) and therefore performed quantitative real-time PCR with RNA from cells separated by CD11b-MACS. Surprisingly, we observed that the relative expression levels of *Ifna1* and *Ifnb1* completely differ between CD11b-positive and flow through fractions. The results showed 23 fold higher relative expression of *Ifna1* in vehicle treated WT flow through compared with CD11b-positive cells and 5-fold higher relative expression of *Ifnb1* in vehicle treated CD11b-positive cells compared with the flow through fraction (Figure 22). In addition, we detected 3-fold higher *Cxcl10* gene expression levels in the flow through fraction of WT OBSCs compared with CD11b-positive cells, whereas the gene

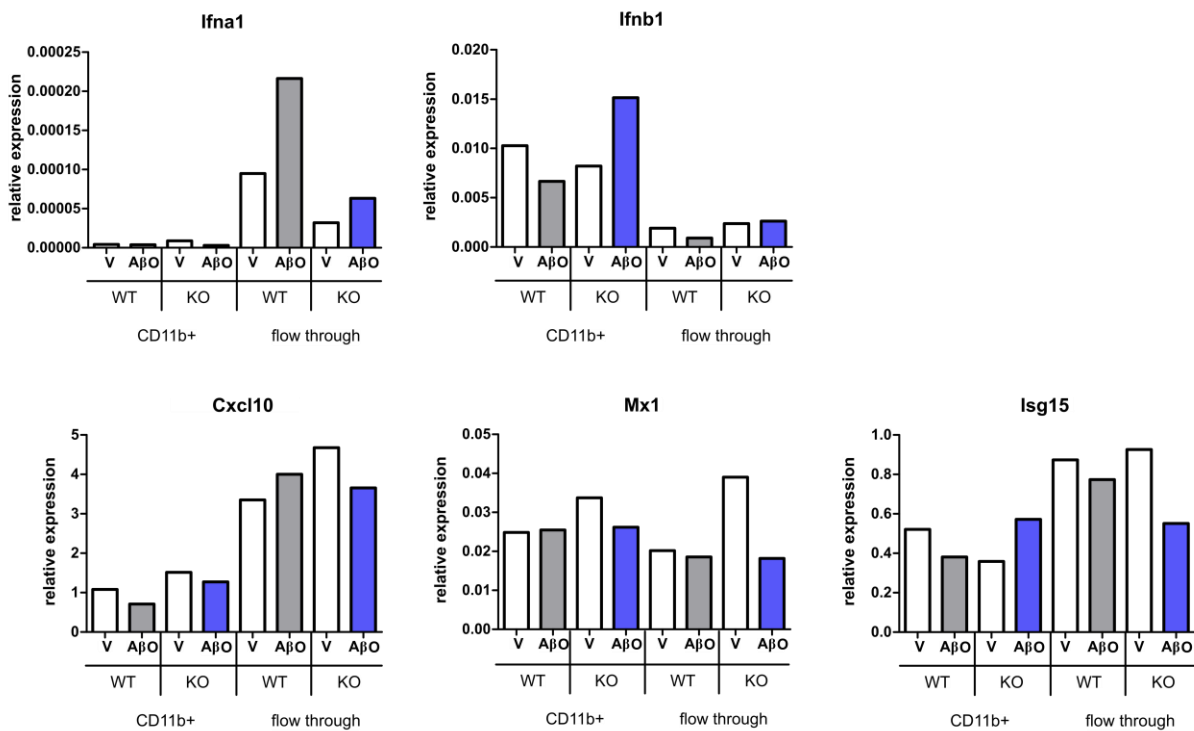


Figure 22: Differential gene expression of A β O-induced Type I IFN response in CD11b-separated microglia.

Gene expression of *Ifna1* and *Ifnb1* and also IFN stimulated genes *Cxcl10*, *Mx1* and *Isg15* relative to housekeeping gene *Hprt*. Bars represent one single measurement (performed in technical duplicates) but includes a sample pool of at least 10 individually treated wells corresponding to 2-3 pups.

expression of Mx1 and Isg15 did not differ considerably between flow through and microglia fraction. Cxcl10 gene expression, however, was slightly elevated 1.2-fold in flow through cells from WT OBSCs treated with A β O while in those from LMP7 KO OBSCs the gene expression of Cxcl10 was decreased 0.8-fold. Interestingly, while gene expression of Mx1 remained nearly unchanged upon A β O-treatment in both CD11b-positive cells and flow through of WT OBSCs, we detected a decrease in Mx1 levels by 0.8-fold in CD11b-positive cells and by 0.5-fold in flow through cells from LMP7 KO OBSCs. Furthermore, we measured slightly decreased levels of Isg15 gene expression in A β O-treated CD11b-positive microglia by 0.7-fold and in flow through cells by 0.9-fold. In contrast, in those cells from immunoproteasome deficient OBSCs the gene expression of Isg15 appeared 1.6-fold higher in CD11b-positive but 0.6-fold lower in flow through cells in response to A β O-treatment (Figure 22).

Finally we analyzed the protein expression of mTOR downstream target S6 ribosomal protein (S6) and its phosphorylation status as well as the protein expression of autophagy marker LC3 in western blot. First we observed lower S6 protein expression in CD11b-positive microglia compared with the respective flow through cells, with lowest signals for microglia derived from LMP7 KO slices. Surprisingly, we detected a higher A β O-induced increase in S6 phosphorylation in flow through cells from LMP7 KO slices (1.9-fold) compared with those from WT slices (1.3-fold). In contrast, in CD11b-separated microglia from WT slices the S6 phosphorylation was 1.2-fold higher in response to A β O whereas the signal was 0.7-fold decreased in microglia from

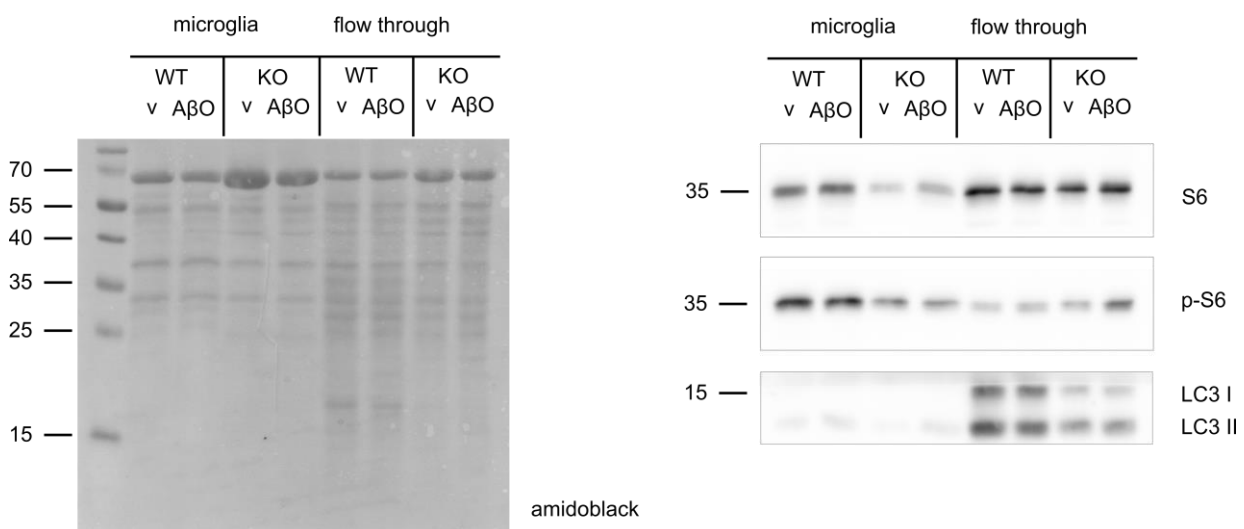


Figure 23: Analysis of mTOR and autophagy activation in CD11b-separated microglia.

Western blot analysis of S6 ribosomal protein (S6) protein expression and S6 phosphorylation as well as LC3-I and LC3-II protein expression. Lanes represent one single measurement (performed in technical duplicates) but includes a sample pool of at least 10 individually treated wells corresponding to 2-3 pups.

LMP7 KO slices. In concordance with data obtained from whole OBSC analysis, we measured a 2.9-fold increase in LC3-II levels in microglia derived from A β O-treated LMP7 KO slices indicating the activation of autophagy. As expected, we did not detect elevated LC3-II levels in both microglia and flow through cells derived from WT slices (Figure 23).

In summary, our results reveal that LMP7 protein expression is clearly higher in CD11b-positive microglia compared with the flow through fraction and both, gene and protein expression, is slightly elevated upon A β O-treatment. *Ifna1* and *Mx1* gene expression seems to be more relevant in those cells in the flow through fraction, namely astrocytes and neurons. On the other hand, *Ifnb1* gene expression appeared higher in CD11b-positive microglia. A β O-induced activation of autophagy was detected in microglia derived from LMP7 KO slices whereas activation of mTOR pathway via S6 phosphorylation was present only in flow through cells, although surprisingly higher in those derived from LMP7 KO slices.

3.1.8. Increased proteasome activity and immunoproteasome expression in aged APP/PS1 mice

Since a recent study suggested an increase in immunoproteasome gene expression during aging and in microglia associated with A β -plaques in APP/PS1 mice [88], we analyzed proteasome activity and LMP7 protein expression in native brain lysates of APP/PS1 mice, LMP7 KO mice and a crossbreed of these two mouse strains at the age of 60, 120 and 250 days and compared them with age matched wild type mice (collaboration with Prof. Heppner, Neuropathology, Charité).

The proteasome activity in native mouse brain lysates was measured using the fluorogenic substrate Suc-LLVY-AMC, reflecting the chymotryptic-like activity of the 26S proteasome. The results revealed that the proteasome activity significantly increased in WT mice with aging, shown by an increase of 1.7-fold in 120 days old and even 1.9-fold in 250 days old mice compared to 60 days old mice. As expected, aged mice deficient for the immunoproteasome showed significantly lower proteasome activity (0.7-fold) compared with age matched WT mice. Interestingly, we detected significantly higher proteasome activity in 250 days old APP/PS1 mice with full established A β -pathology (1.7-fold) compared with 120 days old APP/PS1 mice. However, in aged APP/PS1 mice lacking the immunoproteasome, the proteasome activity was significantly decreased by 0.7-fold in 120 days old mice and by 0.6-fold in 250 old mice compared to age matched WT mice, respectively (Figure 24A). To test if the immunoproteasome is involved in the observed increase in activity, we performed native PAGE with the brain lysates followed by western blot to detect immunoproteasome subunits incorporated into 20S and 26S proteasome complexes. Corresponding to the proteasome activity measured by peptide hydrolysis, the resulting western blot showed an increasing signal with aging for LMP7 at the protein size of both 20S and 26S proteasome complexes in WT mice. Indeed, the signal even appears enhanced for aged APP/PS1 mice compared to WT mice (Figure 24B).

Taken together, we were able to show that proteasome activity is increased upon aging and enhanced in mice with plaque-pathology, accompanied by an increase in the amount of LMP7 containing proteasome complexes. In LMP7 KO and immunoproteasome deficient APP/PS1 mice, however, proteasome activity was decreased compared to WT and APP/PS1 mice. This data has been included in a recent publication [104]

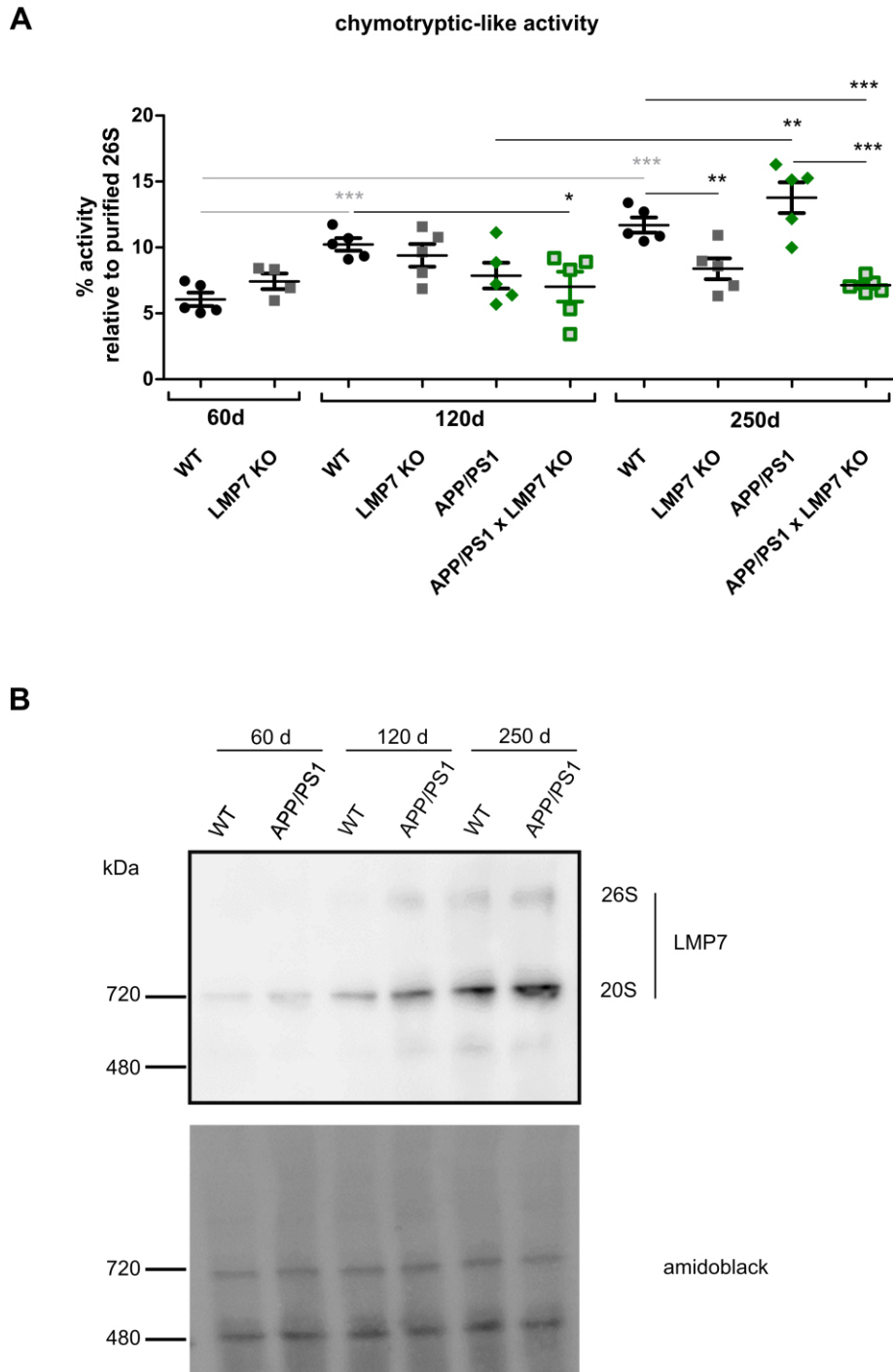


Figure 24: Proteasome activity and immunoproteasome expression is increased in APP/PS1 mice but reversed with immunoproteasome deficiency.

A Analysis of proteasome activity in brain lysates of 60, 120 and 250 d old WT, LMP7 KO, APP/PS1 and APP/PS1 x LMP7 KO mice by measuring hydrolysis of fluorogenic substrate Suc-LLVY-AMC (chymotryptic-like activity). Values represent mean \pm SEM, (* $p < 0.05$ ** $p < 0.005$ *** $p < 0.001$, student-t test). **B** Native PAGE of brain lysates of 60, 120 and 250 d old WT and APP/PS1 mice followed by western blot using in-house LMP7 antibody to visualize 26S and 20S proteasome complexes with LMP7 subunits incorporated. Amidoblack staining served as protein loading control.

3.2. Rapamycin decreases the amount of active proteasome subunits in 5xFAD mice

Earlier, we demonstrated the upregulation of the mTOR pathway via phosphorylation of downstream target S6 ribosomal protein in our ex vivo Alzheimer's disease model using organotypic brain slice culture. In addition, previously it has been shown that intervention in AD pathogenesis in mouse models by reduction of p70 kinase [97] or administration of mTOR inhibitor rapamycin [108] leads to improvements of the disease phenotype. According to these hints to mTOR as a link to AD pathology and using rapamycin as a therapeutic approach, we were further interested in the modulation of the proteasome activity. Therefore, in a collaboration with the lab of Prof. Priller (Molecular Psychiatry, Charité), we analyzed the proteasome activity in native brain lysates from 4 months old 5xFAD mice treated with rapamycin (RAPA) using fluorescently labeled probes targeting the active sites of the proteasome and compared them with equally treated age matched wild type mice.

First, our results demonstrated that in the cortex of 5xFAD mice the $\beta 1/\beta 1i$ subunit activity is 1.4-fold enhanced and $\beta 5/\beta 5i$ subunit activity is significantly enhanced by 1.2-fold compared to WT while the total proteasome activity remained unchanged (Figure

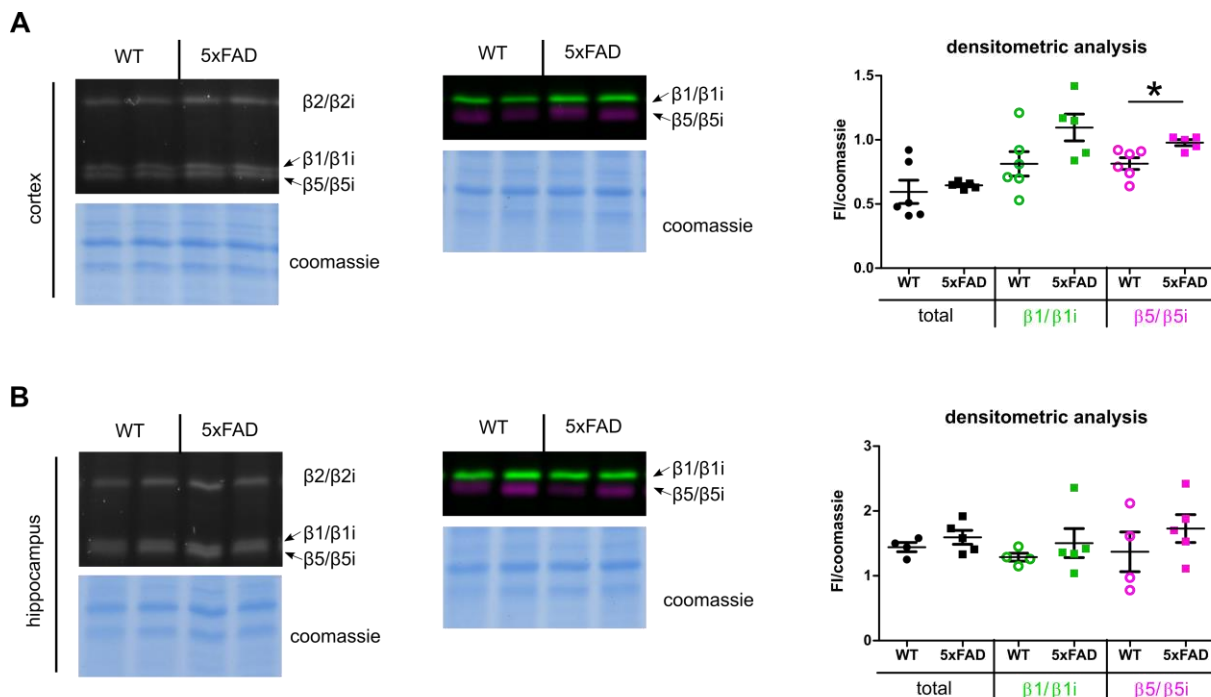


Figure 25: Enhanced proteasome activity in 5xFAD mice.

Left panel: Representative images of $\beta 1/2/5$ subunit activity and specific $\beta 1$ (green) and $\beta 5$ (magenta) subunit activity in native brain lysates of cortex (**A**) and hippocampus (**B**) tissue dissected from vehicle treated 4 months old WT and 5xFAD mice. Coomassie staining served as protein loading control. *Right panel:* Corresponding densitometric analysis normalized to coomassie staining (n = 5-6). Values represent mean with SEM (*p<0.05, student t-test).

25A). In the hippocampus of 5xFAD mice we observed a similar tendency with 1.2-fold higher amount of active $\beta 5/\beta 5i$ subunits compared to WT (Figure 25B).

In order to validate the effect of RAPA on WT mice as well as 5xFAD mice, we analyzed the protein levels and phosphorylation status of mTOR downstream targets p70 S6 kinase and S6 ribosomal protein. As expected, in cortex lysates we found that RAPA inhibits phosphorylation of p70K by 0.7-fold and significantly inhibits phosphorylation of S6 by 0.2-fold in WT mice. In RAPA-treated 5xFAD mice, however, phosphorylation of p70K was significantly increased by 1.7-fold whereas phosphorylation of S6 was decreased by 0.7-fold (Figure 26). Similar results were observed in hippocampus

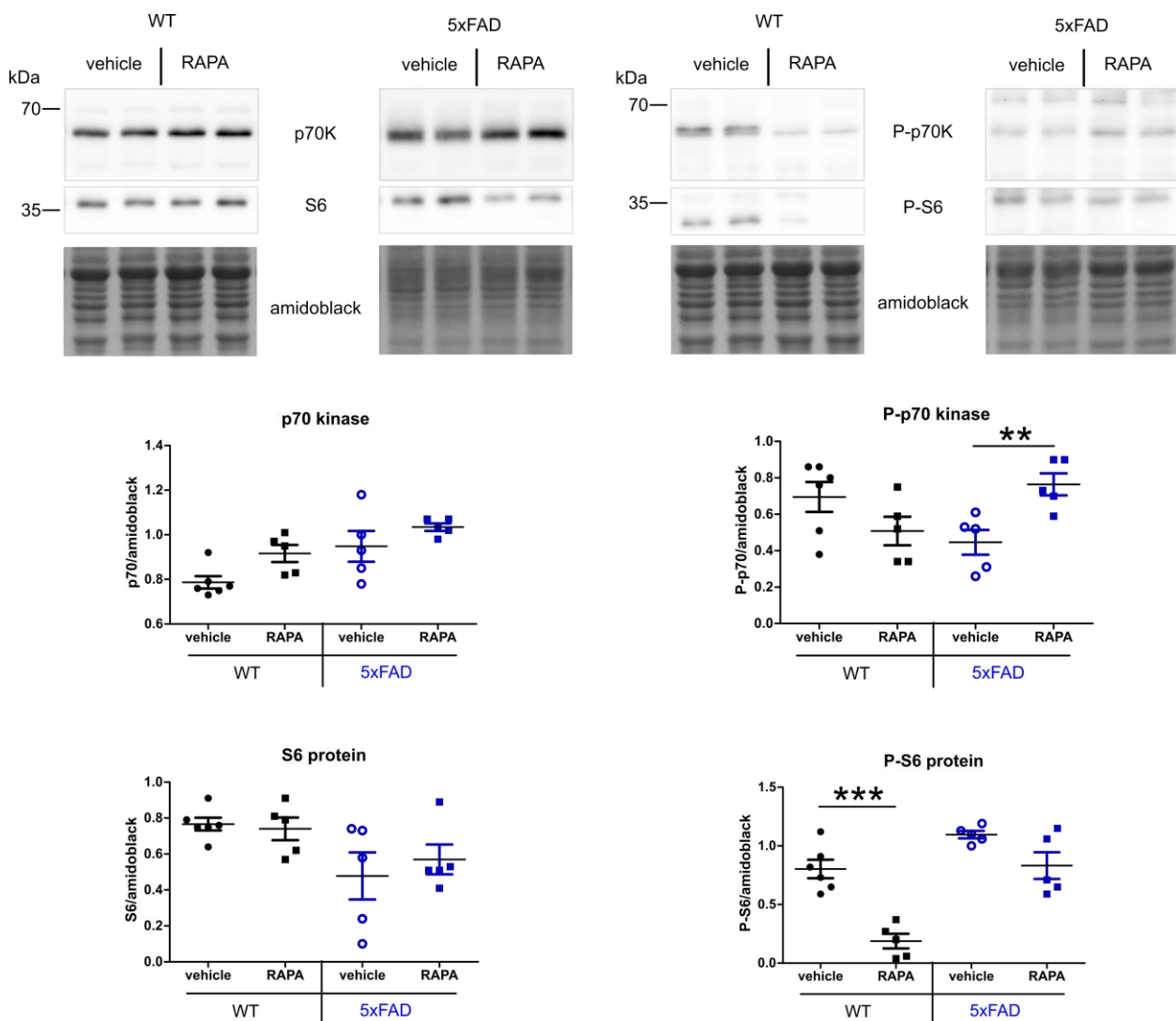


Figure 26: Rapamycin inhibits p70K and S6 phosphorylation in WT mice.

Upper panel: Western blot analysis of p70 kinase, S6 ribosomal protein and its phosphorylation status in native cortex lysates from 4 months old WT and 5xFAD mice treated with Rapamycin or vehicle. Amidoblack staining served as protein loading control. *Lower panel:* Corresponding densitometric analysis of protein levels normalized to amidoblack staining. Values represent mean with SEM (**p < 0.005, ***p < 0.001, student t-test).

lysates (data not shown).

We then measured the amount of active proteasome β -subunits in response to RAPA treatment in WT compared to 5xFAD mice. Surprisingly, by applying the pan-reactive proteasome probe to native lysates from cortex and hippocampus tissue, we found that neither in WT nor in 5xFAD the amount of active β subunits changed in mice treated with RAPA (Figure 27).

Using the proteasome probe mix, containing the inhibitors specific for $\beta 1/\beta 1i$ and $\beta 5/\beta 5i$ and labeled with two distinct fluorophores, we were able to gain more informative results. In native lysates of cortex tissue we found no changes in the amount of $\beta 1/\beta 1i$ active subunits, neither in WT nor in 5xFAD mice treated with RAPA (Figure 28A). In lysates of hippocampus tissue dissected from RAPA-treated WT mice, however, we detected a significant decrease in the amount of active $\beta 1/\beta 1i$ subunits by 0.5-fold. Furthermore, RAPA-treatment of 5xFAD mice resulted in a significant decrease of active $\beta 5/\beta 5i$ subunits by 0.6 - 0.7-fold in native hippocampus lysates (Figure 28B).

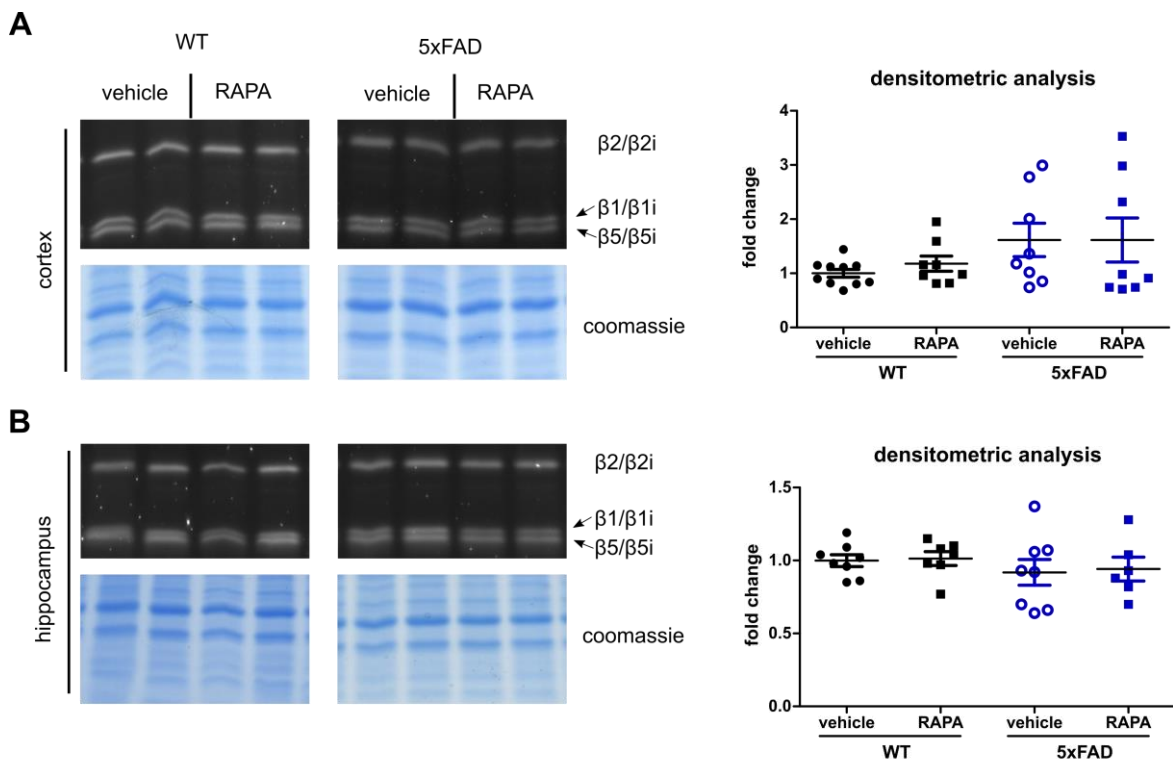


Figure 27: Rapamycin-treatment does not lead to changes in the total amount of active β subunits.

Left panel: Representative images of $\beta 1/2/5$ subunit activity in native brain lysates of cortex (**A**) and hippocampus (**B**) tissue dissected from vehicle- or RAPA-treated 4 months old WT and 5xFAD mice. Right panel: Corresponding densitometric analysis normalized to coomassie staining (n = 7-9). Fold changes were calculated to WT vehicle control. Values represent mean with SEM.

Rapamycin decreases the amount of active proteasome subunits in 5xFAD mice

In summary, we found higher levels of active $\beta 5/\beta 5i$ subunits in brain lysates of 5xFAD mice by 1.2-fold compared with WT mice. Rapamycin-treatment of 5xFAD mice resulted in a decrease in the amount of active $\beta 5/\beta 5i$ subunits in brain lysates by 0.8 – 0.7 fold.

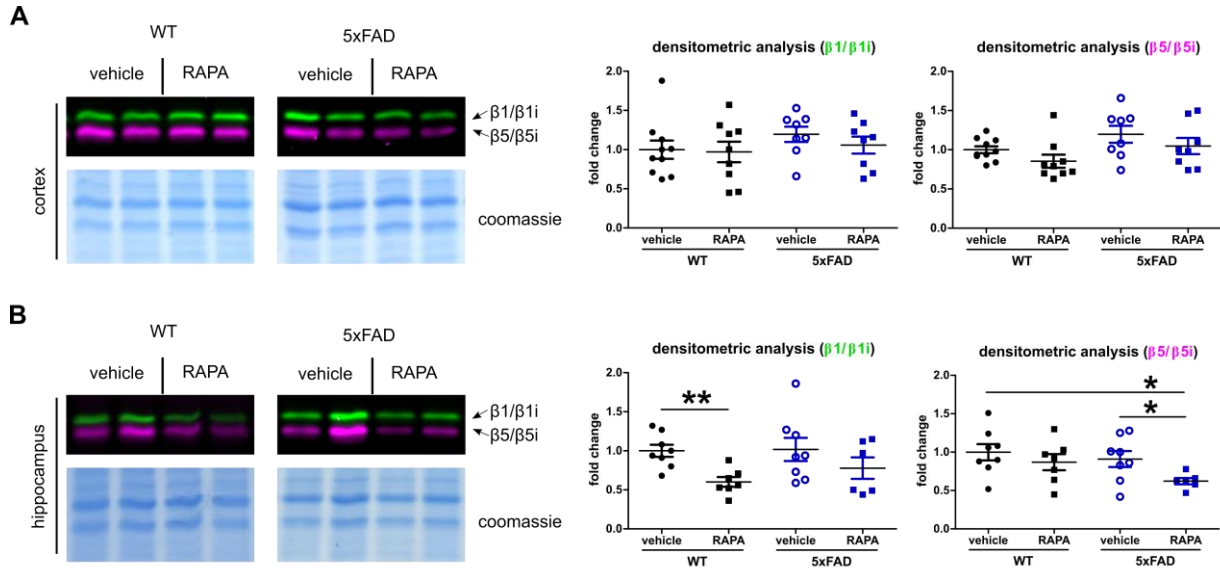


Figure 28: Rapamycin-treatment results in a decrease of active $\beta 1$ and $\beta 5$ subunits.

Left panel: Representative images of specific $\beta 1$ (green) and $\beta 5$ (magenta) subunit activity in native brain lysates of cortex (A) and hippocampus (B) tissue dissected from vehicle- or RAPA-treated 4 months old WT and 5xFAD mice. Right panel: Corresponding densitometric analysis normalized to coomassie staining (n = 7-9). Fold changes were calculated to WT vehicle control. Values represent mean with SEM (* $p < 0.05$, ** $p < 0.005$, student t-test).

4. Discussion

4.1. Perturbations in proteasome networks in experimental models of AD

Studies regarding the effect of amyloid- β on proteasome activity diverge. Inhibitory [82]–[86] as well as activating [87], [88] effects have been reported – in vitro using A β peptides, in vivo using mouse models exhibiting AD pathology as well as in post-mortem brain of AD patients. So far, in-vitro approaches were restricted to either interactions between A β and purified proteasomes or lysates or - if cell cultures were used – to effects of A β on neurons and glial cells cultured separately. Especially when immunomodulatory effects are expected in A β pathology (as presented in chapter 1.1.2.), interactions and communication between different cell types of the brain should be considered. We therefore aimed to elucidate the consequences of A β exposure simultaneous to all brain cells in a tissue network using organotypic brain slice culture (OBSCs). Thereby, we were able to demonstrate that oligomeric A β , that is considered to be a major contributor to AD pathology [103], clearly reduces the activity of proteasome β -subunits which is in concordance with early findings suggesting an inhibitory effect of A β [82]–[85], [109]. Using subunit-specific active site probes we further found that in particular active β 1/ β 1i subunits were significantly reduced in response to A β O-treatment. Unchanged levels of β 5/ β 5i might be due to initiating compensation by upregulation of β 5i activity, indicating initial immunoproteasome formation. Accordingly, we detected a moderate increase in LMP7 protein expression in A β O-treated OBSCs. Surprisingly, we detected no change in active β -subunits in OBSCs lacking the β 5i subunit and therefore the immunoproteasome. This underlines our hypothesis that the immunoproteasome plays a specific role in AD pathology. No changes in proteasome activity indicate the existence of a compensatory mechanism. It is conceivable that other degradation pathways, as for example autophagy, cover the lack of immunoproteasome. Indeed, studies have demonstrated a cross-talk between the UPS and autophagy [107]. To answer the question how A β O-induced proteotoxic stress is compensated when the immunoproteasome is absent, we analyzed the protein expression of autophagy marker LC3b. In fact, while proteasome inhibition by Bortezomib or A β O did not induce autophagy in our OBSC model, immunoproteasome deficient OBSCs react early with activation of autophagy upon A β O exposure. Supporting this finding, in a fly model of neurodegeneration it has been reported that an impaired proteasome induced autophagy as a compensatory mechanism, mediated by

poly-ubiquitin-interacting histone deacetylase 6 (HDAC6) [110]. Considering the absence of the immunoproteasome as an inherent impairment of the UPS, A β O exposure leads to autophagy much earlier than chemical proteasome inhibition or A β -induced proteasome impairment. We therefore propose that induced proteasome inhibition in our model will lead to activation of autophagy at later time points probably due to initial compensation by the immunoproteasome. Indeed, the promotion of autophagy by upregulation of p62 expression, has been shown to improve cognitive deficits in APP/PS1 mice [111]. Thus, the activation of autophagy via the inhibition or deactivation of the immunoproteasome might be a possible treatment strategy for AD.

As expected from previous studies [112], in our ex-vivo OBSC model we were able to show that chemical proteasome inhibition by Bortezomib resulted in a clear accumulation of insoluble poly-Ub-conjugated proteins and elevated protein levels of immunoproteasome β -subunit LMP7. In addition, we confirmed the induction of a type I IFN response with significantly elevated mRNA levels of IFN β and IFN stimulated genes Mx1 and Cxcl-10. This is in line with our previous study demonstrating an enhanced IFN response in patients exhibiting mutations and therefore defects in the proteasome [91]. A possible linkage between proteasome impairment and the production of IFNs has been identified in a current study of two patients with POMP-related autoinflammatory immunodeficiency diseases (PRAID). The analysis of PRAID-patient derived cells that displayed an established interferonopathy, revealed the clear upregulation of unfolded protein response (UPR) genes [113]. We therefore speculate that the accumulation of Ub-conjugates upon proteasome impairment induces endoplasmic reticulum (ER) stress resulting in UPR-mediated production of IFNs promoting inflammatory processes. Interferonopathies, meaning the abnormal production of IFNs and ISGs, have been associated with a number of CNS diseases [92]. In addition, the induction of type I IFNs in AD models have been demonstrated earlier [93]. With the knowledge of interferonopathies associated with proteasome defects and our observation of A β O-induced proteasome impairment, we expected to detect upregulation of IFNs and ISGs in response to A β O as well. Surprisingly, we were not able to show a clear type I IFN response in WT OBSCs treated with A β O. Nonetheless, since we observed significantly elevated levels of soluble Ub-conjugates in A β O-treated OBSCs and occasionally detected elevated levels of IFNs and ISGs, we assume that longer A β O-induced proteasome inhibition would finally lead to the phenotype that we observed by

chemical proteasome inhibition. This assumption is supported by the finding that levels of active $\beta 5/\beta 5i$ subunits remained unchanged upon $A\beta O$ -treatment. We therefore speculate an increase in active $\beta 5/\beta 5i$ subunits at later time points if the amount of insoluble Ub-conjugates further increases with prolonged proteasome impairment. Indeed, our results from analyzing proteasome activity and LMP7 protein levels in APP/PS1 mice clearly showed an increase in chymotryptic-like proteasome activity and LMP7 protein levels in mice exhibiting full established plaque pathology [104]. Furthermore, we detected elevated levels of active $\beta 5/\beta 5i$ subunits in cortex tissue of 5xFAD mice compared to WT. In this context we further conclude that whether $A\beta$ impairs proteasome activity or increases the activity by upregulation of the immunoproteasome depends on the stage of AD pathology or $A\beta$ aggregation state and therefore on the model and time point of analysis.

The analysis of basal levels of active β -subunits revealed significant lower levels in immunoproteasome deficient OBSCs compared to WT, which is in accordance with our previous findings demonstrating lower chymotryptic-like activity in adult LMP7 KO mouse brains [104]. This lack of basal proteasome activity due to the immunoproteasome deficiency in our OBSC model resulted in a mildly more pronounced accumulation of insoluble Ub-conjugates upon $A\beta O$ exposure compared to WT. Corresponding, we have previously shown that immunoproteasome deficiency together with inflammatory stimulation results in the accumulation of Ub-aggregates [48]. Moreover, we found that the presence of the immunoproteasome seems to be important for the activation of mTOR signaling. It has been shown before that proteasome activity is enhanced by inhibiting mTOR via enhancing proteasome assembly and thereby proteasome abundance [59], [60]. Nonetheless, the cross-talk between the proteasome system and mTOR signaling is discussed controversially. Thus, another study demonstrates the opposite phenomenon showing that the activation of mTOR is accompanied by elevated levels of the proteasome [114]. Our results, however, supports the first hypothesis showing that proteasome inhibition by Bortezomib or $A\beta Os$ activates mTOR signaling and confirm the relevance in AD pathology that has been observed before by Caccamo et al. [96]. Interestingly, in a follow-up study it has been demonstrated that reduction of phospho-S6 kinase improved cognitive impairment in an AD mouse model [97]. Supporting this, we found that immunoproteasome deficiency lacks mTOR activation in our $A\beta O$ -treated OBSCs

model and that LMP7 KO improves cognitive behavior in APP/PS1 mice [104]. These findings raise the possibility of the immunoproteasome as therapeutic target in CNS diseases. Similarly, it has been reported that specific inhibition by ONX-0914 or genetic deficiency of the immunoproteasome in mice is beneficial in LCMV-induced meningitis [55], [56]. In contrast, in a model of experimental autoimmune encephalomyelitis (EAE) we observed higher susceptibility to proteotoxic stress under immunoproteasome deficiency [48]. Nonetheless, recently immunoproteasome-specific inhibitor ONX0914 has been reported to display lower neurotoxicity compared to FDA-approved bortezomib and is therefore suggested to be a promising therapeutic alternative for neoplastic autoinflammatory diseases [115].

Using confocal microscopy we were able to verify the reduction in proteasome activity in immunoproteasome deficient brain slices. In addition, we detected less (activated) microglia but more astrocytes in A β O-treated OBSCs of LMP7 KO compared to WT. Interestingly, we found remarkable reduced Iba1+ microglia even in untreated LMP7 KO slices compared to WT. These findings indicate that immunoproteasome deficiency might result in a cellular environment that is less prone to inflammatory responses. This observation confirms our data from immunoproteasome deficient APP/PS1 mice that displayed a reduced microgliosis but enhanced astrogliosis as well as changes in cytokine secretion compared to APP/PS1 mice [104]. Since we observed an improved cognitive phenotype in immunoproteasome deficient APP/PS1 mice in that study, it is tempting to speculate that increasing astrocyte activity might be beneficial in AD pathogenesis. Indeed, it has been shown that attenuating astroglial activity accelerates plaque formation and promotes dystrophic neurites in APP/PS1 mice [116].

Furthermore, we found conspicuously increased proteasome signals nearby activated microglia in WT OBSCs treated with A β O that were not detected in LMP7 KO. An increase in proteasome activity in cultured microglia upon A β -treatment was also observed by Orre et al. [88] and attributed to increased immunoproteasome subunit expression. Nonetheless, they detected an increase in activity in cultured neurons and astrocytes as well. In that study, however, cells were treated 3 times longer (72 hrs) with A β peptides. This underlines our idea that proteasome activation with formation of the immunoproteasome might be a phenomenon of chronic A β exposure and our results reflect a pre-adaptation period with an initial decrease of proteasome activity. In this scenario microglia might be the first to react with immunoproteasome formation.

Our preliminary results obtained by CD11b-MACS separation of microglia supports the idea of the immunoproteasome expression being most abundant in microglia, since we detected much lower LMP7 expression in the flow-through fraction. In a similar manner, Kremer et al. [55] found LMP2 expression mainly co-localizing with microglia in cryosections of LCMV-injected mice brains. LMP2 signals in other than microglia cells were localized to nuclei of astrocytes [55]. Nonetheless, in a study of epileptogenesis in a rat model and human patients, elevated levels of the immunoproteasome subunits LMP2 and LMP7 were found in astrocytes and neurons of the hippocampus [117]. Similarly, in cortical neurons of patients with neurodegenerative disorder Huntington's disease, researchers found elevated levels of LMP2 and LMP7 [118]. We can therefore not exclude neurons as a source for LMP7 protein expression in the flow through as well. Further studies are definitely necessary to elucidate the relevance of immunoproteasome formation in the different cell types of the CNS.

Taken together, our results confirmed that proteasome impairment by specific inhibitor BTZ results in the accumulation of Ub-conjugates, a type I IFN response including STAT-signaling and the activation of mTOR that results in the production of ISGs (Figure 29A). Those ISGs might further promote the communication between neurons and immune cells of the CNS as microglia and astrocytes. Finally, we demonstrated that the effect of A β on the proteasome highly depends on the model and therefore on the time point and the dominating A β species. In particular we confirmed an inhibitory effect of A β O₂ in our OBSC model while we detected an increase in proteasome activity in A β -plaque exhibiting AD mouse models. In addition, we were able to support the hypothesis of the immunoproteasome playing a crucial role in AD pathogenesis. Based on our OBSC model we conclude that the presence of the immunoproteasome is essential for mTOR-mediated response to A β exposure (Figure 29A). The absence of the immunoproteasome, however, induces a fast compensation of A β -induced proteotoxic stress by autophagy (Figure 29B) which has been shown by others before to be beneficial in AD pathogenesis. Moreover, the immunoproteasome seems to be important for the activation of microglia and its absence promotes astroglial activity. Together with our published results showing a beneficial phenotype of immunoproteasome-deficient AD mice, our ex-vivo findings clearly support the idea of the immunoproteasome being a promising target in neurodegeneration.

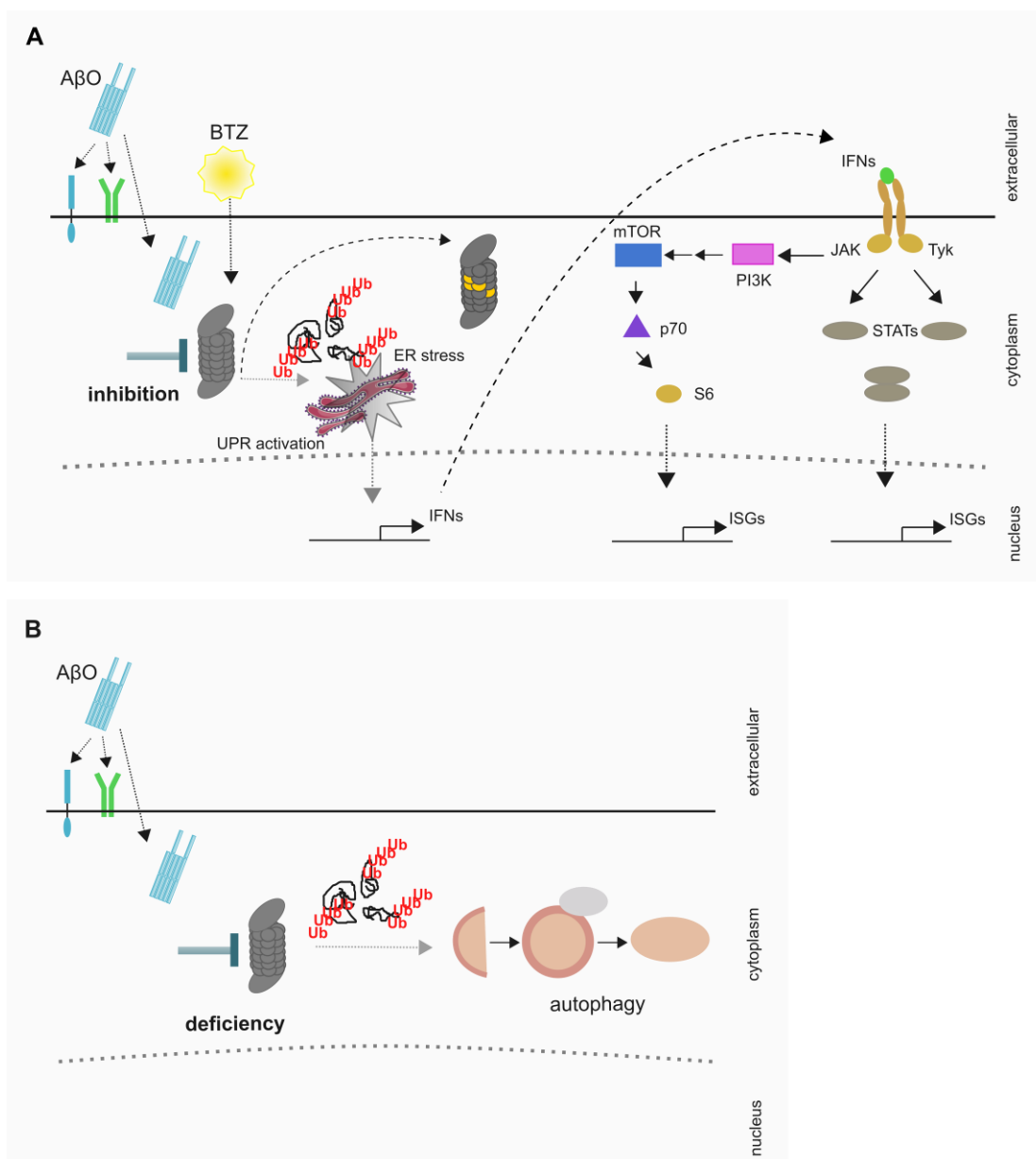


Figure 29: Models for neuroinflammatory events associated with proteasome impairment or deficiency.

A Proteasome impairment results in accumulation of Ub-conjugates that induce the formation of the immunoproteasome and might lead to ER stress that promotes the production of IFNs via UPR activation. IFNs in turn activate signaling via JAK/STAT or mTOR that result in the production of ISGs. A similar pathway is conceivable for AβO-induced proteotoxic stress being induced either indirectly via extracellular interactions with immune receptors or directly via intracellular interactions with the proteasome or its associated network factors. **B** In the absence of the immunoproteasome AβO-induced proteotoxic stress results in the activation of autophagy mechanisms that might compensate impairment of proteasome networks.

4.2. Interventions in proteasome-associated signaling in an AD mouse model

Accumulating evidence suggests that mTOR signaling plays an important role in i) the regulation of the UPS and ii) cross-talk with inflammatory pathways including IFN signaling. Activation of the mTOR pathway in Alzheimer's disease has been shown [96] and was confirmed in our ex-vivo model showing significantly elevated levels of

phospho-S6 ribosomal protein upon A β O exposure. We further demonstrated changes in proteasome activity depending on the experimental model with A β O-induced decrease but A β plaque-associated increase in proteasome activity. The reduction of p70 S6 kinase expression has been shown to improve learning in an AD mouse model [97] and mTOR inhibitor RAPA fed to mice extended their lifespan [61]. Furthermore, it has been demonstrated that neurodegeneration induced by proteasome inhibition was protected by RAPA-induced autophagy [119]. We were therefore interested how RAPA influences proteasome activity in an AD mouse model 5xFAD and its impact on AD pathology (assessed by the group of Prof. Priller, Neuropsychiatry, unpublished data).

First, we confirmed our results from analyzing proteasome activity in APP/PS1 mice and found an increase in β 1/ β 1i and β 5/ β 5i active subunits in 5xFAD mice compared to age matched WT mice. Interestingly, although rapamycin reduced the levels of phospho-S6 in both WT and 5xFAD, the effect was considerably stronger in WT. Surprisingly, in hippocampus tissue we observed a significant reduction in active β 1/ β 1i-subunits in RAPA-treated WT mice as well as a significant reduction in active β 5/ β 5i-subunits in RAPA-treated 5xFAD mice compared to untreated WT and 5xFAD mice. This finding contradicts the study of Zhao et al. [59] that shows an overall increase in protein degradation by mTOR inhibition. Another study, however, demonstrated the suppression of proteasome expression and thereby reduction in proteasome-mediated degradation by mTOR inhibition [114]. In concordance with the observed RAPA-induced reduction of proteasome activity, immunohistochemical analysis of 5xFAD brain sections revealed an increase in A β -plaque load in response to RAPA treatment (unpublished data, AG Priller). Furthermore, microgliosis was enhanced in those 5xFAD mice treated with rapamycin and FACS analysis revealed changes in the microglia phenotype with a decrease in CD11c+ cells (unpublished data, AG Priller). CD11c+ microglia have been described as a plaque-associated subtype that is thought to play a crucial role in A β -uptake and promoting inflammatory events [120]. RAPA has been shown to have immunomodulatory effects due to the role of mTOR in regulating immune cells [62]. In our study this has been manifested in the changes of microglia numbers and phenotype. The question remains if the RAPA-induced decrease of proteasome activity or the reduction in A β -degrading and inflammatory CD11c+ phenotype of microglia is responsible for the increase in plaque load. It is further unclear, if the reduction in proteasome activity accompanied by an increase in plaque

load is beneficial or detrimental for AD pathogenesis including cognitive deficits. It has been shown in 3xTg-AD mice, however, that the time point for RAPA-administration determines the effects on cognition. Thus, it has been found that continuously RAPA-treatment before establishment of disease signs significantly reduced plaque formation and improved cognitive deficits whereas the administration of RAPA at later time points when plaque formation was established had no effect [121]. We found that 5xFAD mice in our study already exhibited A β -plaques at the time point of RAPA-treatment (unpublished data, AG Priller). This might account for the unexpected reduction in proteasome activity and increase in plaque pathology. We therefore conclude that additional studies including much earlier treatment strategies and assessment of cognitive behavior are necessary.

Abbreviations

AD	Alzheimer's disease
A β	amyloid- β
A β O	amyloid- β oligomer
APP	amyloid precursor protein
AICD	amyloid precursor protein intracellular domain
AMC	7-amino-4-methycoumarin
APOE	apolipoprotein E
ASP	active site probe
ATP	adenosinetriphosphate
BACE	beta-secretase
BBB	blood brain barrier
BCA	bicinchoninic acid
bp	base pairs
BSA	bovine serum albumin
BTZ	bortezomib
β -CTF (C99)	short C-terminal fragment
cDNA	complementary desoxyribonucleic acid
CNS	central nervous system
CSF	cerebrospinal fluid
CD	cluster of differentiation
CD11b	cluster of differentiation 11 antigen-like family member b
COX	cyclooxygenase
C _t	threshold cycle
Ctrl	control
Cxcl-10	C-X-C Motif Chemokine Ligand 10
CVB	coxsackie virus B
DIV	days in vitro
DMEM	Dulbecco's Modified Eagle Medium

DMSO	dimethyl sulfoxide
DNA	desoxyribonucleic acid
dNTP	desoxyribonukleosidtriphosphate
DTT	dithiothreitol
DUB	deubiquitinating enzyme
EAE	experimental autoimmune encephalomyelitis
ECL	enhanced chemiluminescence
EDTA	ethylenediaminetetraacetic acid
FAD	familial Alzheimer's disease
FI	fluorescence intensity
g	gravity
GFP	green fluorescent protein
GFAP	glial fibrillary acidic protein
HBSS	Hank's balanced salt solution
HEPES	4-(2-hydroxyethyl)-1-piperazineethanesulfonic acid
HFIP	1,1,1,3,3,3-Hexafluoro-2-propanol
Hprt	Hypoxanthine Phosphoribosyltransferase
HRP	horse radish peroxidase
h	hour
hrs	hours
Iba1	Ionized Calcium-Binding Adapter Molecule 1
IgG	immunoglobulin G
IL	interleukin
IFN	interferon
IFNAR	interferon α receptor
IRF	interferon regulating factor
ISG	interferon stimulated gene
iNOS	inducible nitric oxide synthase
JAK	janus kinase
KCl	potassium chloride

KO	knock out
LC3	light chain 3
LPS	lipopolysaccharide
LMP	large multifunctional peptidase
LCMV	lymphocytic choriomeningitis virus
LTP	long term potentiation
KCa3.1	calcium-dependent potassium channel
MACS	magnetic activated cell sorting
MAP2	microtubuli associated protein 2
MCI	mild cognitive impairment
MECL	multicatalytic endopeptidase complex
MgCl	magnesium chloride
MHC	major histocompatibility complex
min	minutes
µg	mikrogramm
µl	microliter
mL	milliliter
µm	mikrometer
mM	millimolar
mRNA	messenger ribonucleic acid
MS	multiple sclerosis
mTOR	mammalian target of rapamycin
MVB	multi vesicular body
Mx1	Myxovirus Resistance Protein 1
NaCl	sodium chloride
NeuN	Neuronal nucleic antigen
NFκB	nuclear factor κ-light chain enhancer of activated B-cells
nM	nanomolar
nm	nanometer
N _{2(l)}	liquid nitrogen

NO	nitric oxide
NTF	neurofibrillary tangle
OBSC	organotypic brain slice culture
polyI:C	polyriboinosinic-polyribocytidilic acid
P	postnatal
p	probability (statistics)
p	phosphorylated (protein)
p70	p70 S6 ribosomal protein kinase
PA	proteasome activator
PAGE	polyacrylamide gelelectrophoresis
PBS	phosphate buffered saline
qRT-PCR	quantitative real-time polymerase chain reaction
PBS	phosphate buffered saline
PSMB	proteasome subunit beta
PSD	postsynaptic density
PS1	Presenilin 1
PRAAS	proteasome-associated autoinflammatory syndrome
PVDF	polyvinylidene difluoride
RAGE	receptor for advanced glycation end products
RAPA	rapamycin
RE	relative expression
ROS	reactive oxygen species
rpm	rounds per minute
RNA	ribonucleic acid
RNS	reactive nitrogen species
RT	room temperature
sAPP β	soluble amyloid precursor protein β
s	seconds
S6	S6 ribosomal protein
SDS	sodium dodecyl sulfate

SEM	standard error mean
SRA	scavenger receptor A
STAT	signal transducer and activator of transcription
SH-SY5Y	human neuroblastoma cell line
SP	stratum pyramidale
SR	stratum radiatum
TAE	Tris acetic acid EDTA
TAMRA	tetramethylrhodamine
TBS	tris buffered saline
TNF α	tumor necrosis factor α
TREM2	triggering receptor expressed on myeloid cells 2
TLR	toll-like receptor
UPS	ubiquitin protein system
Ub	ubiquitin
UV	ultra violet
V	volt
v or vctrl	vehicle control
WI	water immersion
WT	wild type

List of figures

Figure 1: Cleavage of amyloid- β from APP.	6
Figure 2: The structure of the proteasome and degradation of Ub-conjugated proteins.	10
Figure 3: Intersections between IFN signaling and the UPS.	13
Figure 4: Experimental setup for organotypic brain slice culture.	21
Figure 5: Characterization of A β O preparation.	33
Figure 6: Concentration depended decrease of active subunits upon A β O treatment.	34
Figure 7: A β O-induced decrease of active β 1 subunits in WT OBSCs.	35
Figure 8: Proteasome inhibition by Bortezomib results in higher insoluble Ubiquitin positive fraction.	36
Figure 9: Chemical proteasome inhibition by Bortezomib upregulates LMP7 protein expression.	37
Figure 10: Type I IFN induced JAK-STAT signaling.	38
Figure 11: Bortezomib induces a Type I IFN response.	39
Figure 12: Bortezomib but not A β O activate STAT1 and ISG transcription.	41
Figure 13: Proteasome inhibition by Bortezomib results in p70/S6 activation.	43
Figure 14: A β O-induced p70/S6 (mTOR) pathway in WT OBSCs.	44
Figure 15: Suppression of autophagy upon Bortezomib and A β O-induced autophagy in LMP7 KO OBSCs.	45
Figure 16: Experimental setup for confocal imaging.	46
Figure 17: Reduced proteasome activity in immunoproteasome deficient OBSCs.	47
Figure 18: A β O-induced microgliosis.	48
Figure 19: A β O-induced astrogliosis in immunoproteasome deficient OBSCs.	49
Figure 20: MACS-separating of Cd11b-positive microglia from OBSCs.	51
Figure 21: Differential expression of iP subunits in MACS-separated microglia versus flow through.	52
Figure 22: Differential gene expression of A β O-induced Type I IFN response in CD11b-separated microglia.	53
Figure 23: Analysis of mTOR and autophagy activation in CD11b-separated microglia.	54
Figure 24: Proteasome activity and immunoproteasome expression is increased in APP/PS1 mice but reversed with immunoproteasome deficiency.	57
Figure 25: Enhanced proteasome activity in 5xFAD mice.	58
Figure 26: Rapamycin inhibits p70K and S6 phosphorylation in WT mice.	59
Figure 27: Rapamycin-treatment does not lead to changes in the total amount of active β subunits.	60
Figure 28: Rapamycin-treatment results in a decrease of active β 1 and β 5 subunits.	61

Figure 29: Models for neuroinflammatory events associated with proteasome impairment or deficiency.....	67
---	----

List of tables

Table 1: Primer sequences for LMP7 genotyping.....	20
Table 2: PCR conditions for LMP7 genotyping.....	20
Table 3: Antibodies used for immunodetection in western or dot blot.....	26
Table 4: Antibodies for immunofluorescence stainings in organotypic brain slices.....	28
Table 5: cDNA synthesis master mix.....	29
Table 6: Pre-amplification protocol.....	30
Table 7: Taqman primer assays.....	30
Table 8: Quantitative real-time PCR master mix.....	31
Table 9: Quantitative real-time PCR program.....	31

References

- [1] A. Alzheimer, "Über eine eigenartige Erkrankung der Hirnrinde.," *Allg. Zeitschrift für Psychiatr. und Psych. Medizin*, vol. 64, pp. 146–148, 1907.
- [2] P. Scheltens, K. Blennow, M. B. M. Breteler, B. de Strooper, G. B. Frisoni, S. Salloway, W. M. Van der Flier, "Alzheimer ' s disease," *Lancet*, vol. 388, no. 10043, pp. 505–517, 2016.
- [3] R. Vassar, P.-H. Kuhn, C. Haass, M. E. Kennedy, L. Rajendran, P. C. Wong, and S. F. Lichtenthaler, "Function, therapeutic potential and cell biology of BACE proteases: Current status and future prospects," *Journal of Neurochemistry*, vol. 130, no. 1. pp. 4–28, 2014.
- [4] M. Takami, Y. Nagashima, Y. Sano, S. Ishihara, M. Morishima-Kawashima, S. Funamoto, and Y. Ihara, "γ-Secretase: Successive Tripeptide and Tetrapeptide Release from the Transmembrane Domain of -Carboxyl Terminal Fragment," *J. Neurosci.*, vol. 29, no. 41, pp. 13042–13052, 2009.
- [5] E. Portelius, E. Price, G. Brinkmalm, M. Stiteler, M. Olsson, R. Persson, A. Westman-Brinkmalm, H. Zetterberg, A. J. Simonb, K. Blennowa, "A novel pathway for amyloid precursor protein processing," *Neurobiol. Aging*, vol. 32, no. 6, pp. 1090–1098, 2011.
- [6] J. T. Jarrett, E. P. Berger, and P. T. Lansbury, "The Carboxy Terminus of the β Amyloid Protein Is Critical for the Seeding of Amyloid Formation: Implications for the Pathogenesis of Alzheimer's Disease," *Biochemistry*, vol. 32, no. 18, pp. 4693–4697, 1993.
- [7] J. C. Polanco, C. Li, L. G. Bodea, R. Martinez-Marmol, F. A. Meunier, and J. Götz, "Amyloid-β and tau complexity - Towards improved biomarkers and targeted therapies," *Nature Reviews Neurology*, vol. 14, no. 1. Nature Publishing Group, pp. 22–40, 2018.
- [8] F. M. LaFerla, K. N. Green, and S. Oddo, "Intracellular amyloid-β in Alzheimer's disease," *Nature Reviews Neuroscience*, vol. 8, no. 7. pp. 499–509, 2007.
- [9] B. De Strooper and E. Karran, "The Cellular Phase of Alzheimer ' s Disease," *Cell*, vol. 164, no. 4, pp. 603–615, 2016.
- [10] M. T. Heneka, D. T. Golenbock, and E. Latz, "Innate immunity in Alzheimer ' s disease," *Nat. Publ. Gr.*, vol. 16, no. 3, pp. 229–236, 2015.
- [11] F. L. Heppner, R. M. Ransohoff, and B. Becher, "Immune attack : the role of inflammation in Alzheimer disease," *Nat. Publ. Gr.*, vol. 16, no. 6, pp. 358–372, 2015.
- [12] B. A. In ' T Veld, A. Ruitenber, A. Hofman, L. J. Launer, C. M. V. Duijn, T. Stijnen, M. M.B. Breteler, and B. H.C. Stricker, "Nonsteroidal Antiinflammatory Drugs and the Risk of Alzheimer ' S Disease," *N. Engl. J. Med.*, vol. 345, no. 21, pp. 1515–1521, 2001.
- [13] S. Weggen, J. L. Eriksen, P. Das, S. A. Sagi, R. Wang, C. U. Pietrzik, K. A. Findlay, T. E. Smith, M. P. Murphy, T. Bulter, D. E. Kang, N. Marquez-Sterling, T. E. Golde and E. H. Koo, "A subset of NSAIDs lower amyloidogenic Aβ42 independently of cyclooxygenase activity," *Nature*, vol. 414, no. 6860, pp. 212–216, 2001.
- [14] M. Sastre, I. Dewachter, G. E. Landreth, T. M. Willson, T. Klockgether, F. van Leuven, and M. T. Heneka, "Nonsteroidal anti-inflammatory drugs and peroxisome proliferator-activated receptor-gamma agonists modulate immunostimulated processing of amyloid precursor protein through regulation of beta-secretase.," *J. Neurosci.*, vol. 23, no. 30, pp.

- 9796–804, 2003.
- [15] F. Brosseron, M. Krauthausen, M. Kummer, and M. T. Heneka, “Body Fluid Cytokine Levels in Mild Cognitive Impairment and Alzheimer’s Disease: a Comparative Overview,” *Mol. Neurobiol.*, vol. 50, no. 2, pp. 534–544, 2014.
- [16] E. M. Bradshaw, L. B. Chibnik, B. T. Keenan, L. Ottoboni, T. Raj, A. Tang, L. L. Rosenkrantz, S. Imboywa, M. Lee, A. Von Korff, The Alzheimer’s Disease Neuroimaging Initiative, M. C. Morris, D. A. Evans, K. Johnson, R. A. Sperling, J. A. Schneider, D. A. Bennett and P. L. De Jager, “CD33 Alzheimer ’ s disease locus: altered monocyte function and amyloid biology,” *Nat. Publ. Gr.*, vol. 16, no. 7, pp. 848–850, 2013.
- [17] T. Jonsson, H. Stefansson, S. Steinberg, I. Jonsdottir, P. V. Jonsson, J. Snaedal, S. Bjornsson, J. Huttenlocher, A. I. Levey, J. J. Lah, D. Rujescu, H. Hampel, I. Giegling, O. A. Andreassen, K. Engedal, I. Ulstein, S. Djurovic, C. Ibrahim-Verbaas, A. Hofman, M. A. Ikram, C. M. van Duijn, U. Thorsteinsdottir, A. Kong, and K. Stefansson, “Variant of TREM2 Associated with the Risk of Alzheimer’s Disease,” *N. Engl. J. Med.*, vol. 368, no. 2, pp. 107–116, 2013.
- [18] R. Guerreiro, A. Wojtas, J. Bras, M. Carrasquillo, E. Rogaeva, E. Majounie, C. Cruchaga, C. Sassi, J. S. K. Kauwe, S. Younkin, L. Hazrati, J. Collinge, J. Pocock, T. Lashley, J. Williams, J.-C. Lambert, P. Amouyel, A. Goate, R. Rademakers, K. Morgan, J. Powell, P. St. George-Hyslop, A. Singleton, and J. Hardy for the Alzheimer Genetic Analysis Group, “TREM2 Variants in Alzheimer’s Disease,” *N. Engl. J. Med.*, vol. 368, no. 2, pp. 117–127, 2013.
- [19] D. Krstic, A. Madhusudan, J. Doehner, P. Vogel, T. Notter, and C. Imhof, “Systemic immune challenges trigger and drive Alzheimer-like neuropathology in mice Systemic immune challenges trigger and drive Alzheimer-like neuropathology in mice,” 2012.
- [20] I. Benilova, E. Karran, and B. De Strooper, “The toxic A β oligomer and Alzheimer’s disease: an emperor in need of clothes,” *Nat. Neurosci.*, vol. 15, no. 3, pp. 349–357, 2012.
- [21] I. Maezawa, P. I. Zimin, H. Wulff, and L. W. Jin, “Amyloid- β protein oligomer at low nanomolar concentrations activates microglia and induces microglial neurotoxicity,” *J. Biol. Chem.*, vol. 286, no. 5, pp. 3693–3706, 2011.
- [22] T.-I. Kam, S. Song, Y. Gwon, H. Park, J.-J. Yan, I. Im, J.-W. Choi, T.-Y. Choi, J. Kim, D.-K. Song, T. Takai, Y.-C. Kim, K.-S. Kim, S.-Y. Choi, S. Choi, W. L. Klein, J. Yuan, and Y.-K. Jung, “Fc γ RIIb mediates amyloid- β neurotoxicity and memory impairment in Alzheimer ’ s disease,” *J. Clin. Invest.*, vol. 123, no. 7, pp. 2791–2802, 2013.
- [23] E. Sturchler, A. Galichet, M. Weibel, E. Leclerc, and C. W. Heizmann, “Site-Specific Blockade of RAGE-V d Prevents Amyloid-beta Oligomer Neurotoxicity,” *J Neurosci*, vol. 28, no. 20, pp. 5149–5158, 2008.
- [24] C. Balducci, A. Frasca, M. Zotti, P. La Vitola, E. Mhillaj, E. Grigoli, M. Iacobellis, F. Grandi, M. Messa, L. Colombo, M. Molteni, L. Trabace, C. Rossetti, M. Salmona, and G. Forloni, “Brain , Behavior , and Immunity Toll-like receptor 4-dependent glial cell activation mediates the impairment in memory establishment induced by b -amyloid oligomers in an acute mouse model of Alzheimer ’ s disease,” *Brain Behav. Immun.*, vol. 60, pp. 188–197, 2017.
- [25] M. Calvo-Rodríguez, C. de la Fuente, M. García-Durillo, C. García-Rodríguez, C. Villalobos, and L. Núñez, “Aging and amyloid β oligomers enhance TLR4 expression, LPS-induced Ca $^{2+}$ responses, and neuron cell death in cultured rat hippocampal neurons,” *J. Neuroinflammation*, vol. 14, no. 1, pp. 1–13, 2017.

- [26] M. T. Ferretti, M. A. Bruno, A. Ducatzenzeiler, W. L. Klein, and A. C. Cuervo, "Intracellular A β -oligomers and early inflammation in a model of Alzheimer's disease," *Neurobiol. Aging*, vol. 33, no. 7, pp. 1329–1342, 2012.
- [27] M. Prinz and J. Priller, "Microglia and brain macrophages in the molecular age: from origin to neuropsychiatric disease," *Nat. Publ. Gr.*, vol. 15, no. 5, pp. 300–312, 2014.
- [28] M. Stalder, A. Phinney, A. Probst, B. Sommer, M. Staufenbiel, and M. Jucker, "Association of Microglia with Amyloid Plaques in Brains of APP23 Transgenic Mice," *Am. J. Pathol.*, vol. 154, no. 6, pp. 1673–1684, 1999.
- [29] G. Krabbe, A. Halle, V. Matyash, J. L. Rinnenthal, G. D. Eom, U. Bernhardt, K. R. Miller, S. Prokop, H. Kettenmann, F. L. Heppner, "Functional Impairment of Microglia Coincides with Beta-Amyloid Deposition in Mice with Alzheimer-Like Pathology," *PLoS One*, vol. 8, no. 4, 2013.
- [30] M. Orre, W. Kamphuis, L. M. Osborn, A.H.P. Jansen, L. Kooijman, K. Bossers, and E. M. Hol, "Isolation of glia from Alzheimer's mice reveals inflammation and dysfunction," *Neurobiol. Aging*, vol. 35, no. 12, pp. 2746–2760, 2014.
- [31] K. M. Lucin, C. E. O'Brien, G. Bieri, E. Czirr, K. I. Mosher, R. J. Abbey, D. F. Mastroeni, J. Rogers, B. Spencer, E. Masliah, and T. Wyss-Coray, "Microglial Beclin 1 Regulates Retromer Trafficking and Phagocytosis and Is Impaired in Alzheimer's Disease," *Neuron*, vol. 79, no. 5, pp. 873–886, 2013.
- [32] S. A. Grathwohl, R. E. Kälin, T. Bolmont, S. Prokop, G. Winkelmann, S. A. Kaeser, J. Odenthal, R. Radde, T. Eldh, S. Gandy, A. Aguzzi, M. Staufenbiel, P. M. Mathews, H. Wolburg, F. L. Heppner, and M. Jucker, "Formation and maintenance of Alzheimer's disease β -amyloid plaques in the absence of microglia," *Nat. Neurosci.*, vol. 12, no. 11, pp. 1361–1363, 2009.
- [33] S. A. Liddelow and B. A. Barres, "Reactive Astrocytes: Production, Function, and Therapeutic Potential," *Immunity*, vol. 46, no. 6. Elsevier Inc., pp. 957–967, 2017.
- [34] M. V. Sofroniew and H. V. Vinters, "Astrocytes: Biology and pathology," *Acta Neuropathologica*, vol. 119, no. 1. pp. 7–35, 2010.
- [35] S. A. Liddelow, K. A. Guttenplan, L. E. Clarke, F. C. Bennett, C. J. Bohlen, L. Schirmer, M. L. Bennett, A. E. Münch, W.-S. Chung, T. C. Peterson, D. K. Wilton, A. Frouin, B. A. Napier, N. Panicker, M. Kumar, M. S. Buckwalter, D. H. Rowitch, V. L. Dawson, T. M. Dawson, B. Stevens and B. A. Barres, "Neurotoxic reactive astrocytes are induced by activated microglia," *Nature*, vol. 541, no. 7638, pp. 481–487, 2017.
- [36] R. Medeiros and F. M. LaFerla, "Astrocytes: Conductors of the Alzheimer disease neuroinflammatory symphony," *Experimental Neurology*, vol. 239, no. 1. Elsevier Inc., pp. 133–138, 2013.
- [37] I. Carrero, M. R. Gonzalo, B. Martin, J. M. Sanz-Anquela, J. Arévalo-Serrano, and A. Gonzalo-Ruiz, "Oligomers of beta-amyloid protein (A β 1-42) induce the activation of cyclooxygenase-2 in astrocytes via an interaction with interleukin-1beta, tumour necrosis factor-alpha, and a nuclear factor kappa-B mechanism in the rat brain," *Exp. Neurol.*, vol. 236, no. 2, pp. 215–227, 2012.
- [38] T. Wyss-Coray, J. D. Loike, T. C. Brionne, E. Lu, R. Anankov, F. Yan, S. C. Silvesterstein and J. Husemann "Adult mouse astrocytes degrade amyloid-beta in vitro and in situ.," *Nat. Med.*, vol. 9, no. 4, pp. 453–457, 2003.
- [39] M. Koistinaho, S. Lin, X. Wu, M. Esterman, D. Koger, J. Hanson, R. Higgs, F. Liu, S. Malkani, K. R. Bales and S. M. Paul, "Apolipoprotein E promotes astrocyte colocalization and degradation of deposited amyloid- β peptides," *Nat. Med.*, vol. 10, no. 7, pp. 719–726,

- 2004.
- [40] D. Terwel, K. R. Steffensen, P. B. Verghese, M. P. Kummer, J.-Å. Gustafsson, D. M. Holtzman, and M. T. Heneka, "Critical Role of Astroglial Apolipoprotein E and Liver X Receptor- Expression for Microglial A Phagocytosis," *J. Neurosci.*, vol. 31, no. 19, pp. 7049–7059, 2011.
- [41] R. Pihlaja, J. Koistinaho, R. Kauppinen, J. Sandholm, H. Tanila, and M. Koistinaho, "Multiple cellular and molecular mechanisms Are involved in human A β clearance by transplanted adult astrocytes," *Glia*, vol. 59, no. 11, pp. 1643–1657, 2011.
- [42] M. Olabarria, H. N. Noristani, A. Verkhratsky, and J. J. Rodríguez, "Concomitant astroglial atrophy and astrogliosis in a triple transgenic animal model of Alzheimer's disease," *Glia*, vol. 58, no. 7, pp. 831–838, 2010.
- [43] I. Livneh, V. Cohen-Kaplan, C. Cohen-Rosenzweig, N. Avni, and A. Ciechanover, "The life cycle of the 26S proteasome: from birth, through regulation and function, and onto its death," *Cell Res.*, vol. 26, no. 8, pp. 869–885, 2016.
- [44] P. M. Kloetzel, "Antigen processing by the proteasome.," *Nat. Rev. Mol. Cell Biol.*, vol. 2, no. 3, pp. 179–187, 2001.
- [45] A. Brehm and E. Krüger, "Dysfunction in protein clearance by the proteasome : impact on autoinflammatory diseases," pp. 323–333, 2015.
- [46] E. Krüger and P.-M. Kloetzel, "Immunoproteasomes at the interface of innate and adaptive immune responses: two faces of one enzyme.," *Curr. Opin. Immunol.*, vol. 24, no. 1, pp. 77–83, Feb. 2012.
- [47] F. Ebstein, A. Voigt, N. Lange, A. Warnatsch, F. Schroeter, T. Prozorovski, U. Kuckelkorn, O. Aktas, U. Seifert, P.-M. Kloetzel, and E. Krueger, "Immunoproteasomes are important for proteostasis in immune responses.," *Cell*, vol. 152, no. 5, pp. 935–7, Feb. 2013.
- [48] U. Seifert *et al.*, "Immunoproteasomes preserve protein homeostasis upon interferon-induced oxidative stress.," *Cell*, vol. 142, no. 4, pp. 613–24, Aug. 2010.
- [49] G. A. Collins and A. L. Goldberg, "The Logic of the 26S Proteasome," *Cell*, vol. 169, no. 5, pp. 792–806, 2017.
- [50] M. Aki, N. Shimbara, M. Takashina, K. Akiyama, S. Kagawa, T. Tamura, N. Tanahashi, T. Yoshimura, K. Tanaka, and A. Ichihara, "Interferon-gamma induces different subunit organizations and functional diversity of proteasomes.," *J. Biochem.*, vol. 115, no. 2, pp. 257–269, 1994.
- [51] P. M. Kloetzel, "Generation of major histocompatibility complex class I antigens : functional interplay between proteasomes and TPPII," vol. 5, no. 7, pp. 661–669, 2004.
- [52] R. Stohwasser, U. Kuckelkorn, R. Kraft, S. Kostka, and P. M. Kloetzel, "20S proteasome from LMP7 knock out mice reveals altered proteolytic activities and cleavage site preferences," *FEBS Lett.*, vol. 383, no. 1–2, pp. 109–113, 1996.
- [53] B. Rada and T. L. Leto, "Oxidative innate immune defenses by Nox / Duox family NADPH oxidases," *Trends Innate Immun.*, vol. 15, pp. 164–187, 2008.
- [54] H. Fehling, W. Swat, C. Laplace, and R. Kuhn, "MHC class I expression in mice lacking the proteasome subunit LMP-7," no. April, 1994.
- [55] M. Kremer, A. Henn, C. Kolb, M. Basler, J. Moebius, B. Guillaume, M. Leist, B. J. Van den Eynde and M. Groettrup, "Reduced Immunoproteasome Formation and Accumulation of Immunoproteasomal Precursors in the Brains of Lymphocytic

- Choriomeningitis Virus-Infected Mice,” *J. Immunol.*, vol. 185, no. 9, pp. 5549–5560, 2010.
- [56] S. Mundt, B. Engelhardt, C. J. Kirk, M. Groettrup, and M. Basler, “Inhibition and deficiency of the immunoproteasome subunit LMP7 attenuates LCMV-induced meningitis,” *Eur. J. Immunol.*, vol. 46, no. 1, pp. 104–113, 2016.
- [57] J. Reis, F. Hassan, X. Qin Guan, J. Shen, J. J. Monaco, C. J. Papasian, A. A. Qureshi, C. W. Van Way III, S. N. Vogel, D. C. Morrison, N. Qureshi, “The Immunoproteasomes Regulate LPS-Induced TRIF/TRAM Signaling Pathway in Murine Macrophages,” *Cell Biochem. Biophys.*, vol. 60, no. 1–2, pp. 119–126, 2011.
- [58] E. Opitz, A. Koch, K. Klingel, F. Schmidt, S. Prokop, A. Rahnefeld, M. Sauter, F. L. Heppner, U. Voelker, R. Kandolf, U. Kuckelkorn, K. Stangl, Elke Krueger, P. M. Kloetzel, A. Voigt, “Impairment of immunoproteasome function by $\beta 5i/Imp7$ subunit deficiency results in severe enterovirus myocarditis,” *PLoS Pathog.*, vol. 7, no. 9, 2011.
- [59] J. Zhao, B. Zhai, S. P. Gygi, and A. L. Goldberg, “mTOR inhibition activates overall protein degradation by the ubiquitin proteasome system as well as by autophagy,” *Proc. Natl. Acad. Sci.*, vol. 112, no. 52, pp. 15790–15797, 2015.
- [60] A. Rousseau and A. Bertolotti, “An evolutionarily conserved pathway controls proteasome homeostasis,” *Nature*, vol. 536, no. 7615, pp. 184–189, 2016.
- [61] D. E. Harrison, R. Strong, Z. Dave Sharp, J. F. Nelson, C. M. Astle, K. Flurkey, N. L. Nadon, J. Erby Wilkinson, K. Frenkel, C. S. Carter, M. Pahor, M. A. Javors, E. Fernandez and R. A. Miller, “Rapamycin fed late in life extends lifespan in genetically heterogeneous mice,” *Nature*, vol. 460, no. 7253, pp. 392–395, 2009.
- [62] A. W. Thomson, H. R. Turnquist, and G. Raimondi, “Immunoregulatory functions of mTOR inhibition,” vol. 9, no. mAy, pp. 324–337, 2009.
- [63] W. Cao, S. Manicassamy, H. Tang, S. Pai Kasturi, A. Pirani, N. Murthy and B. Pulendran, “Toll-like receptor – mediated induction of type I interferon in plasmacytoid dendritic cells requires the rapamycin-sensitive PI (3) K-mTOR-p70S6K pathway,” vol. 9, no. 10, pp. 1157–1164, 2008.
- [64] S. Kaur, A. Sassano, B. Dolniak, S. Joshi, B. Majchrzak-Kita, D. P. Baker, N. Hay, E. N. Fish, and L. C. Plataniias, “Role of the Akt pathway in mRNA translation of interferon-stimulated genes,” *Proc. Natl. Acad. Sci. U. S. A.*, vol. 105, no. 12, pp. 4808–13, 2008.
- [65] F. Lekmine, S. Uddin, A. Sassano, S. Parmar, S. M. Brachmann, B. Majchrzak, N. Sonenberg, N. Hay, E. N. Fish and L. C. Plataniias, “Activation of the p70 S6 kinase and phosphorylation of the 4E-BP1 repressor of mRNA translation by type I interferons,” *J. Biol. Chem.*, vol. 278, no. 30, pp. 27772–27780, 2003.
- [66] D. Saleiro and L. C. Plataniias, “Intersection of mTOR and STAT signaling in immunity,” *Trends Immunol.*, vol. 36, no. 1, pp. 21–29, 2015.
- [67] H.-C. Tai and E. M. Schuman, “Ubiquitin, the proteasome and protein degradation in neuronal function and dysfunction,” *Nat. Rev. Neurosci.*, vol. 9, no. 11, pp. 826–838, 2008.
- [68] N. Myeku and K. E. Duff, “Targeting the 26S Proteasome To Protect Against Proteotoxic Diseases,” *Trends Mol. Med.*, vol. 24, no. 1, pp. 18–29, 2018.
- [69] K. Willeumier, S. M. Pulst, and F. E. Schweizer, “Proteasome Inhibition Triggers Activity-Dependent Increase in the Size of the Recycling Vesicle Pool in Cultured Hippocampal Neurons,” *J. Neurosci.*, vol. 26, no. 44, pp. 11333–11341, 2006.
- [70] I. Yao, H. Takagi, H. Ageta, T. Kahyo, S. Sato, K. Hatanaka, Y. Fukuda, T. Chiba, N.

- Morone, S. Yuasa, K. Inokuchi, T. Ohtsuka, G. R. MacGregor, K. Tanaka, and M. Setou, "SCRAPPER-Dependent Ubiquitination of Active Zone Protein RIM1 Regulates Synaptic Vesicle Release," *Cell*, vol. 130, no. 5, pp. 943–957, 2007.
- [71] M. D. Ehlers, "Activity level controls postsynaptic composition and signaling via the ubiquitin-proteasome system," *Nat. Neurosci.*, vol. 6, no. 3, pp. 231–242, 2003.
- [72] F. Cai, J. U. Frey, P. P. Sanna, and T. Behnisch, "Protein degradation by the proteasome is required for synaptic tagging and the heterosynaptic stabilization of hippocampal late-phase long-term potentiation," *Neuroscience*, vol. 169, no. 4, pp. 1520–1526, 2010.
- [73] R. Fonseca, R. M. Vabulas, F. U. Hartl, T. Bonhoeffer, and U. V. Nägerl, "A Balance of Protein Synthesis and Proteasome-Dependent Degradation Determines the Maintenance of LTP," *Neuron*, vol. 52, no. 2, pp. 239–245, 2006.
- [74] Y.-H. Jiang, D. Armstrong, U. Albrecht, C. M. Atkins, J. L. Noebels, G. Eichele, J. D. Sweatt, and A. L. Beaudet, "Mutation of the Angelman ubiquitin ligase in mice causes increased cytoplasmic p53 and deficits of contextual learning and long-term potentiation," *Neuron*, vol. 21, no. 4, pp. 799–811, 1998.
- [75] S. V Dindot, B. A. Antalffy, M. B. Bhattacharjee, and A. L. Beaudet, "The Angelman syndrome ubiquitin ligase localizes to the synapse and nucleus, and maternal deficiency results in abnormal dendritic spine morphology," *Hum. Mol. Genet.*, vol. 17, no. 1, pp. 111–118, 2008.
- [76] B. Bingol and E. M. Schuman, "Activity-dependent dynamics and sequestration of proteasomes in dendritic spines," *Nature*, vol. 441, no. 7097, pp. 1144–1148, 2006.
- [77] B. Bingol, C. Wang, D. Arnott, D. Cheng, J. Peng, and M. Sheng, "Autophosphorylated CaMKII α Acts as a Scaffold to Recruit Proteasomes to Dendritic Spines," *Cell*, vol. 140, no. 4, pp. 567–578, 2010.
- [78] H. Mori, J. Kondo, and Y. Ihara, "Ubiquitin is a component of paired helical filaments in Alzheimer's disease," *Science (80-.)*, vol. 235, pp. 1641–1644, 1987.
- [79] G. Perry, R. Friedman, G. Shaw, and V. Chau, "Ubiquitin is detected in neurofibrillary tangles and senile plaque neurites of Alzheimer disease brains," *Proc. Natl. Acad. Sci.*, vol. 84, no. 9, pp. 3033–3036, 1987.
- [80] F. W. van Leeuwen, D. P. V. de Kleijn, H. H. van den Hurk, A. Neubauer, M. A. F. Sonnemans, J. A. Sluijs, S. Koeycue, R. D. J. Ramdjielal, A. Salehi, G. J. M. Martens, F. G. Grosveld, J. P. H. Burbach, E. M. Hol, "Frameshit mutants of β amyloid precursor protein and ubiquitin-b in alzheimers and down patients," *Science (80-.)*, vol. 279, no. 5348, pp. 242–247, 1998.
- [81] Y. A. Lam *et al.*, "Inhibition of the ubiquitin-proteasome system in Alzheimer's disease," *Proc Natl Acad Sci U S A*, vol. 97, no. 18, pp. 9902–9906, 2000.
- [82] J. N. Keller, K. B. Hanni, and W. R. Markesbery, "Impaired proteasome function in Alzheimer's disease," *J. Neurochem.*, vol. 75, no. 1, pp. 436–439, 2000.
- [83] L. Gregori, J. F. Hainfeld, M. N. Simon, and D. Goldgaber, "Binding of amyloid ?? protein to the 20 S proteasome," *J. Biol. Chem.*, vol. 272, no. 1, pp. 58–62, 1997.
- [84] L. Gregori, C. Fuchs, M. E. Figueiredo-Pereira, W. E. Van Nostrand, and D. Goldgaber, "Amyloid β -protein inhibits ubiquitin-dependent protein degradation in vitro," *Journal of Biological Chemistry*, vol. 270, no. 34, pp. 19702–19708, 1995.
- [85] V. Cecarini, L. Bonfili, M. Amici, M. Angeletti, J. N. Keller, and A. M. Eleuteri, "Amyloid

- peptides in different assembly states and related effects on isolated and cellular proteasomes," *Brain Res.*, vol. 1209, no. Mc, pp. 8–18, 2008.
- [86] C. G. Almeida, R. H. Takahashi, and G. K. Gouras, "Beta-amyloid accumulation impairs multivesicular body sorting by inhibiting the ubiquitin-proteasome system.," *J. Neurosci.*, vol. 26, no. 16, pp. 4277–88, Apr. 2006.
- [87] F. Gillardon, A. Kloß, M. Berg, M. Neumann, K. Mechtler, B. Hengerer and B. Dahlmann, "The 20S proteasome isolated from Alzheimer's disease brain shows post-translational modifications but unchanged proteolytic activity." *J. Neurochem.*, vol. 101, no. 6, pp. 1483–1490, 2007.
- [88] M. Orre, W. Kamphuis, S. Dooves, L. Kooijman, E. T. Chan, C. J. Kirk, V. D. Smith, S. Koot, C. Mamber, A. H. Jansen, H. Ovaa and E. M. Hol, "Reactive glia show increased immunoproteasome activity in Alzheimer's disease," *Brain*, vol. 136, no. 5, pp. 1415–1431, 2013.
- [89] M. Mishtoa, E. Bellavistaa, A. Santoroa, A. Stolzingh, C. Ligoriod, B. Nacmiasc, L. Spazzafumob, M. Chiappellia, F. Licastroa, S. Sorbic, A. Pessiond, T. Ohme, T. Gruneg, C. Franceschia, "Immunoproteasome and LMP2 polymorphism in aged and Alzheimer's disease brains," *Neurobiol. Aging*, vol. 27, no. 1, pp. 54–66, 2006.
- [90] E. Aso, S. Lomoio, I. López-González, L. Joda, M. Carmona, N. Fernández-Yagüe, J. Moreno. S. Juvés, A. Pujol, R. Pamplona, M. Portero-Otin, V. Martín, M. Díaz, I. Ferrer "Amyloid generation and dysfunctional immunoproteasome activation with disease progression in animal model of familial Alzheimer's disease," *Brain Pathol.*, vol. 22, no. 5, pp. 636–653, 2012.
- [91] A. Brehm, Y. Liu, A. Sheikh, B. Marrero, E. Omoyinmi, Q. Zhou, G. Montealegre, A. Biancotto, A. Reinhardt, A. Almeida de Jesus, M. Pelletier, W. L. Tsai, E. F. Remmers, L. Kardava, S. Hill, H. Kim, H. J. Lachmann, A. Megarbane, J. Jin Chae, J. Brady, R. D. Castillo, D. Brown, A. V. Casano, L. Gao, D. Chapelle, Y. Huang, D. Stone, Y. Chen, F. Sotzny, C.-C. R. Lee, D. L. Kastner, A. Torrelo, A. Zlotogorski, S. Moir, M. Gadina, P. McCoy, R. Wesley, K. I. Rother, P. W. Hildebrand, P. Brogan, E. Krüger, I. Aksentijevich, and R. Goldbach-Mansky "Additive loss-of-function proteasome subunit mutations in CANDL / PRAAS patients promote type I IFN production," *J Clin Invest.*;125(11):4196–4211, 2015.
- [92] T. Blank and M. Prinz, "Type I interferon pathway in CNS homeostasis and neurological disorders," *Glia*, no. October 2016, pp. 1–10, 2017.
- [93] J. M. Taylor, M. R. Minter, A. G. Newman, M. Zhang, P. A. Adlard, and P. J. Crack, "Type-1 interferon signaling mediates neuro-inflammatory events in models of Alzheimer's disease.," *Neurobiol. Aging*, vol. 35, no. 5, pp. 1012–23, May 2014.
- [94] M. R. Minter, B. S. Main, K. M. Brody, M. Zhang, J. M. Taylor, and P. J. Crack, "Soluble amyloid triggers a myeloid differentiation factor 88 and interferon regulatory factor 7 dependent neuronal type-1 interferon response in vitro.," *J. Neuroinflammation*, vol. 12, p. 71, 2015.
- [95] M. R. Minter, Z. Moore, M. Zhang, K. M. Brody, N. C. Jones, S. R. Shultz, J. M. Taylor and P. J. Crack, "Deletion of the type-1 interferon receptor in APPSWE/PS1ΔE9 mice preserves cognitive function and alters glial phenotype," *Acta Neuropathol. Commun.*, vol. 4, no. 1, p. 72, 2016.
- [96] A. Caccamo, M. A. Maldonado, S. Majumder, D. X. Medina, W. Holbein, A. Magrí, and S. Oddo, "Naturally secreted amyloid-β increases mammalian target of rapamycin (mTOR) activity via a PRAS40-mediated mechanism," *J. Biol. Chem.*, vol. 286, no. 11, pp. 8924–8932, 2011.

- [97] A. Caccamo, C. Branca, J. S. Talboom, D. M. Shaw, D. Turner, L. Ma, A. Messina, Z. Huang, J. Wu, and S. Oddo, "Reducing Ribosomal Protein S6 Kinase 1 Expression Improves Spatial Memory and Synaptic Plasticity in a Mouse Model of Alzheimer's Disease.," *J. Neurosci.*, vol. 35, no. 41, pp. 14042–56, 2015.
- [98] F. Ahmad, K. Singh, D. Das, R. Gowaikar, E. Shaw, A. Ramachandran, K. V. Rupanagudi, R. P. Kommaddi, D. A. Bennett, and V. Ravindranath, "Reactive Oxygen Species-Mediated Loss of Synaptic Akt1 Signaling Leads to Deficient Activity-Dependent Protein Translation Early in Alzheimer's Disease," *Antioxid. Redox Signal.*, vol. 00, no. 00, p. ars.2016.6860, 2017.
- [99] R. Radde, T. Bolmont, S. A. Kaeser, J. Coomaraswamy, D. Lindau, L. Stoltze, M. E. Calhoun, F. Jaeggi, H. Wolburg, S. Gengler, C. Haass, B. Ghetti, C. Czech, C. Hoelscher, P. M. Mathews, and M. Jucker, "A β 42-driven cerebral amyloidosis in transgenic mice reveals early and robust pathology," *EMBO Rep.*, vol. 7, no. 9, pp. 940–946, 2006.
- [100] H. Oakley, S. L. Cole, S. Logan, E. Maus, P. Shao, J. Craft, A. Guillozet-Bongaarts, M. Ohno, J. Disterhoft, L. Van Eldik, R. Berry, and R. Vassar, "Intraneuronal beta-Amyloid Aggregates, Neurodegeneration, and Neuron Loss in Transgenic Mice with Five Familial Alzheimer's Disease Mutations: Potential Factors in Amyloid Plaque Formation," *J. Neurosci.*, vol. 26, no. 40, pp. 10129–10140, 2006.
- [101] W. L. Klein, "A β -toxicity in Alzheimer's disease: Globular oligomers (ADDLs) as new vaccine and drug targets," *Neurochem. Int.*, vol. 41, no. 5, pp. 345–352, 2002.
- [102] B. A. Chromy, R. J. Nowak, M. P. Lambert, K. L. Viola, L. Chang, P. T. Velasco, B. W. Jones, S. J. Fernandez, P. N. Lacor, P. Horowitz, C. E. Finch, G. A. Krafft, and W. L. Klein, "Self-assembly of A β (1-42) into globular neurotoxins," *Biochemistry*, vol. 42, no. 44, pp. 12749–12760, 2003.
- [103] J. J. Palop and L. Mucke, "Amyloid- β -induced neuronal dysfunction in Alzheimer's disease: from synapses toward neural networks," *Nat. Neurosci.*, vol. 13, no. 7, pp. 812–818, 2010.
- [104] L. K. Wagner, K. E. Gilling, E. Schormann, P. M. Kloetzel, F. L. Heppner, E. Krüger, and S. Prokop "Immunoproteasome deficiency alters microglial cytokine response and improves cognitive deficits in Alzheimer's disease-like APPPS1 mice," pp. 1–16, 2017.
- [105] U. Seifert and E. Krüger, "Remodelling of the ubiquitin-proteasome system in response to interferons.," *Biochem. Soc. Trans.*, vol. 36, no. Pt 5, pp. 879–84, Oct. 2008.
- [106] J. Zhao, A. L. Goldberg, J. Zhao, and A. L. Goldberg, "Coordinate regulation of autophagy and the ubiquitin proteasome system by MTOR Coordinate regulation of autophagy and the ubiquitin proteasome system by MTOR," *Autophagy*, vol. 12, no. 10, pp. 1967–1970, 2016.
- [107] V. I. Korolchuk, F. M. Menzies, and D. C. Rubinsztein, "Mechanisms of cross-talk between the ubiquitin-proteasome and autophagy-lysosome systems," *FEBS Lett.*, vol. 584, no. 7, pp. 1393–1398, 2010.
- [108] R. Siman, R. Cocca, and Y. Dong, "The mTOR inhibitor rapamycin mitigates perforant pathway neurodegeneration and synapse loss in a mouse model of early-stage Alzheimer-type tauopathy," *PLoS One*, vol. 10, no. 11, pp. 1–21, 2015.
- [109] C. G. Almeida, R. H. Takahashi, and G. K. Gouras, "beta-Amyloid Accumulation Impairs Multivesicular Body Sorting by Inhibiting the Ubiquitin-Proteasome System," *J. Neurosci.*, vol. 26, no. 16, pp. 4277–4288, 2006.
- [110] U. B. Pandey, Z. Nie, Y. Batlevi, B. A. McCray, G. P. Ritson, N. B. Nedelsky, S. L. Schwartz, N. A. DiProspero, M. A. Knight, O. Schuldiner, R. Padmanabhan, M. Hild, D. L.

- Berry, D. Garza, C. C. Hubbert, T.-P. Yao, E. H. Baehrecke, and J. P. Taylor, "HDAC6 rescues neurodegeneration and provides an essential link between autophagy and the UPS," vol. 447, no. June, pp. 859–863, 2007.
- [111] A. Caccamo, E. Ferreira, C. Branca, and S. Oddo, "p62 improves AD-like pathology by increasing autophagy," *Nat. Publ. Gr.*, vol. 22, no. 6, pp. 865–873, 2016.
- [112] J. Steffen, M. Seeger, A. Koch, and E. Krüger, "Proteasomal degradation is transcriptionally controlled by TCF11 via an ERAD-dependent feedback loop.," *Mol. Cell*, vol. 40, no. 1, pp. 147–58, Oct. 2010.
- [113] M. C. Poli, F. Ebstein, S. K. Nicholas, M. De Guzman, L.R. Forbes, I. K. Chinn, E.M. Mace, T. P. Vogel, A. Carisey, F. Benavides, Z. H. Coban-Akdemir, R. A. Gibbs, S. N. Jhangiani, D.M. Muzny, C. Carvalho, D. A. Schady, M. Jain, J. A. Rosenfeld, L. Emrick, R. A. Lewis, B. Lee, B. A. Zieba, S. Küry, E. Krüger, J. R. Lupski, L. B. Bostwick, and J.S. Orange, "Heterozygous truncating variants in POMP that escape nonsense-mediated decay and cause a unique immune dysregulatory syndrome.," *Am. J. Hum. Genet.*
- [114] Y. Zhang, J. Nicholatos, J.R. Dreier, S. J. H. Ricoult, S. B. Widenmaier, G.S. Hotamisligil, D. J. Kwiatkowski, and B. D. Manning, "Coordinated regulation of protein synthesis and degradation by mTORC1," *Nature*, vol. 513, no. 7518, pp. 440–443, 2014.
- [115] L. von Brzezinski, P. Säring, P. Landgraf, C. Cammann, U. Seifert, and D. C. Dieterich, "Low neurotoxicity of ONX-0914 supports the idea of specific immunoproteasome inhibition as a side-effect-limiting, therapeutic strategy," *Eur. J. Microbiol. Immunol.*, vol. 7, no. 3, pp. 234–245, 2017.
- [116] A. W. Kraft, X. Hu, H. Yoon, P. Yan, Q. Xiao, Y. Wang, S. C. Gil, J. Brown, U. Wilhelmsson, J. L. Restivo, J. R. Cirrito, D. M. Holtzman, J. Kim, M. Pekny, and J.-M. Lee, "Attenuating astrocyte activation accelerates plaque pathogenesis in APP/PS1 mice," *FASEB J.*, vol. 27, no. 1, pp. 187–198, 2013.
- [117] D. W. M. Broekaart, J. van Scheppingen, K. W. Geijtenbeek, M. R. J. Zuidberg, J. J. Anink, J. C. Baayen, A. Muhlebner, E. Aronica, J. A. Gorter, and E. A. van Vliet., "Increased expression of (immuno) proteasome subunits during epileptogenesis is attenuated by inhibition of the mammalian target of rapamycin pathway," pp. 1–11, 2017.
- [118] M. Di´az-Herna´ndez, F. Herna´ndez, E. Marti´n-Aparicio, P. Go´mez-Ramos, M. A. Mora´n, J. G. Casta´no, I. Ferrer, J. Avila, and J. J. Lucas, "Neuronal induction of the immunoproteasome in Huntington's disease.," *J. Neurosci.*, vol. 23, no. 37, pp. 11653–11661, 2003.
- [119] T. Pan, S. Kondo, W. Zhu, W. Xie, J. Jankovic, and W. Le, "Neuroprotection of rapamycin in lactacystin-induced neurodegeneration via autophagy enhancement," *Neurobiol. Dis.*, vol. 32, no. 1, pp. 16–25, 2008.
- [120] W. Kamphuis, L. Kooijman, S. Schettters, M. Orre, and E. M. Hol, "Biochimica et Biophysica Acta Transcriptional pro fi ling of CD11c-positive microglia accumulating around amyloid plaques in a mouse model for Alzheimer ' s disease," *BBA - Mol. Basis Dis.*, vol. 1862, no. 10, pp. 1847–1860, 2016.
- [121] S. Majumder, A. Richardson, R. Strong, and S. Oddo, "Inducing Autophagy by Rapamycin Before , but Not After , the Formation of Plaques and Tangles Ameliorates Cognitive Deficits," vol. 6, no. 9, 2011.

Eidesstattliche Versicherung

„Ich, Eileen Schormann, versichere an Eides statt durch meine eigenhändige Unterschrift, dass ich die vorgelegte Dissertation mit dem Thema: „*Perturbations of proteostasis networks in Alzheimer’s disease: Focus on the ubiquitin proteasome system.*“ selbstständig und ohne nicht offengelegte Hilfe Dritter verfasst und keine anderen als die angegebenen Quellen und Hilfsmittel genutzt habe.

Alle Stellen, die wörtlich oder dem Sinne nach auf Publikationen oder Vorträgen anderer Autoren beruhen, sind als solche in korrekter Zitierung (siehe „Uniform Requirements for Manuscripts (URM)“ des ICMJE -www.icmje.org) kenntlich gemacht. Die Abschnitte zu Methodik (insbesondere praktische Arbeiten, Laborbestimmungen, statistische Aufarbeitung) und Resultaten (insbesondere Abbildungen, Graphiken und Tabellen) entsprechen den URM (s.o) und werden von mir verantwortet.

Meine Anteile an etwaigen Publikationen zu dieser Dissertation entsprechen denen, die in der untenstehenden gemeinsamen Erklärung mit dem/der Betreuer/in, angegeben sind. Sämtliche Publikationen, die aus dieser Dissertation hervorgegangen sind und bei denen ich Autor bin, entsprechen den URM (s.o) und werden von mir verantwortet.

Die Bedeutung dieser eidesstattlichen Versicherung und die strafrechtlichen Folgen einer unwahren eidesstattlichen Versicherung (§156,161 des Strafgesetzbuches) sind mir bekannt und bewusst.“

Datum

Unterschrift

Lebenslauf

Mein Lebenslauf wird aus datenschutzrechtlichen Gründen in der elektronischen Version meiner Arbeit nicht veröffentlicht.

Mein Lebenslauf wird aus datenschutzrechtlichen Gründen in der elektronischen Version meiner Arbeit nicht veröffentlicht.

Publikationen

Wagner LK, Gilling KE, Schormann E, Kloetzel PM, Heppner FL, Krüger E, Prokop S. **Immunoproteasome deficiency alters microglial cytokine response and improves cognitive deficits in Alzheimer's disease-like APPS1 mice.** Acta Neuropathol Commun. 2017 Jun 24;5(1):52. doi: 10.1186/s40478-017-0453-5.

Sotzny F, Schormann E, Kühlewindt I, Koch A, Brehm A, Goldbach-Mansky R, Gilling KE, Krüger E. **TCF11/Nrf1-Mediated Induction of Proteasome Expression Prevents Cytotoxicity by Rotenone.** Antioxid Redox Signal. 2016 Dec 1;25(16):870-885. Epub 2016 Nov 14.

Jonigk D, Izykowski N, Maegel L, Schormann E, Ludewig B, Kreipe H, Hussein K. **Tumour angiogenesis in Epstein-Barr virus-associated post-transplant smooth muscle tumours.** Clin Sarcoma Res. 2014 Jan 7;4(1):1. doi: 10.1186/2045-3329-4-1.

Jonigk D, Izykowski N, Maegel L, Schormann E, Maecker-Kolhoff B, Laenger F, Kreipe H, Hussein K. **MicroRNA expression in Epstein-Barr virus-associated post-transplant smooth muscle tumours is related to leiomyomatous phenotype.** Clin Sarcoma Res. 2013 Jul 6;3(1):9. doi: 10.1186/2045-3329-3-9.

Pilatz A, Altinkilic B, Schormann E, Maegel L, Izykowski N, Becker J, Weidner W, Kreipe H, Jonigk D. **Congenital phimosis in patients with and without lichen sclerosus: distinct expression patterns of tissue remodeling associated genes.** J Urol. 2013 Jan;189(1):268-74. doi: 10.1016/j.juro.2012.09.010. Epub 2012 Nov 20.

Anteilserklärung an etwaigen erfolgten Publikationen

Eileen Schormann hatte während ihrer Tätigkeit als wissenschaftliche Mitarbeiterin im Institut für Biochemie, Charité Universitätsmedizin, folgenden Anteil an den folgenden Publikationen:

Publikation 1: Sotzny F, Schormann E, Kühlewindt I, Koch A, Brehm A, Goldbach-Mansky R, Gilling KE, Krüger E. TCF11/Nrf1-Mediated Induction of Proteasome Expression Prevents Cytotoxicity by Rotenone. *Antioxid Redox Signal*. 2016

Beitrag im Einzelnen (bitte kurz ausführen):

Meine experimentelle Arbeit mit nigrostriatalen organotypischen Hirnkulturen hat zu den Abbildungen 2. (D) und (E), Abbildung 3. (B), Abbildung 4 (B) beigetragen.

Publikation 2: Wagner LK, Gilling KE, Schormann E, Kloetzel PM, Heppner FL, Krüger E, Prokop S. Immunoproteasome deficiency alters microglial cytokine response and improves cognitive deficits in Alzheimer's disease-like APPPS1 mice. *Acta Neuropathol Commun*. 2017

Beitrag im Einzelnen (bitte kurz ausführen):

Meine experimentelle Arbeit zur Analyse von Proteasomaktivität und LMP7 Proteinexpression in post-mortem Hirngewebe von APP/PS1 Mausmodellen hat zu der Abbildung 1 c und d beigetragen.

Unterschrift Prof. Dr. Elke Krüger

Unterschrift Eileen Josephine Schormann

Danksagung

Die experimentelle Arbeit im Labor - sei es für die Bachelor-, Master- oder nun sogar die Doktorarbeit – ist geprägt von Erschöpfung, Frustration, Selbstzweifeln aber auch von Überraschungen, Stolz und Freude. Ohne die Unterstützung von Fachleuten, Kollegen, Freunden und Familie wäre dieses Wechselbad der Gefühle kaum zu meistern gewesen. Dafür bin ich allen Beteiligten unendlich dankbar!

Meine Doktormutter Prof. Dr. Elke Krüger hat es geschafft mich nicht nur fachlich kompetent zu unterstützen sondern daneben immer Verständnis zu zeigen. Sie hat mir vollstes Vertrauen geschenkt in der Organisation und Durchführung meines Forschungsprojektes, mir die Möglichkeiten eingeräumt meine Erkenntnisse auf Konferenzen zu präsentieren und sogar meinen Forschungsaustausch in Amsterdam unterstützt. Aber noch viel wichtiger und daher umso dankbarer bin ich, dass Elke immer ein offenes Ohr für meine Probleme hatte und mir in schwierigen Zeiten den nötigen Freiraum einräumte etwas kürzer zu treten. Ebenso dankbar bin ich der sowohl fachlichen als auch moralischen Unterstützung meiner Co-Betreuer Prof. Harms und Dr. Progione. Christoph und Alessandro haben mir stets wertvolles Feedback in den Progress-Meetings gegeben und mir auch darüber hinaus zur Seite gestanden, wenn ich Probleme hatte. Ich hätte mir keine bessere Betreuung wünschen können.

Ein besonderer Dank gilt auch Dr. Danny Jonigk, in dessen Labor ich meine ersten wissenschaftlichen Erfahrungen sammeln durfte. Mit „Blut, Schweiß und Tränen“ habe ich meine ersten Forscher-Schritte in der Pathologie gemacht und wurde dabei nachhaltig geprägt. Ohne diese wertvollen Erfahrungen wäre ich heute nicht die Person, die ich heute bin. Damals hörte ich das erste Mal von Rudolf Virchow, dem Begründer der modernen Pathologie, ohne zu ahnen, dass ich schon bald für meine Doktorarbeit in der wichtigsten Wirkungsstätte Virchows landen würde, der Charité.

Während der letzten 3 ½ Jahre habe ich immer wieder auf die Unterstützung anderer Wissenschaftler/innen und technischer Assistenten/innen zählen können. Seien es Materialien und Reagenzien, Protokolle oder technische Ratschläge oder einfach der moralische Support. Die Hilfsbereitschaft innerhalb der Charité und darüber hinaus war enorm. Namentlich bedanken möchte ich mich insbesondere bei Kate Elizabeth Gilling, Daniela Ludwig, Elke Bürger, Yves Leestemaker, Betty Jurek, Bettina Schmerl, Alex

Haake und Judith Houtman. Ganz besonders bedanken möchte ich mich bei Larissa Kraus, die mich durch das Korrekturlesen meiner Dissertation unterstützt hat und mir als Freundin immer den Rücken stärkt und frei hält.

Auch Christian möchte ich danken, der mich mit so viel Verständnis und Liebe aufgefangen hat. Auf dich kann ich mich immer verlassen. Das lässt sich mit nichts in der Welt aufwiegen!

Nicht vergessen habe ich wo ich herkomme und den beschwerlichen Weg, den ich hinter mir habe. Meine Familiengeschichte hat mich gelehrt stark zu sein und niemals aufzugeben. Mein vorrangiges Ziel war immer meine Familie stolz zu machen und ich hoffe, das ist mir hiermit gelungen.

Berlin, Juni 2018